NASA/CR—2004-213199/VOL2

Numerical, Analytical, Experimental Study of Fluid Dynamic Forces in Seals

Volume 2—Description of Gas Seal Codes GCYLT and GFACE

Wilbur Shapiro
Mechanical Technology, Inc., Latham, New York

October 2004

The NASA STI Program Office . . . in Profile

Since its founding, NASA has been dedicated to the advancement of aeronautics and space science. The NASA Scientific and Technical Information (STI) Program Office plays a key part in helping NASA maintain this important role.

The NASA STI Program Office is operated by Langley Research Center, the Lead Center for NASA's scientific and technical information. The NASA STI Program Office provides access to the NASA STI Database, the largest collection of aeronautical and space science STI in the world. The Program Office is also NASA's institutional mechanism for disseminating the results of its research and development activities. These results are published by NASA in the NASA STI Report Series, which includes the following report types:

- TECHNICAL PUBLICATION. Reports of completed research or a major significant phase of research that present the results of NASA programs and include extensive data or theoretical analysis. Includes compilations of significant scientific and technical data and information deemed to be of continuing reference value. NASA's counterpart of peer-reviewed formal professional papers but has less stringent limitations on manuscript length and extent of graphic presentations.
- TECHNICAL MEMORANDUM. Scientific and technical findings that are preliminary or of specialized interest, e.g., quick release reports, working papers, and bibliographies that contain minimal annotation. Does not contain extensive analysis.
- CONTRACTOR REPORT. Scientific and technical findings by NASA-sponsored contractors and grantees.
- CONFERENCE PUBLICATION. Collected papers from scientific and technical conferences, symposia, seminars, or other meetings sponsored or cosponsored by NASA.
- SPECIAL PUBLICATION. Scientific, technical, or historical information from NASA programs, projects, and missions, often concerned with subjects having substantial public interest.
- TECHNICAL TRANSLATION. English-language translations of foreign scientific and technical material pertinent to NASA's mission.

Specialized services that complement the STI Program Office's diverse offerings include creating custom thesauri, building customized databases, organizing and publishing research results . . . even providing videos.

For more information about the NASA STI Program Office, see the following:

- Access the NASA STI Program Home Page at ***http://www.sti.nasa.gov***
- E-mail your question via the Internet to help@sti.nasa.gov
- Fax your question to the NASA Access Help Desk at 301–621–0134
- Telephone the NASA Access Help Desk at 301–621–0390
- Write to:
  NASA Access Help Desk
  NASA Center for AeroSpace Information
  7121 Standard Drive
  Hanover, MD 21076

NASA/CR—2004-213199/VOL2

Numerical, Analytical, Experimental Study of Fluid Dynamic Forces in Seals

Volume 2—Description of Gas Seal Codes GCYLT and GFACE

Wilbur Shapiro
Mechanical Technology, Inc., Latham, New York

Prepared under Contract NAS3–25644

National Aeronautics and
Space Administration

Glenn Research Center

October 2004

Available from

NASA Center for Aerospace Information
7121 Standard Drive
Hanover, MD 21076

National Technical Information Service
5285 Port Royal Road
Springfield, VA 22100

Available electronically at http://gltrs.grc.nasa.gov

FOREWORD

The Computational Fluid Dynamics (CFD) computer codes and Knowledge-Based System (KBS) were generated under NASA contract NAS3-25644 originating from the Office of Advanced Concepts and Technology and administered through NASA-Lewis Research Center. The support of the Program Manager, Anita Liang, and the advice and direction of the Technical Monitor, Robert Hendricks, are gratefully appreciated. Major contributors to code development were:

- Dr. Bharat Aggarwal: KBS and OS/2 PC conversion of labyrinth seal code KTK
- Dr. Antonio Artiles: cylindrical and face seal codes ICYL and IFACE
- Dr. Mahesh Athavale and Dr. Andrzej Przekwas: CFD code SCISEAL
- Mr. Wilbur Shapiro: gas cylindrical and face seal codes GCYLT, GFACE, and seal dynamics code DYSEAL
- Dr. Jed Walowit: spiral groove gas and liquid cylindrical and face seal codes SPIRALG and SPIRALI.

The labyrinth seal code, KTK, was developed by Allison Gas Turbine Division of General Motors Corporation for the Aero Propulsion Laboratory, Air Force Wright Aeronautical Laboratories, Wright-Patterson Air Force Base, Ohio. It is included as part of the CFD industrial codes package by the permission of the Air Force.

TABLE OF CONTENTS

SECTION	PAGE
FORWARD	iii
LIST OF FIGURES	vii
LIST OF TABLES	ix
NOMENCLATURE	xi
1.0 INTRODUCTION	1
2.0 THEORETICAL DESCRIPTION AND NUMERICAL METHODS FOR CODE GCYLT	9
2.1 General Theory	9
2.2 Formation of Equations for Determining Pressure Distribution	9
2.3 The Column Method Solution of Newton-Raphson Equations	17
2.4 Film Thickness Distribution with Eccentricity and Misalignment	22
2.5 Power Loss (Torque)	25
2.6 Computation of Flows	30
2.7 Frequency-Dependent Spring and Damping Coefficients	31
2.8 Critical Mass and Frequency	34
2.9 Force Balance	36
3.0 SAMPLE PROBLEMS FOR CODE GCYLT	39
3.1 Sample Problem 1 - Rayleigh-Step Seal	39
3.2 Sample Problem 2 - Nongrooved Lobe Seal	44
3.3 Sample Problem 3 - Three-Lobe Seal	49
3.4 Sample Problem 4 - T-Shaped Sectored Seal	55
3.5 Sample Problem 5 - Rayleigh-Step, Floating-Ring Seal	61
3.6 Sample Problem 6 - Rayleigh-Step Seal with Eccentricity	67
3.7 Critical Mass - Sample Problem	71
4.0 COMPARISONS OF GCYLT WITH GCYL	73
5.0 VERIFICATION	79
6.0 THEORETICAL DESCRIPTION AND NUMERICAL METHODS FOR CODE GFACE	89
6.1 Governing Equations	89
6.2 Film Thickness Distribution and Misalignment	91
7.0 SAMPLE PROBLEMS OF CODE GFACE	93
7.1 Multipad Rayleigh Step Seal	93
7.2 Tapered Land Seal	93
7.3 Hydrostatic Recess Seal	95
7.4 Inherently Compensated Hydrostatic Seal	96

TABLE OF CONTENTS (Continued)

SECTION		PAGE
	7.5 Radial Taper Seal	97
8.0	VERIFICATION OF CODE GFACE	113
	8.1 Tilted Slider	113
	8.2 Ausman Rayleigh-Step Analysis	114
	8.3 Internal Verification	115
9.0	REFERENCES	121

LIST OF FIGURES

NUMBER		PAGE
1	GCYLT Hydrodynamic and Hydrostatic Configurations	3
2	Floating Ring Concept with Jointed Segmented Rings	4
3	Unwrapped Seal Surface	5
4	GFACE Configurations	7
5	Polar Grid Mesh System	8
6	Flow-Balance Cell and Associated Grid Network	11
7	Flow-Balance Across Cell	11
8	Couette Turbulence Coefficients	13
9	Poiseuille Turbulence Coefficients	14
10	Film Thickness Parameters	23
11	Preloaded Configuration	24
12	Rayleigh-Step	26
13	Axial Taper	27
14	Viscous Power Loss	28
15	Flow Across Circumferential Line	32
16	Flow Across Axial Line	32
17	Rayleigh-Step Geometry	40
18	Rayleigh-Step Seal Clearance Distribution	42
19	Rayleigh-Step Seal Pressure Distribution	43
20	Sectored Lobe Seal	45
21	Clearance Distribution, Sectored Lobe Seal	47
22	Pressure Distribution, Sectored Lobe Seal	48
23	Three-Lobe Seal	50
24	Clearance Distribution, Three-Lobe Seal	52
25	Pressure Distribution, Three-Lobe Seal	53
26	Pressure Distribution, Viewing in Axial Direction	54
27	T-Shaped Sectored Ring Seal	56
28	Pressure Distribution and Force Balance, Sectored Seal	57
29	Clearance Distribution, Sectored Seal	59
30	Pressure Distribution, Sectored Seal	60
31	Rayleigh-Step, Floating Ring Seal	62
32	Developed View of 50-mm Rayleigh-Step Pad	63
33	Clearance Distribution, Rayleigh-Step Pad	65
34	Pressure Distribution, Rayleigh-Step Pad	66
35	Clearance Distribution, Rayleigh-Step Seal with Eccentricity	69
36	Pressure Distribution, Rayleigh-Step Seal with Eccentricity	70
37	Rayleigh-Step Seal, Critical Mass versus Speed	71
38	Rayleigh-Step Seal, Critical Frequency versus Speed	72
39	Rayleigh-Step, Program Verification	81
40	Dimensionless Load Capacity versus Λ	82

LIST OF FIGURES (Continued)

NUMBER **PAGE**

41 Attitude Angle versus Λ 83
42 Coordinate System for GFACE 90
43 Non-Uniform Clearance Geometries 92
44 Sample Problem 1, Rayleigh-Step Seal, Clearance Distribution 99
45 Sample Problem 1, Rayleigh-Step Seal, Pressure Distribution 100
46 Sample Problem 1, Rayleigh-Step Seal, Pressure Distribution, Looking Along Radius 101
47 Sample Problem 2, Tapered Land Seal, Grid Regions 102
48 Sample Problem 2, Tapered Land Seal, Clearance Distribution 103
49 Sample Problem 2, Tapered Land Seal, Pressure Distribution 104
50 Sample Problem 4, Four-Recess Seal Configuration 105
51 Sample Problem 4, Four-Recess Seal, Clearance Distribution 106
52 Sample Problem 4, Four-Recess Seal, Pressure Distribution 107
53 Sample Problem 6, Inherently Compensated Seal, Clearance Distribution . . 108
54 Sample Problem 6, Inherently Compensated Seal, Pressure Distribution . . . 109
55 Sample Problem 6, Inherently Compensated Seal, Pressure Distribution Along Radius 110
56 Sample Problem 7, Radial Taper Seal, Clearance Distribution 111
57 Sample Problem 7, Radial Taper Seal, Pressure Distribution 112
58 Validation, Step Pad, Load vs. Step Height 116
59 Validation, Step-Pad, Load/Power vs. Step Height 117

LIST OF TABLES

NUMBER		PAGE
1	Sample Case 1: Raleigh Step Seal	41
2	Sample Case 2: Sectored Seal	46
3	Sample Case 3: Three-Lobe Gas Seal	51
4	Sectored Buffer Seal Sample Problem	58
5	Single-Pad Rayleigh-Step Seal Problem	64
6	Multipad Rayleigh-Step Seal Problem	68
7	Rayleigh-Step Seal Comparison	73
8	Three-Pad Sectored Seal Comparison	74
9	Three-Lobe Seal Comparison	75
10	Hydrostatic Sector Comparison	76
11	Rayleigh-Step Seal, Single Pad Comparison	77
12	Four-Pad Rayleigh-Step Seal Comparison	78
13	360° Plain Seal Parameters	79
14	Laminar Check of GCYLT	80
15	Couette Turbulence Comparison	84
16	Poiseuille Turbulence Comparison	84
17	Recessed Pad Flow Comparisons	86
18	Comparative Studies - Discrete Orifices versus Grid Size A	87
19	GFACE Multipad Step Seal	94
20	GFACE Single Tapered Land Seal	95
21	GFACE Recess Seal	96
22	GFACE Hydrostatic Source Seal	98
23	GFACE Inside Radial Tapered Land Seal	98
24	Comparisons of GFACE with Etsion and Fleming Load Capacity	113
25	Comparison of GFACE with ETSION and Fleming Power Loss	114
26	GFACE Comparison with Ausman Rayleigh-Step Pad	114
27	Forces and Moments as a Function of Displacements	119
28	Stiffness Comparisons Between Automatic and Manual Computed Values; Rayleigh-Step Pad	119

NOMENCLATURE FOR CODE GCYLT

C_d = inherently compensated orifice coefficient of discharge

C_o = reference clearance (concentric clearance)

d_o = orifice diameter

e = shaft displacement from concentric position

F_f = viscous friction force

FF = dimensionless viscous friction force = $F_f/(p_o C_o R)$

G = turbulent modifier of power loss

G_C = universal gas constant

G_x = turbulent modifier in direction of rotation

G_z = turbulent modifier in direction normal to rotation

h = local film thickness

H = dimensionless film thickness = h/C_o

l = bearing length

L = dimensionless length = l/R

M_c = critical mass

p = pressure

p_o = reference pressure

P = dimensionless pressure = p/p_o

P_{CR} = critical pressure ratio

P_R = orifice downstream pressure

P_S = supply pressure upstream of orifice

q = mass flow

r = orifice hole radius

R = journal radius

R_e = Couette Reynolds number

R_e* = modified Poiseuille Reynolds number

t = time

t_o = reference time $= \dfrac{12\mu R^2}{p_o C_o^2}$

T = dimensionless time = t/t_o

T_a = absolute temperature

T_f = viscous friction torque

TF = dimensionless viscous friction torque = $T_f/(p_o C_o R^2)$

U = journal surface velocity

z = axial direction coordinate

Z = dimensionless axial coordinate = z/R

α = misalignment angle about x-x axis

β = misalignment angle about y-y axis

γ = ratio of specific heats

ε = eccentricity ratio = e/C_o

θ = angular direction (direction of sliding)

θ_p = angular extent of pad

Λ = compressibility parameter = $\dfrac{6\mu\omega R^2}{p_o C_o^2}$

μ = absolute viscosity

ω = rotating speed

NOMENCLATURE FOR CODE GFACE

C_d = inherently compensated orifice coefficient of discharge

C_o = reference clearance

d_o = orifice diameter

F_f = viscous friction force

FF = dimensionless viscous friction force = $F_f/(p_oC_oR)$

G_C = universal gas constant

h = local film thickness

H = dimensionless film thickness = h/C_o

N = number of orifices in a row

p = pressure

p_o = reference pressure

P = dimensionless pressure = p/p_o

P' = absolute dimensionless pressure = P + 1

P_{CR} = critical pressure ratio

P_R = orifice downstream pressure

P_S = supply pressure upstream of orifice

q = mass flow

r = orifice hole radius

r_i = inner radius

r_o = outer radius

R = journal radius

S_c = source correction factor

t = time

t_o = reference time $= \dfrac{12\mu R^2}{p_o C_o^{\,2}}$

T = dimensionless time = t/t_o

T_a = absolute temperature

T_f = viscous friction torque

T_F = dimensionless viscous friction torque = $T_f/(p_o C_o R^2)$

U = journal surface velocity

z = axial direction coordinate

Z = dimensionless axial coordinate = z/R

α = misalignment angle about x-x axis

ß = misalignment angle about y-y axis

γ = ratio of specific heats

θ = angular direction (direction of sliding)

θ_p = angular extent of pad

Λ = compressibility parameter $= \dfrac{6\mu\omega R_o^2}{p_o C_o^{\,2}}$

μ = absolute viscosity

ω = rotating speed

1.0 INTRODUCTION

NASA's advanced engine programs are aimed at progressively higher efficiencies, greater reliability, and longer life. Recent studies have indicated that significant engine performance advantages can be achieved by employing advanced seals[1]*, and dramatic life extensions can also be achieved. Advanced seals are not only required to control leakage, but are necessary to control lubricant and coolant flow, prevent entrance of contamination, inhibit the mixture of incompatible fluids, and assist in the control of rotor response.

Recognizing the importance and need of advanced seals, NASA, in 1990, embarked on a five-year program (Contract NAS3-25644) to provide the U.S. aerospace industry with computer codes that would facilitate configuration selection and the design and application of advanced seals.

The program included four principal activities:

1. Development of a scientific code called SCISEAL, which is a Computational Fluid Dynamics (CFD) code capable of producing full three-dimensional flow field information for a variety of cylindrical configurations. The code is used to enhance understanding of flow phenomena and mechanisms, to predict performance of complex situations, and to furnish accuracy standards for the industrial codes. The SCISEAL code also has the unique capability to produce stiffness and damping coefficients that are necessary for rotordynamic computations.
2. Generation of industrial codes for expeditious analysis, design, and optimization of turbomachinery seals. The industrial codes consist of a series of separate stand-alone codes that were integrated by a Knowledge-Based System (KBS).
3. Production of a KBS that couples the industrial codes with a user friendly Graphical User Interface (GUI) that can in the future be integrated with an expert system to assist in seal selection and data interpretation and provide design guidance.
4. Technology transfer via four multiday workshops at NASA facilities where the results of the program were presented and information exchanged among suppliers and users of advanced seals. A Peer Panel also met at the workshops to provide guidance and suggestions to the program.

This final report has been divided into separate volumes, as follows:

Volume 1: Executive Summary and Description of Knowledge-Based System
Volume 2: Description of Gas Seal Codes GCYLT and GFACE
Volume 3: Description of Spiral-Groove Codes SPIRALG and SPIRALI
Volume 4: Description of Incompressible Seal Codes ICYL and IFACE
Volume 5: Description of Seal Dynamics Code DYSEAL and Labyrinth Seal Code KTK
Volume 6: Description of Scientific CFD Code SCISEAL.

This volume describes two industrial codes used to determine performance of fluid film gas seals. The codes are GCYLT (gas, cylindrical, turbulent) and GFACE (gas, face), which predict performance of a variety of film-riding gas seal configurations.

*Numbers in brackets indicate references located in Section 9.0.

Both codes were written for a PC environment using OS/2 as an operating system. The FORTRAN codes, however, are amenable to other systems that use FORTRAN 77, as long as memory is sufficient. References 2 and 3 provide the details of code implementation.

GCYLT is used for analyzing cylindrical gas seals. The turbulent version supplants a previous laminar version, GCYL. The laminar results are identical to the previous code, but GCYLT includes Couette and Poiseuille turbulence when Reynolds numbers dictate the presence of turbulence. The code will automatically determine the presence of turbulence throughout the grid field and make the necessary adjustments when computing the pressure distribution. Figure 1 shows solid ring configurations and Figure 2 shows typical sectored ring configurations that the program analyzes. Program capabilities include the following:

- Varying geometries, as indicated on Figures 1 and 2
- Variable or constant grid representation. Maximum grid size is 30 grid points in the axial direction and 74 grid points in the circumferential direction. Figure 3 shows a typical grid network. The circumferential parameter is θ, and the axial parameter is Z. The grid points are identified in the axial direction as I and in the circumferential direction as J. The extent of I is $1 \rightarrow M$, and the extent of J is $1 \rightarrow N$.
- Specified boundary pressures or periodic boundary conditions in the circumferential direction
- Axial symmetry option
- Four degrees of freedom, x and y translations and angular displacements about the x and y axes through the seal center
- Determining load as a function of shaft position or determining shaft position to satisfy a given load
- External pressurization (hydrostatic) of inherently compensated orifices, spot recesses or full recesses
- Choice of English or SI units.

The output of the program includes:

- Clearance distribution
- Pressure distribution
- Leakage along specified flow paths
- Load and load angle
- Righting moments
- Viscous dissipation
- Cross-coupled, frequency-dependent, stiffness and damping coefficients
- Plotting routines for the pressure and clearance distribution
- Critical mass and frequency.

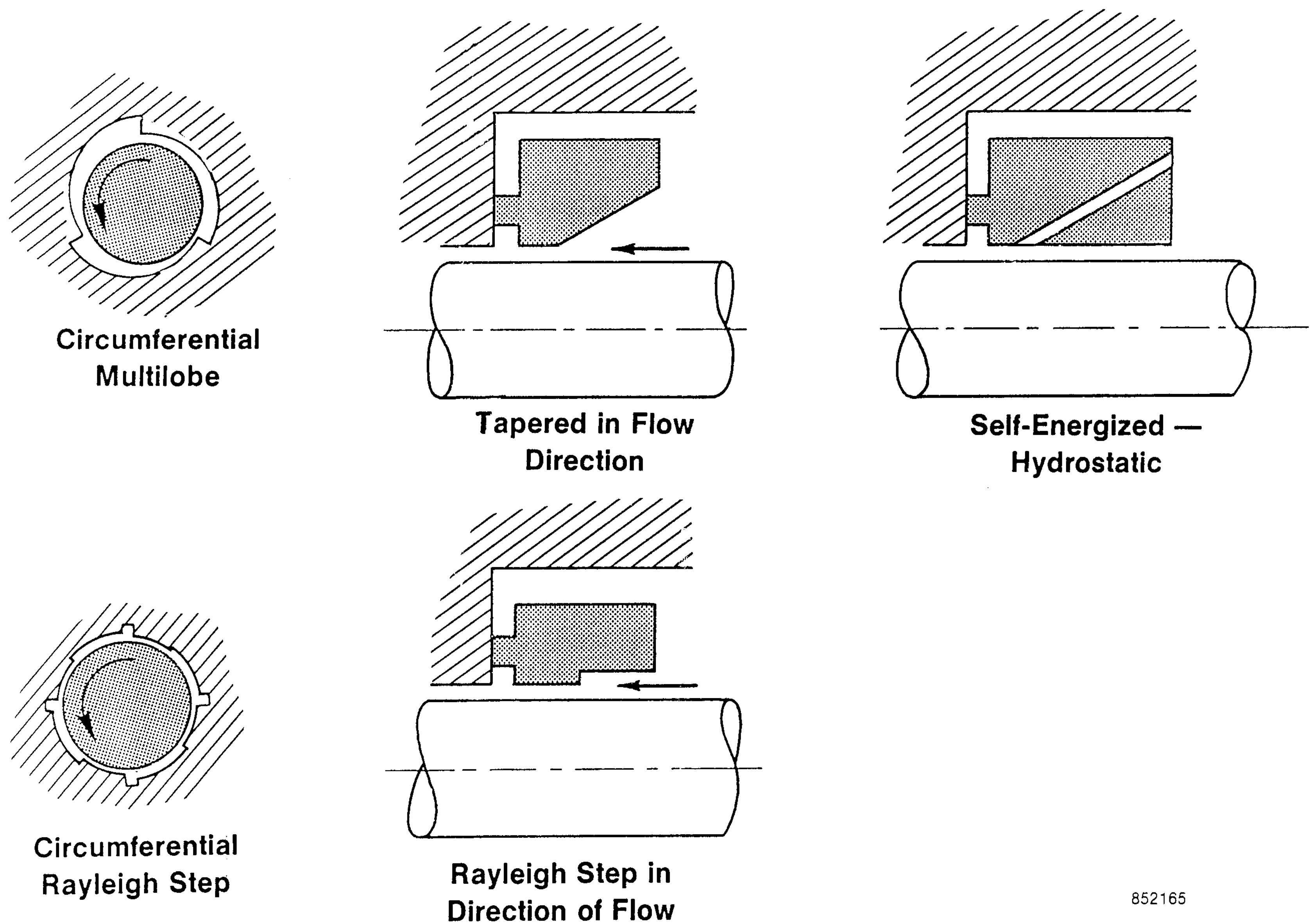

Figure 1. GCYLT Hydrodynamic and Hydrostatic Configurations

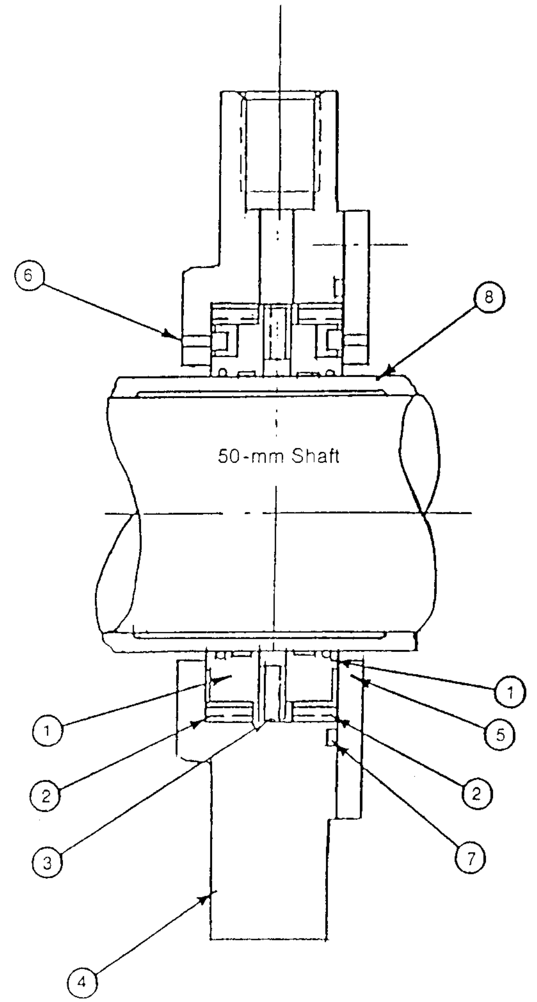

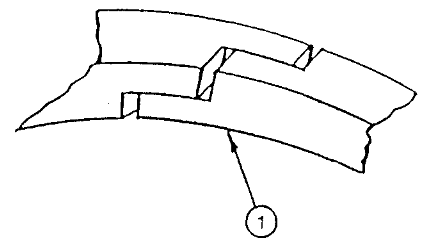

Item	Description	Material
1	Segmented Ring Rayleigh Step	Carbon
2	Spring-Radial	Inconel X-750
3	Spring-Axial	Inconel X-750
4	Housing	Stainless Steel 17-4 PH
5	Cover	Stainless Steel 17-4 PH
6	Stop Pin	Stainless Steel 17-4 PH
7	Seal	Teflon
8	Sleeve	Inconel 718 Hard Chromium Plated

852166

Figure 2. Floating Ring Concept with Jointed Segmented Rings

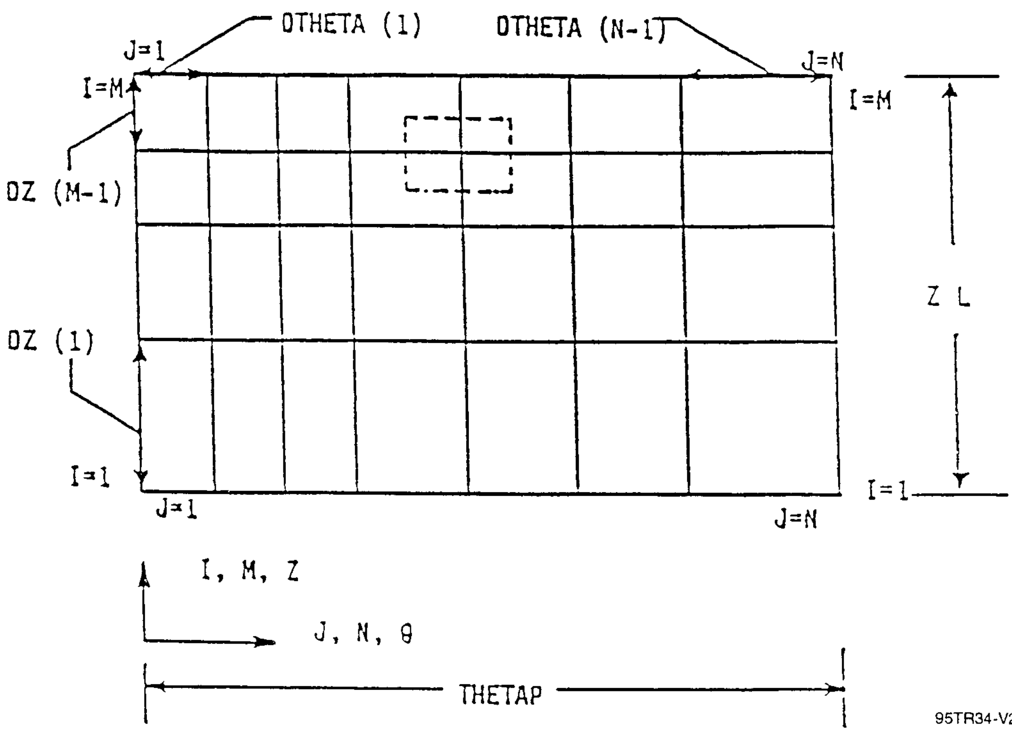

Figure 3. Unwrapped Seal Surface

The GFACE code is used for a variety of seals that can be defined in a polar coordinate reference frame. Figure 4 shows typical configurations that the program analyzes. The capabilities of the program include the following:

- Varying geometries as indicated on Figure 4
- Variable or constant grid representation. Maximum grid size is 51 grid points in the radial direction and 361 grid points in the circumferential direction. Figure 5 shows a typical grid network. The circumferential variable is θ and the radial variable is R. The grid points are identified in the radial direction as I and in the circumferential direction as J. The extent of I is $1 \rightarrow M$, and the extent of J is $1 \rightarrow N$.
- Specified boundary pressures or circumferential periodic boundaries
- Three degrees of freedom; axial, z translation and α and β rotations about the x and y axes through the rotor origin
- Determining load as a function of shaft position or determining shaft position to satisfy a given load
- External pressurization (hydrostatic) of inherently compensated orifices, spot recesses or full recesses
- Choice of English or SI units.

The output of the program includes:

- Clearance distribution
- Pressure distribution
- Leakage along specified flow paths
- Load capacity
- Righting moments
- Viscous dissipation
- Cross-coupled, frequency dependent, stiffness and damping coefficients
- Plotting routines for the pressure and clearance distribution

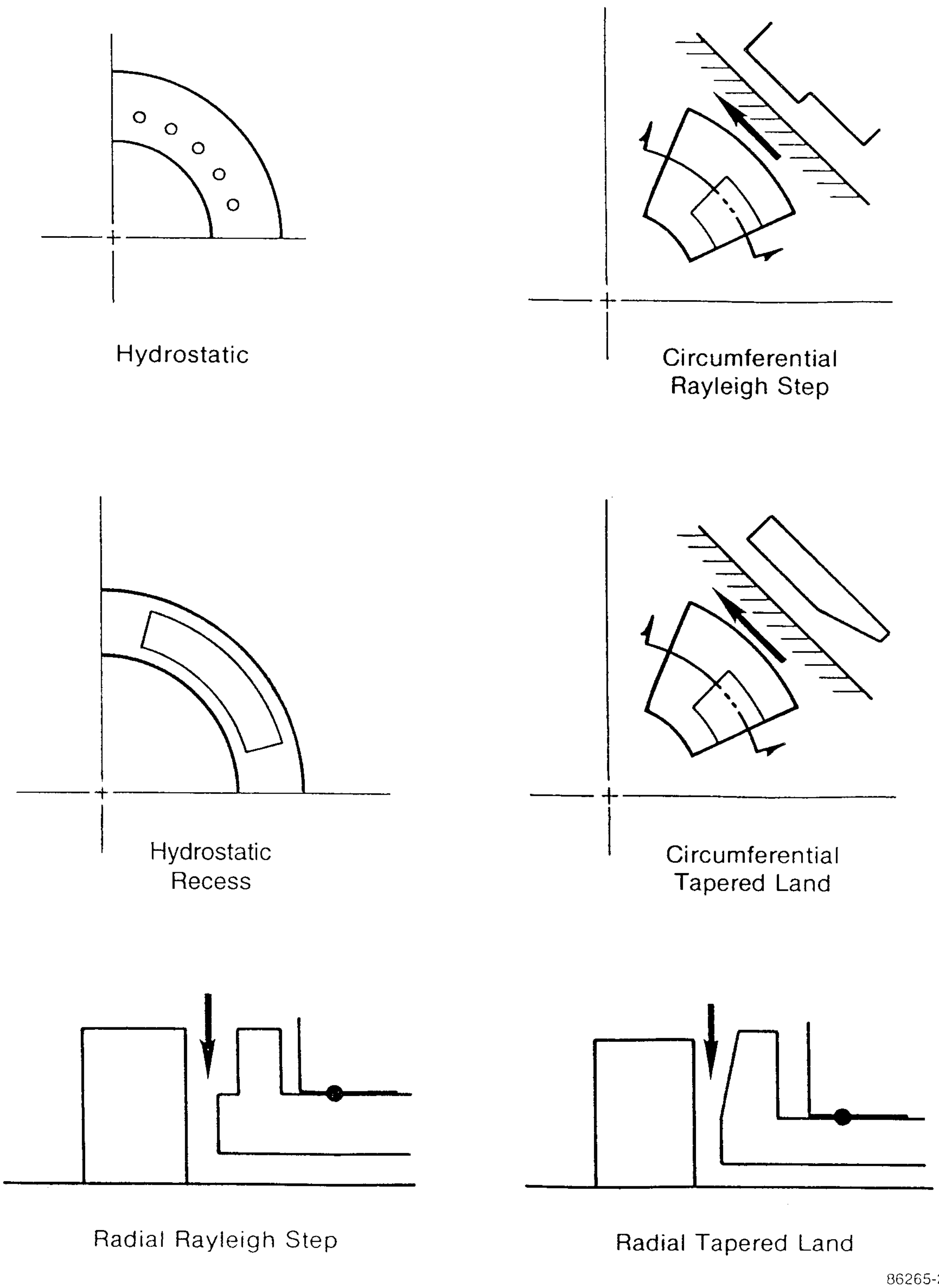

Figure 4. GFACE Configurations

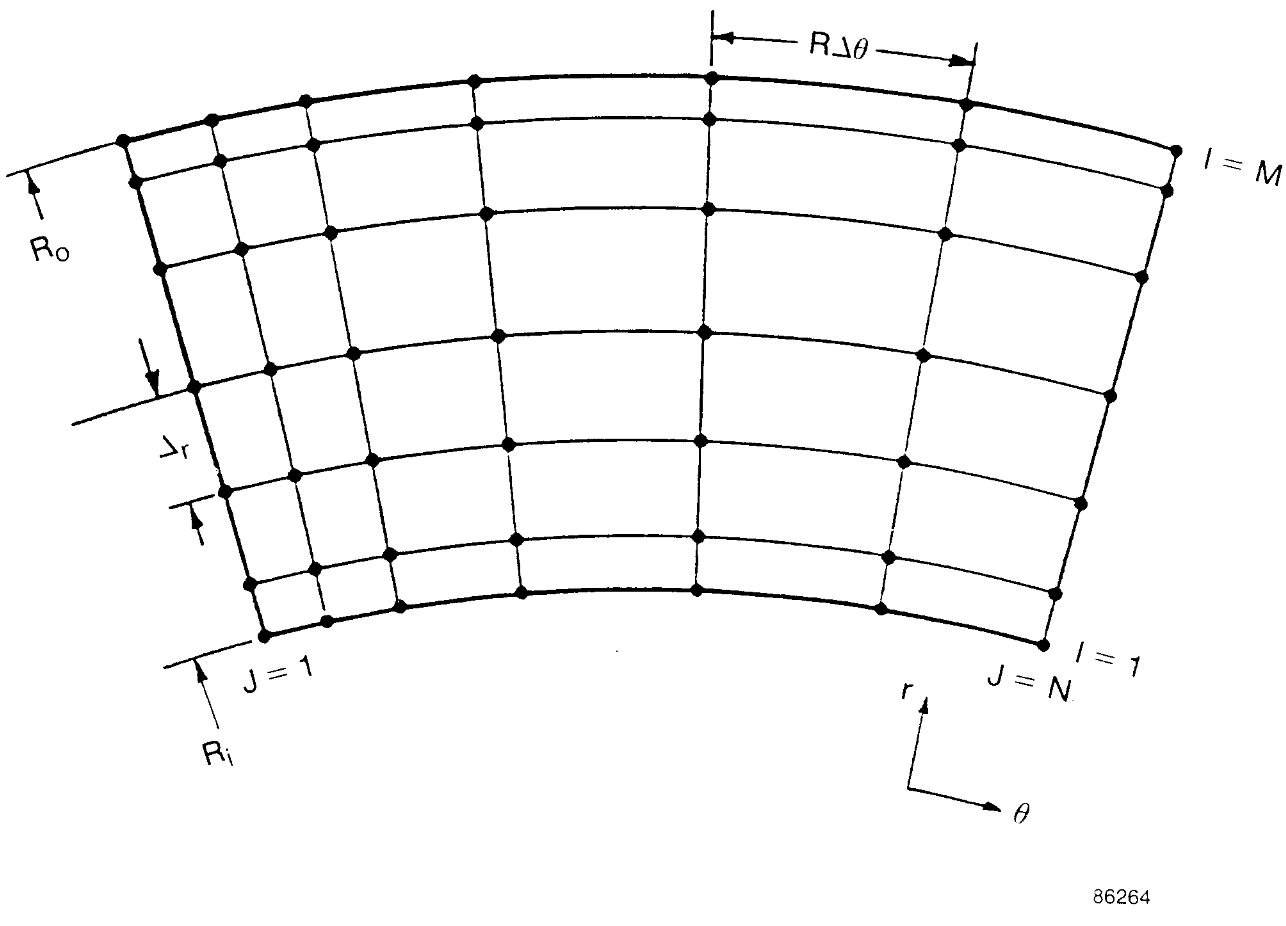

Figure 5. Polar Grid Mesh System

2.0 THEORETICAL DESCRIPTION AND NUMERICAL METHODS FOR CODE GCYLT

2.1 General Theory

Reynolds equation for turbulent compressible flow for journal bearings is as follows:

$$\frac{1}{R^2}\frac{\partial}{\partial\theta}\left(ph^3 G_x \frac{\partial p}{\partial\theta}\right) + \frac{\partial}{\partial z}\left(ph^3 G_z \frac{\partial p}{\partial z}\right) = 6\mu\omega\frac{\partial(ph)}{\partial\theta} + 12\mu\frac{\partial(ph)}{\partial t} \qquad \textbf{(2-1)}$$

The equation is made dimensionless with the following definitions. (Upper case variables are dimensionless).

$$Z = z/R,\ \ H = h/C_o,\ \ T = t/t_o,\ \ P = p/p_o,$$

$$\Lambda = \frac{6\mu\omega R^2}{p_o C_o^2},\ t_o = \frac{12\mu R^2}{p_o C_o^2},\ G_x \textit{ and } G_z = \textit{turbulence modifiers}$$

Substituting the dimensionless variables into the turbulent Reynolds equation produces a dimensionless equation.

$$\frac{\partial}{\partial\theta}\left(PH^3 G_x \frac{\partial P}{\partial\theta}\right) + \frac{\partial}{\partial Z}\left(PH^3 G_z \frac{\partial P}{\partial Z}\right) = \Lambda\frac{\partial(PH)}{\partial\theta} + \frac{\partial(PH)}{\partial T} \qquad \textbf{(2-2)}$$

For steady-state solutions, the time-dependent term on the right-hand side is eliminated except for the computation of spring and damping coefficients.

In the solution methods subsequently described, the Reynolds equation is not applied directly. The Reynolds equation represents the divergence of the mass flow at any grid point. The more convenient cell method[4] is to conduct a mass balance directly, and not the divergence of the mass flow at each point.

2.2 Formation of Equations for Determining Pressure Distribution

Solving for the pressure distribution is accomplished by a method[4] that uses a flow balance through a cell volume. The perimeter of the cell extends halfway between the grid point and its four neighboring points. A typical cell is shown by the dashed lines on Figure 6. The principal grid point is at Row i (length direction) and Column j (circumferential direction). For convenience of programming, the grid points are numbered for each cell sequentially from 1 to 9, with grid point 5 being the principal point. The corners of the cell boundaries are also numbered from 1 to 4.

Figure 7 shows the flow balance through the cell. There are eight flows across the cell boundaries, and there can also be a source (or sink) flow into or out of the cell control volume. The reason eight flows are used in lieu of four is that it permits discontinuous clearance boundaries at grid lines (such as Rayleigh steps) without taking derivatives across a discontinuous boundary.

The net flow through a cell can be expressed as:

$$\begin{aligned}&Q_{12}^{+}\frac{\Delta Z_i}{2} + Q_{12}^{-}\frac{\Delta Z_{i-1}}{2} + Q_{14}^{+}\frac{\Delta\theta_j}{2} + Q_{14}^{-}\frac{\Delta\theta_{j-1}}{2}\\ &-Q_{34}^{+}\frac{\Delta Z_i}{2} - Q_{34}^{-}\frac{\Delta Z_{i-1}}{2} - Q_{23}^{+}\frac{\Delta\theta_j}{2} - Q_{23}^{-}\frac{\Delta\theta_{j-1}}{2} = Q_{in}\end{aligned} \tag{2-3}$$

Q_{12}^{+} means the mass flow per unit length across the plus side of cell boundary 1-2, etc.

The Q's are dimensionless mass flows per unit length, except for Q_{in} which is a dimensionless source inlet flow. (Primed values of P are absolute pressures; unprimed values are gage pressures).

In the θ direction:

$$Q = -P'H^3 \frac{\partial P}{\partial\theta} G_x \frac{\Delta Z}{2} + \Lambda P'H \frac{\Delta Z}{2} \tag{2-4}$$

In the length or Z direction:

$$Q = -P'H^3 \frac{\partial P}{\partial Z} G_z \frac{\Delta\theta}{2} \tag{2-5}$$

where Q is defined as

$$Q = \frac{12\mu G_c T_a q}{p_o^2 C_o^3} \tag{2-6}$$

An optional flow can enter the cell from an external source, which can be treated as an inherently compensated orifice, or a conventional orifice restriction. Inherent compensation presumes the orifice area is the surface area of a cylinder circumvented by the hole size and length equal to the clearance under the inlet hole. The conventional orifice area is the area of the hole. The conventional orifice generally discharges into a recess that allows the flow velocity to dissipate into a region of constant pressure. Two types of recesses are permitted; a spot recess, which is treated as a source at one grid point, or a recess of finite length in the axial and circumferential directions, which is fed by an inlet orifice.

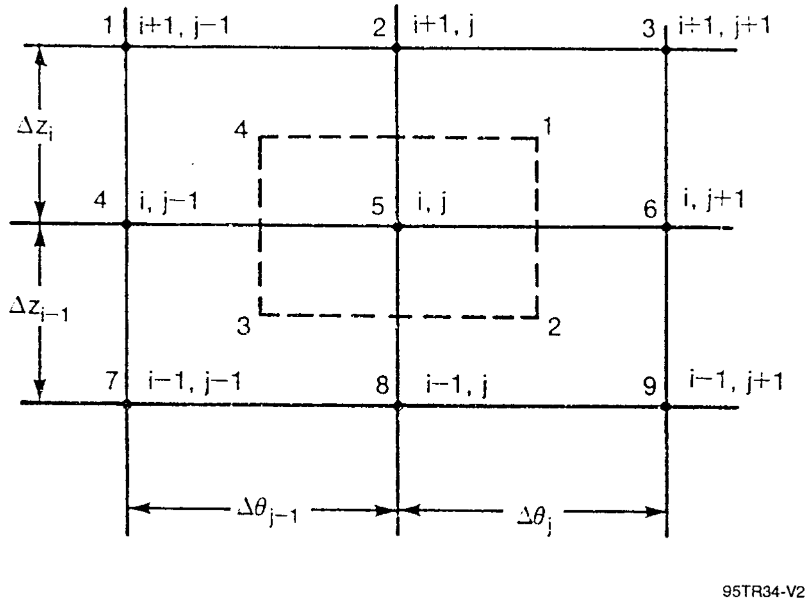

Figure 6. Flow-Balance Cell and Associated Grid Network

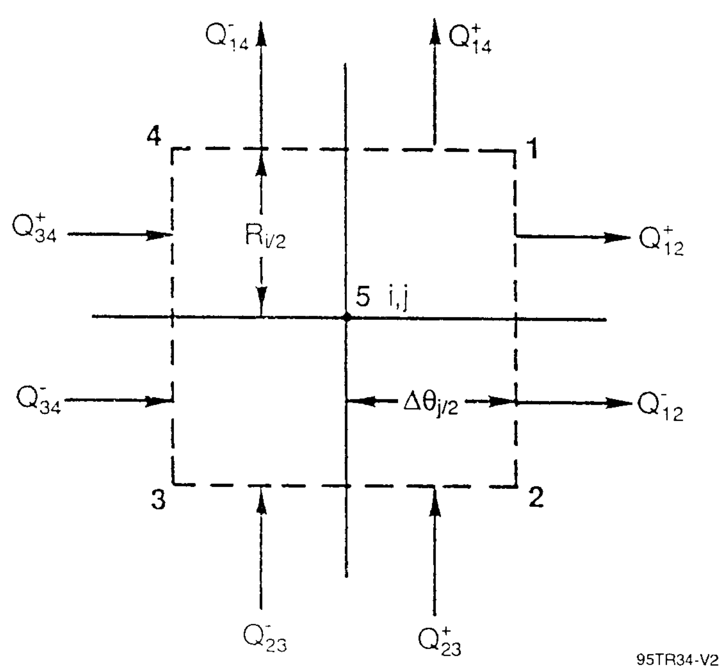

Figure 7. Flow-Balance Across Cell

Pressures are taken as the average pressure across the boundary. For example:

$$P_{12} = \frac{P_{i,j} + P_{i,j+1}}{2} \tag{2-7}$$

and

$$\frac{\partial P}{\partial \theta}\Big|_{12} = \frac{P_{i,j+1} - P_{i,j}}{\Delta\theta_j} \tag{2-8}$$

etc.

The turbulent G factors are dependent upon the Couette and Poiseuille Reynolds numbers which are computed at each grid point[5].

The Couette Reynolds number is

$$Re = \frac{CR\omega p_o}{\mu G_c T_a} \; P_c H_c \tag{2-9}$$

where the subscript c refers to the cell corner point (e.g., for Q_{12}^+, $P_c = P_1$). The Poiseuille Reynolds number is defined as:

$$R_e^* = R_{e0}^* \left|\nabla P\right| H_c^3 P_c$$

$$where \; R_{e0}^* = \frac{C^3 p_o^2}{\mu^2 R G_c T_a} \tag{2-10}$$

$$\left|\nabla P\right| = \left[\left(\frac{\partial P}{\partial \theta}\right)^2 + \left(\frac{\partial P}{\partial Z}\right)^2\right]^{1/2}$$

The value of P_c is the average of the four surrounding grid points, i.e.,

$$P_c = \frac{P_{i+i,j} + P_{i+1,j+1} + P_{ij} + P_{i,j+1}}{4}$$

The variation of the G factors with Reynolds numbers are shown on Figures 8 and 9. Once the Reynolds numbers have been computed at the cell corner points, the appropriate G coefficients are obtained from curve fitting routines.

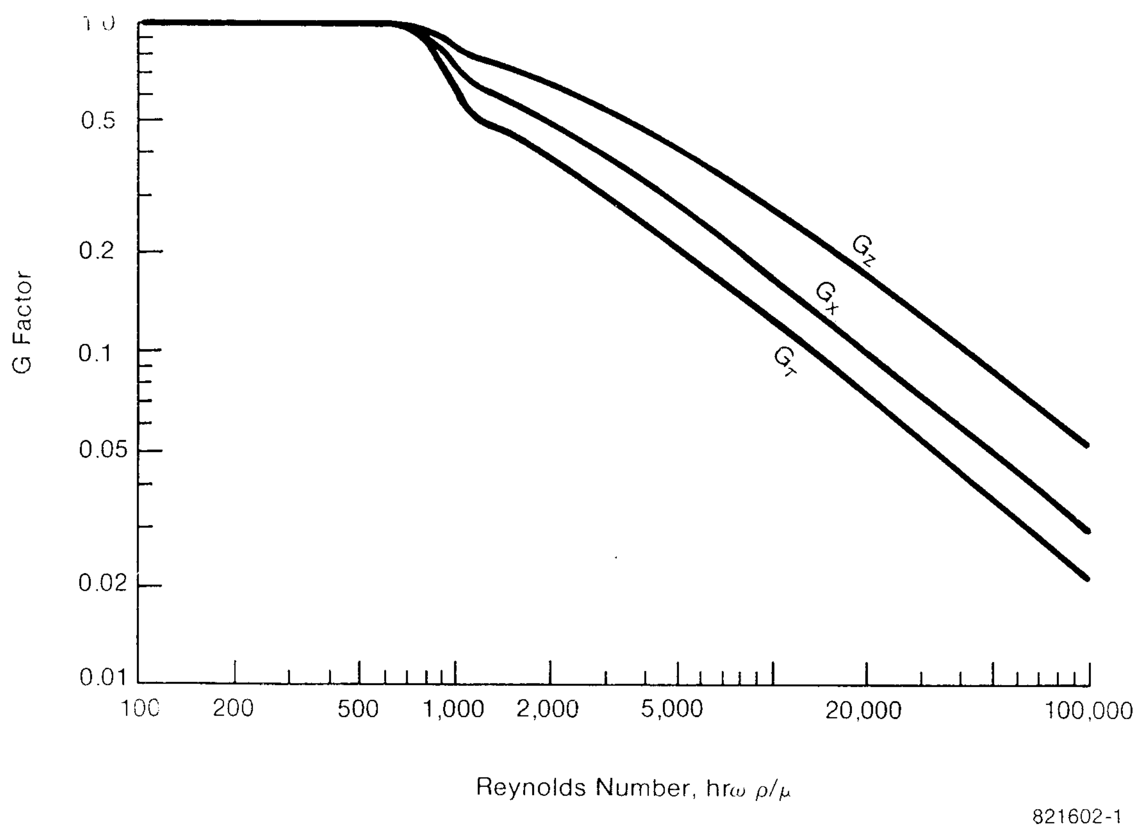

Figure 8. Couette Turbulence Coefficients

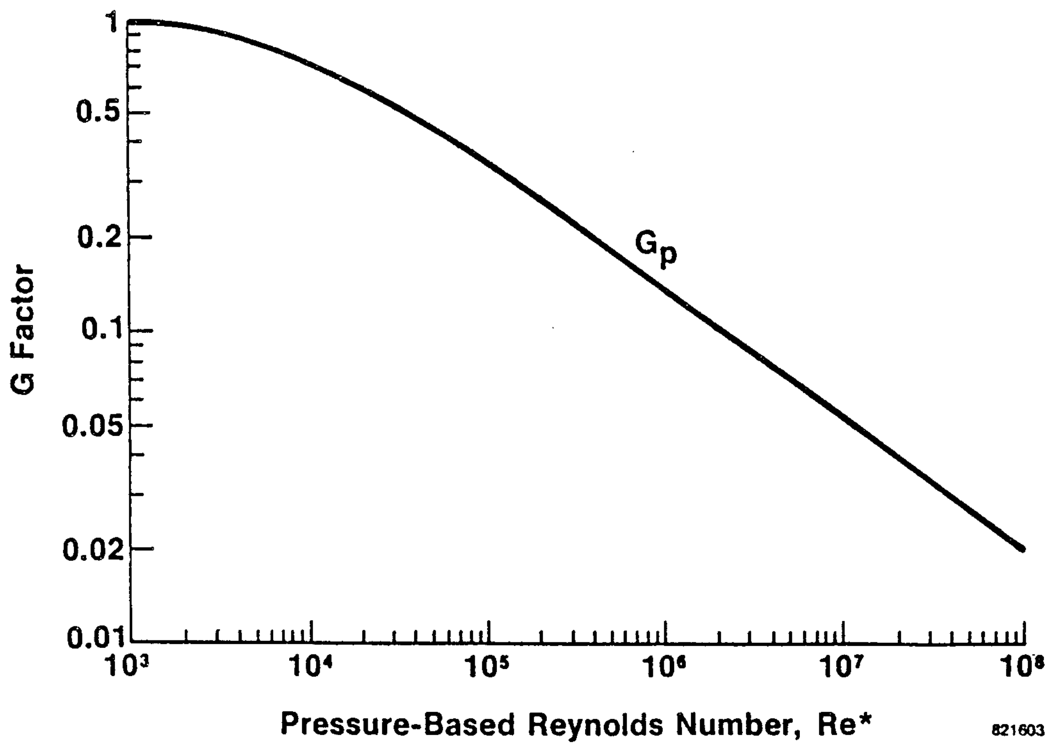

Figure 9. Poiseuille Turbulence Coefficients

The final values utilized are:

$$G_x = Min\left[G_x(R_e),\ G_p(R_e^*)\right] \tag{2-11}$$

$$G_z = Min\left[G_z(R_e),\ G_p(R_e^*)\right] \tag{2-12}$$

where G_x (R_e) and G_z (R_e) are Couette, and G_p are Poiseuille factors. This procedure selects the dominant turbulence factor for each of the eight cell flows.

By substituting the pressures and pressure derivatives (Equations 2-7 and 2-8) into the mass flow balance equations (2-3 and 2-4), an equation is derived that is a function of the nine pressures, P_1 through P_9, and the clearances taken at the cell corner points, H_1 -- H_4. Each cell corner point film thickness is computed in the clearance routine by appropriate values of Z and θ and is designated as HC_i, i = 1, 4. For example, HC_1 is the clearance at the cell corner point 1.

An optional flow can enter the cell from an external source, which is treated as an inherently compensated orifice or the usual hole size orifice restriction. Point sources pose numerical instability problems, which are circumvented by applying fine grids surrounding the source points. Flow through the orifice is given as:

$$Q_{in} = OFCxAOx\acute{P}_S \left\{ \left(\frac{\acute{P}_R}{\acute{P}_S}\right)^{2/\gamma} \left[1 - \left(\frac{\acute{P}_R}{\acute{P}_S}\right)^{\frac{\gamma-1}{\gamma}}\right] \right\}^{1/2} \tag{2-13}$$

where

$$OFC = \frac{12\mu C_d}{p_o C_o^3} \sqrt{\frac{2\gamma G_c T_a}{\gamma - 1}} \tag{2-14}$$

$$A_o = \begin{cases} \pi do H_5 C_o \ \textit{for Inherent Compensation} \\ \dfrac{\pi do^2}{4} \quad \textit{for Orifice Compensation} \\ \quad (\textit{spot recess or full recess}) \end{cases} \tag{2-15}$$

If

$$\left(\frac{\acute{P}_R}{\acute{P}_S}\right) \le P_{CR} \quad then \quad \left(\frac{\acute{P}_R}{\acute{P}_S}\right) = P_{CR} \tag{2-16}$$

$$where\ P_{CR} = \left[\frac{2.0}{(\gamma+1)}\right]\left(\frac{\gamma}{\gamma-1}\right) \tag{2-17}$$

$$Also,\ if\ \frac{\acute{P}_R}{\acute{P}_S} > 1.0,\ \frac{\acute{P}_R}{\acute{P}_S} = \frac{1}{\acute{P}_R/\acute{P}_S}\ and\ \acute{P}_S = \acute{P}_R \tag{2-18}$$

This condition implies backflow through the orifice.

The primed values indicate absolute pressure (i.e., $\acute{P}_R = P_R+1$).

Thus, a system of numerical equations can be derived as a function of nine pressures. There is an equation for every grid point.

$$f\ (P_1,\ P_2,\ ....\ P_9)\ i,j\ = 0 \tag{2-19}$$

The system is nonlinear since it is dependent upon multiples of P and its derivatives.

The solution process starts by assuming a pressure distribution, and using Newton-Raphson iteration until the functions f converge to zero within a prespecified truncation error. In equation form, the iteration process is:

$$f_{i,j}^{(old)} + \sum_{k=1}^{9} \frac{\partial f_{i,j}^{(old)}}{\partial P_K}\left(P_K^{(new)} - P_K^{(old)}\right) = 0 \tag{2-20}$$

where the partial derivatives are explicitly determined, e.g.,

$$\frac{\partial f_{i,j}}{\partial P_K} = \frac{f(P_1,P_2,\ ...\ P_{K+\varepsilon/2}\ ...\ P_9)_{i,j} - f(P_1,P_2,\ ...\ P_{K-\varepsilon/2},\ ...\ P_9)_{i,j}}{\varepsilon} \tag{2-21}$$

The actual convergence is not on f, but on $P_K^{(new)}$ - $P_K^{(old)}$, for when the difference vanishes, the condition that f = 0 is satisfied.

2.3 The Column Method Solution of Newton-Raphson Equations

The column method[6] is used to solve the new pressures in the set of M x N equations defined by Equation 2-20. The advantage of the column matrix method is that its inversions are M x M rather than M x N so that its use saves computational time.

The linearized N-R equations may be written in the form:

$$C_j\, P_j + E_j\, P_{j-1} + D_j\, P_{j+1} = R_j \tag{2-22}$$

For each value of j, P_j is a vector containing the jth column of new pressures, R_j is the right-hand side column vector and C_j, E_j and D_j are in general tri-diagonal matrices.

Case 1 - Pressure Prescribed at Start and End of Pads

Equations of form 2-22 are written at all points in the grid corresponding to i = 1, 2, →M and j = 2, 3, →N-1 with boundary column vectors P_1 and P_N prescribed. Look for a solution in the form:

$$P_{j-1} = A_j\, P_j + B_j \tag{2-23}$$

Where A_j is an M x M matrix and B_j is a vector. Use Equation 2-23 to eliminate P_{j-1} appearing in Equation 2-22.

$$(C_j + E_j\, A_j)\, P_j + E_j\, B_j + D_j\, P_{j+1} = R_j \tag{2-24}$$

Solve Equation 2-24 for P_j to obtain:

$$P_j = -I_j\, D_j\, P_{j+1} + I_j (R_j - E_j\, B_j) \tag{2-25}$$

Where $I_j = (C_j + E_j\, A_j)^{-1}$ (M x M matrix)

Set j = j+1 in Equation 2-23 to obtain

$$P_j = A_{j+1}\, P_{j+1} + B_{j+1} \tag{2-26}$$

Compare coefficients in Equations 2-25 and 2-26.

$$A_{j+1} = -I_j\, P_j\ ,\ B_{j+1} = I_j\, (R_j - E_j\, B_j) \tag{2-27}$$

Set $A_2 = 0$, $B_2 = P_1$.

Use Equation 2-27 to compute A_3, A_4, --, A_N and B_3, B_4 -- B_N.

Since P_N is given and all A_j and B_j are computed, we may use Equation 2-23 to compute P_{N-1}, P_{N-2}, P_{N-3}, ---, P_2.

Review of General Procedure for Nonperiodic Boundaries

1) *Set* $A_2 = 0$

$$B_2 = P_1$$

2) *Compute* A_{j+1}, B_{j+1}

$$A_{j+1} = -I_j\, D_j$$

$$B_{j+1} = I_j\,(R_j - E_j\, B_j)$$

$$j \rightarrow 2,\ N\text{-}1$$

where $I_j = (C_j + E_j\, A_j)^{-1}$

3) *Compute* P_j

$$P_{j-1} = A_j\, P_j + B_j$$

$$j \rightarrow N,\ 2$$

Case 2 - Column Method for Periodic Boundaries

P_j , B_j , R_j , Z_j are vectors. $\acute{N} = N - 1$

For periodic boundaries, the condition is that $P_1 = P_N$. At the boundary, j = 1, the general equation is:

$$C_1\, P_1 + E_1\, P_{\acute{N}} + D_1\, P_2 = R_1 \tag{2-28}$$

At column $\acute{N}$, the equation becomes

$$C_{N'}\, P_{N'} + E_{N'}\, P_{N'-1} + D_N\, P_1 = R_{N'} \tag{2-29}$$

To satisfy the boundary conditions, a solution is assumed of the form:

$$P_{j-1} = A_j\, P_j + B_j + F_j\, P_{N'} \tag{2-30}$$

$$A_1 = 0,\ B_1 = 0,\ F_1 = \delta\ (\textit{Kronecker delta matrix}) \tag{2-31}$$

Returning to the general equation:

$$C_j\, P_j + E_j\, P_{j-1} + D_j\, P_{j+1} = R_j \tag{2-32}$$

Substituting for P_{j-1} from Equation 2-30, the following results:

$$(C_j + E_j A_j) P_j + E_j B_j + E_j F_j P_{N'} + D_j P_{j+1} = R_j \qquad \textbf{(2-33)}$$

$$I_j = (C_j + E_j A_j)^{-1} \qquad \textbf{(2-34)}$$

Then,

$$P_j = -I_j D_j P_{j+1} + I_j (R_j - E_j B_j) - I_j E_j F_j P_{N'} \qquad \textbf{(2-35)}$$

From Equation 2-30:

$$P_j = A_{j+1} P_{j+1} + B_{j+1} + F_{j+1} P_{N'} \qquad \textbf{(2-36)}$$

Comparing Equations 2-35 and 2-36:

$$A_{j+1} = -I_j D_j \; B_{j+1} = I_j (R_j - E_j B_j), \; F_{j+1} = -I_j E_j F_j \; j = 1, 2, \text{---}, N-1 \qquad \textbf{(2-37)}$$

For $P_N = P_1$, we obtain from Equation 2-30:

$$P_{N'} = A_{N'+1} P_1 + B_{N'+1} + F_{N'+1} P_{N'} \qquad \textbf{(2-38)}$$

After rearranging:

$$P_{N'} = (\delta - F_{N'+1})^{-1} (A_{N'+1} P_1 + B_{N'+1}) \qquad \textbf{(2-39)}$$

or

$$P_{N'} = Y_{N'} P_1 + Z_{N'} \qquad \textbf{(2-40)}$$

where

$$Y_{N'} = (\delta - F_{N'+1})^{-1} A_{N'+1}, \; Z_{N'} = (\delta - F_{N'+1})^{-1} B_{N'+1} \qquad \textbf{(2-41)}$$

Substituting Equation 2-40 into 2-30 we obtain:

$$\begin{aligned} P_{N'-1} &= A_{N'} (Y_{N'} P_1 + Z_{N'}) + B_{N'} + F_{N'} (Y_{N'} P_1 + Z_{N'}) \\ &= (A_{N'} Y_{N'} + F_{N'} Y_{N'}) P_1 + A_{N'} Z_{N'} + B_{N'} + F_{N'} Z_{N'} \\ &= Y_{N'-1} P_1 + Z_{N'-1} \end{aligned} \tag{2-42}$$

where

$$Y_{N'-1} = A_{N'} Y_{N'} + F_{N'} Y_{N'} \text{ , } Z_{N'-1} = A_{N'} Z_{N'} + B_{N'} + F_{N'} Z_{N'} \tag{2-43}$$

Similarly,

$$\begin{aligned} P_{N'-2} &= A_{N'-1} (Y_{N'-1} P_1 + Z_{N'-1}) + B_{N'-1} + F_{N'-1} (Y_{N'} P_1 + Z_{N'}) \\ &= (A_{N'-1} Y_{N'-1} + F_{N'-1} Y_{N'}) P_1 + A_{N'-1} Z_{N'-1} + B_{N'-1} + F_{N'-1} Z_{N'} \end{aligned} \tag{2-44}$$

$$= Y_{N'-2} P_1 + Z_{N'-2} \tag{2-45}$$

$$\begin{aligned} Y_{j-1} &= A_j Y_j + F_j Y_{N'} \\ Z_{j-1} &= A_j Z_j + B_j + F_j Z_{N'} \end{aligned} \tag{2-46}$$

Therefore, in general:

$$P_{j-1} = Y_{j-1} P_1 + Z_{j-1} \text{ or } P_j = Y_j P_1 + Z_j \tag{2-47}$$

$$P_1 = (\delta - Y_1)^{-1} Z_1 \tag{2-48}$$

Review of General Procedure for Joined or Periodic Boundaries

1) *Compute* A_{j+1}, B_{j+1}, F_{j+1}

$$\begin{aligned} A_{j+1} &= -I_j D_j \\ B_{j+1} &= I_j (R_j - E_j B_j) \\ & j=1, N-1 \\ F_{j+1} &= -I_j E_j F_j \\ A_1 &= 0 \\ I_j &= (C_j + E_j A_j)^{-1} \\ B_1 &= 0 \\ F_1 &= \delta \end{aligned}$$

2) *Compute* Y_N', Z_N'

$$Y_N' = (\delta - F_N)^{-1} A_N$$

$$Z_N' = (\delta - F_N)^{-1} B_N$$

3) *Compute*

$$Y_{j-1} = A_j\, Y_j + F_j\, Y_N'$$

$$j = \acute{N} \rightarrow 2$$

$$Z_{j-1} = A_j\, Z_j + B_j + F_j\, Z_N'$$

4) *Compute* $P_1 = (\delta - Y_1)^{-1}\, Z_1$

5) *Compute* $P_j = Y_j\, P_1 + Z_j$
$j = 2 \rightarrow \acute{N}$

The coefficient matrices C_j, E_j and D_j, and the right-hand side vector R_j, are easily formulated. C_j contains all the coefficients multiplied by P_j. By examining Equation 2-20, it is seen that for any row i and column j that values of C are:

$$C_{i,i-1,j} = \frac{\partial f_5}{\partial P_8}$$

$$C_{i,i,j} = \frac{\partial f_5}{\partial P_5} \tag{2-49}$$

$$C_{i,i+1,j} = \frac{\partial f_5}{\partial P_2}$$

Similarly, the coefficient matrix E_j contains the elements:

$$E_{i,i,j} = \frac{\partial f_5}{\partial P_4},\; E_{i,i+1,j} = \frac{\partial f_5}{\partial P_1},\; E_{i,i-1,j} = \frac{\partial f_5}{\partial P_7} \tag{2-50}$$

and

$$D_{i,i,j} = \frac{\partial f_5}{\partial P_6},\; D_{i,i+1,j} = \frac{\partial f_5}{\partial P_3},\; D_{i,i-1,j} = \frac{\partial f_5}{\partial P_9} \tag{2-51}$$

R_j contains all elements not multiplied by the pressure

$$R_j = -f_{ij}^{(old)} + \sum_{k=1}^{9} \frac{\partial f_{ij}}{\partial P_K}\, P_K^{(old)} \tag{2-52}$$

2.4 Film Thickness Distribution with Eccentricity and Misalignment (see Figure 10)

In vector format, the clearance due to eccentricity and misalignment at any angle θ and at distance z' from the mid-plane is:

$$\bar{h} = \left(C_o \bar{e}_r - e_x \hat{i} - e_y \hat{j} - \alpha \hat{i}\ x\ z' \hat{k} - \beta \hat{j}\ x\ z' \hat{k}\right) . \hat{e}_r \tag{2-53}$$

$$\begin{aligned} h &= C_o - e_x \cos\theta - e_y \sin\theta + \alpha z' \sin\theta - \beta z' \cos\theta \\ &= C_o - (e_x + \beta z') \cos\theta - (e_y - \alpha z') \sin\theta \end{aligned} \tag{2-54}$$

Using dimensionless variables, Equation (2-54) becomes:

$$\begin{aligned} H = 1 &- \left(\varepsilon_x + \beta \frac{(Z - L/2)R}{C_o}\right) \cos\theta \\ &- \left(\varepsilon_y - \alpha \frac{(Z - L/2)R}{C_o}\right) \sin\theta \end{aligned} \tag{2-55}$$

which is set equal to

$$H = 1 - (\varepsilon_x + \varepsilon_\beta) \cos\theta - (\varepsilon_y + \varepsilon_\alpha) \sin\theta \tag{2-56}$$

where

$$\begin{aligned} \varepsilon_\beta &= \beta \ \frac{(Z - L/2)R}{C_o} \\ \varepsilon_\alpha &= \alpha \ \frac{(Z - L/2)R}{C_o} \end{aligned} \tag{2-57}$$

Preloaded Configurations

Preloaded configurations (see Figure 11) can be modeled by adding an additional eccentricity in the x and y directions.

$$\begin{aligned} \varepsilon_{PR}^x &= \varepsilon_{PR} \cos\theta_p \\ \varepsilon_{PR}^y &= \varepsilon_{PR} \sin\theta_p \end{aligned} \tag{2-58}$$

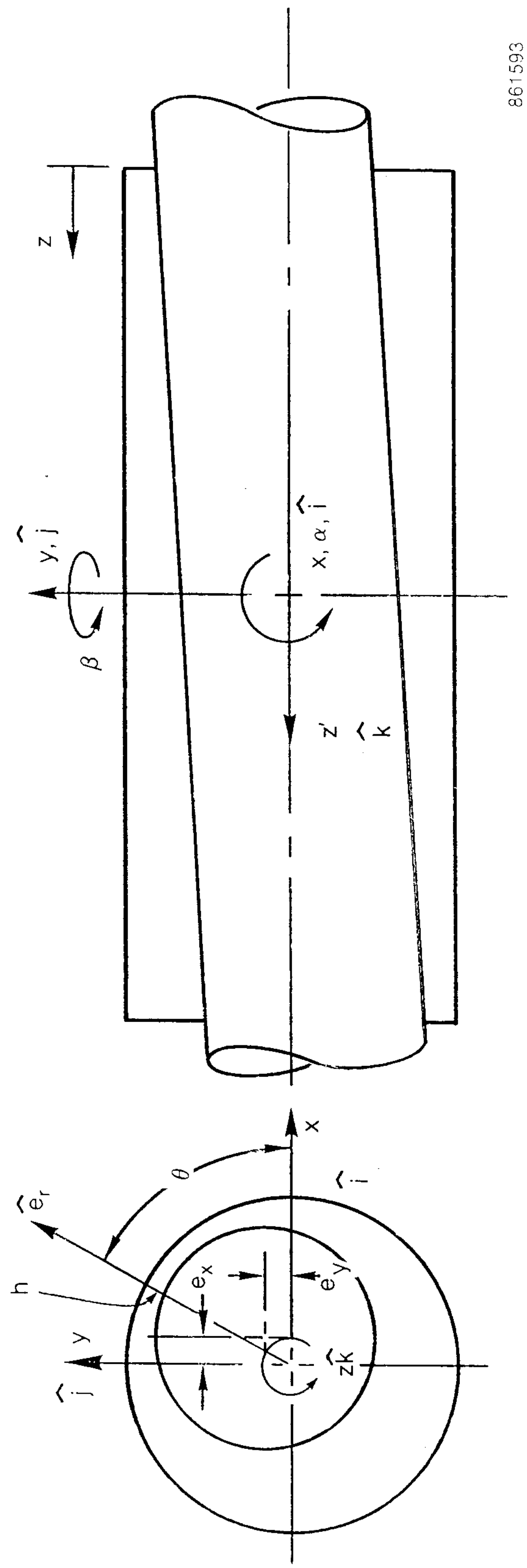

Figure 10. Film Thickness Parameters

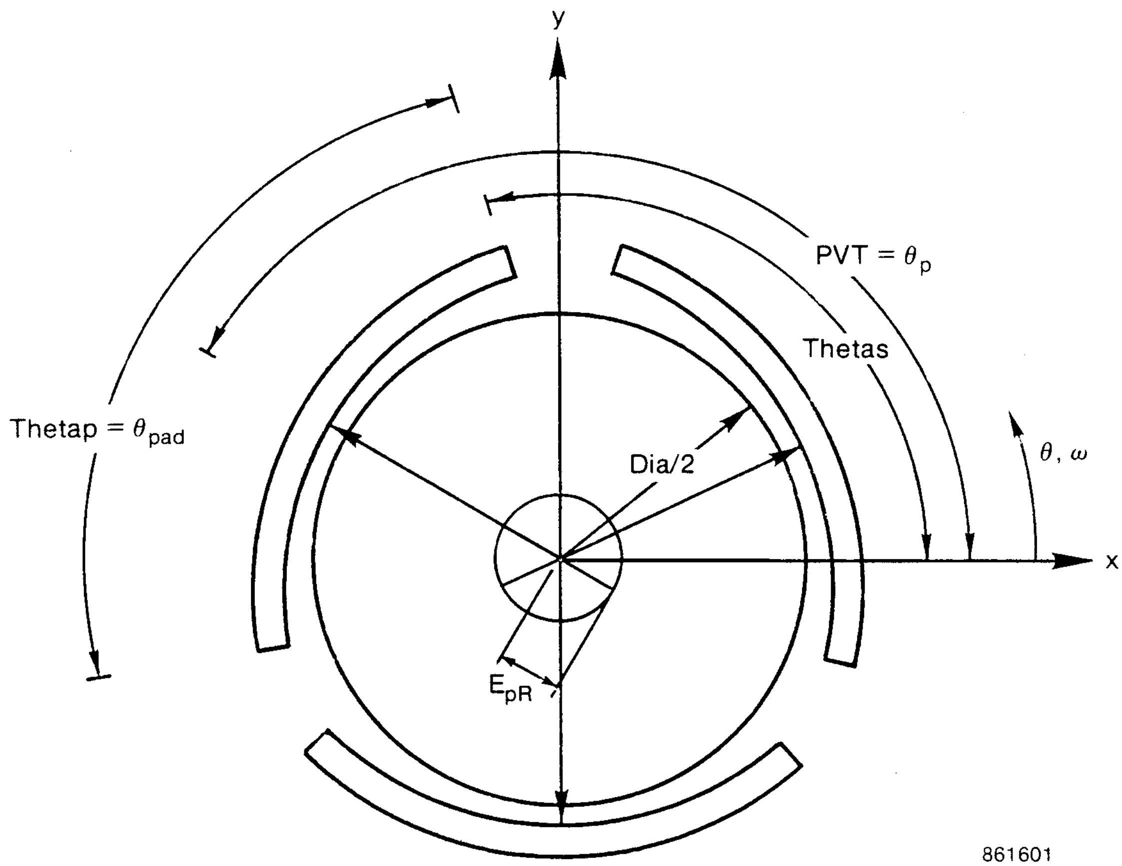

Keyword	Variable	Description
START	THETAS	Pad Start Angle
PADANGLE	THETAP	Pad Angle
PIVOT	PVT	Pivot Angle
PRELOAD	EPR	Offset/Clearance

Figure 11. Preloaded Configuration

where

ε_{PR}^{x} = x eccentricity due to preload

ε_{PR}^{y} = y eccentricity due to preload

θ_p = preload angle.

Rayleigh Step

The grid network for the Rayleigh step is shown on Figure 12. The boundaries of the step are defined by the lower left and upper right corners of the depressed region. Interior grid points include the step height in the clearance distribution.

Axial Taper

An axial taper is indicated as Figure 13. If $Z \geq Z_t$ then

$$H = H + \delta (Z - Z_t) \tag{2-59}$$

2.5 Power Loss (Torque)

Power loss is obtained by integrating the viscous shear forces across the film. From Figure 14, a force balance on an element produces:

$$\frac{\partial p}{\partial x} = \frac{\partial \tau}{\partial z} , \tag{2-60}$$

but

$$\tau = \mu \frac{\partial U}{\partial z} \tag{2-61}$$

Therefore,

$$\frac{\partial p}{\partial x} = \frac{\mu}{G\tau} \frac{\partial U^2}{\partial z^2} \tag{2-62}$$

where G_τ is the turbulence shear modifier. See Figure 8.

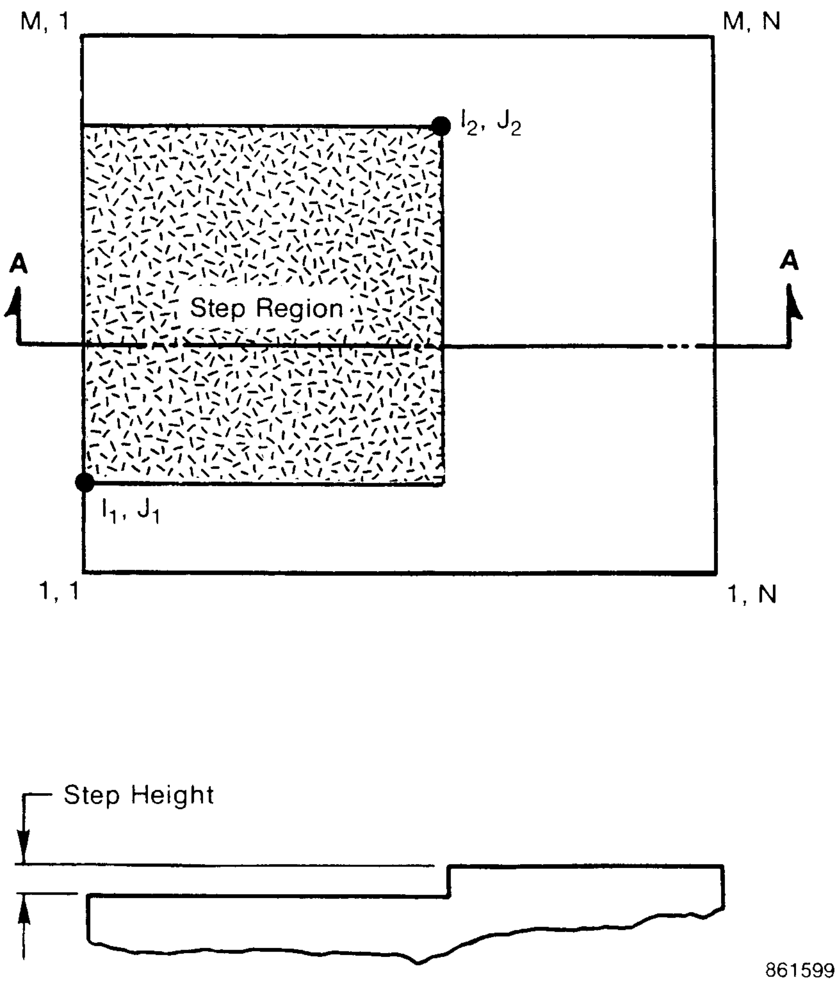

Figure 12. Rayleigh-Step

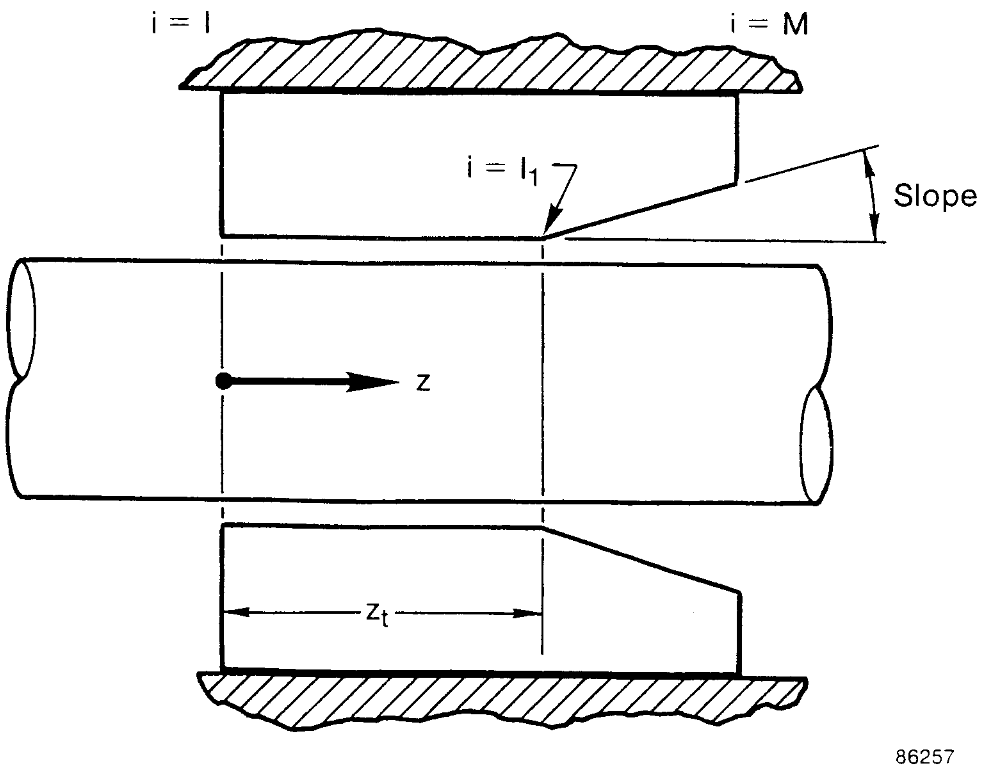

Figure 13. Axial Taper

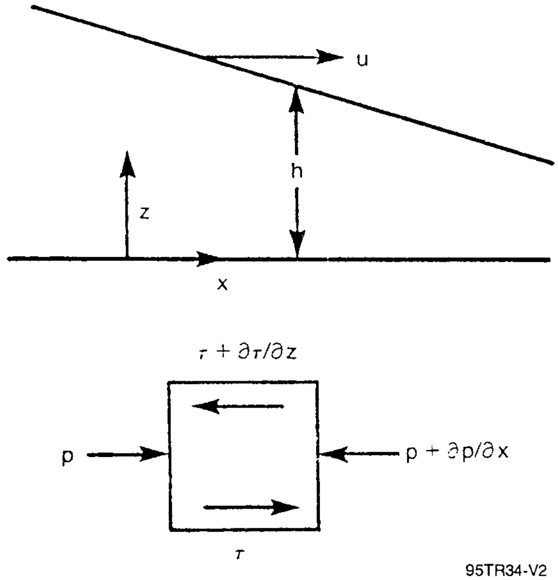

Figure 14. Viscous Power Loss

Integrating,

$$\frac{\partial U}{\partial z} = \frac{G_\tau}{\mu}\frac{\partial p}{\partial x} z + C_1 \tag{2-63}$$

$$U = \frac{G_\tau}{\mu}\frac{\partial p}{\partial x}\frac{z^2}{2} + C_1 z + C_2 \tag{2-64}$$

The boundary conditions are:

$$\begin{gathered} U = 0 \quad z = 0 \;\therefore\; C_2 = 0 \\ U = U \quad when\; z = h \end{gathered} \tag{2-65}$$

Substituting:

$$U = \frac{G_\tau}{\mu}\frac{\partial p}{\partial x}\frac{h^2}{2} + C_1 h \tag{2-66}$$

Therefore,

$$C_1 = \frac{U}{h} - \frac{G}{\mu}\frac{\partial p}{\partial x}\frac{h}{2} \tag{2-67}$$

and

$$U = \frac{G}{\mu}\frac{\partial p}{\partial x}\left[\frac{z^2}{2} - \frac{h}{2}z\right] + \frac{U}{h}z \tag{2-68}$$

$$\frac{\partial U}{\partial z} = \frac{1}{\mu}\frac{\partial p}{\partial x}\left[z - \frac{h}{2}\right] + \frac{U}{h} \tag{2-69}$$

$$\tau = \frac{\mu}{G}\frac{\partial u}{\partial z} = \frac{\partial p}{\partial x}\left[z - \frac{h}{2}\right] + \frac{U}{h}\frac{\mu}{G} \tag{2-70}$$

$$\tau\ (at\ z=h) = \frac{\partial p}{\partial x}\frac{h}{2} + \frac{\mu}{G}\frac{U}{h} \tag{2-71}$$

$$\begin{aligned} F_f &= friction\ force = \iint \tau dA \\ &= \iint \left[\frac{\partial P}{R\partial\theta}\frac{h}{2} + \frac{\mu}{G}\frac{R\omega}{h}\right] Rd\theta dZ \\ &= \iint \left[\frac{p_o C_o}{2R} H \frac{\partial P}{\partial\theta} + \frac{\mu}{C_o}\frac{R\omega}{HG}\right] R^2 d\theta dZ \\ &= \iint \left[p_o C_o R\frac{h}{2}\frac{\partial P}{\partial\theta} + \frac{\mu}{G}\frac{\omega R^3}{C_o H}\right] d\theta dZ \end{aligned} \tag{2-72}$$

$$\begin{aligned} FF &= \iint \left[p_o C_o \frac{H}{2}\frac{\partial P}{\partial\theta} + \frac{\Lambda}{G}\frac{C_o p_o}{6} R \frac{1}{H}\right] d\theta dZ \\ FF &= \iint \left[\frac{H}{2}\frac{\partial P}{\partial\theta} + \frac{\Lambda}{G6H}\right] d\theta dZ \end{aligned} \tag{2-73}$$

$$TF = \iint \left[\frac{H}{2} \frac{\partial P}{\partial \theta} + \frac{\Lambda}{G6H} \right] d\theta dZ \tag{2-74}$$

G, the turbulence modifier for friction, is the minimum of the Couette and Poiseuille values. The Couette and Poiseuille Reynolds numbers are computed as before (see Section 2-2). For the Couette number, G_τ, as shown on Figure 8, is obtained. For the Poiseuille flow, G_p, as shown on Figure 9, is obtained. The value of G is the minimum of G_τ and G_p.

2.6 Computation of Flows

The program computes the flow across specified axial and circumferential grid lines. A total of four grid lines can be prespecified.

Circumferential Flow Line (see Figure 15)

There are three types of points to consider. A point on a grid boundary J = 1 or J = N, and an interior point. Also, a flow line on I = M requires special consideration. For each point, a flow balance is accomplished through the cell surrounding the point as depicted on Figure 15. Consider an interior grid point on an interior grid line (I ≠ M).

$$Q_C\ (I,\ J) = Q_{14}^- + Q_{14}^+ + Q_{12}^+ - Q_{34}^+ \tag{2-75}$$

where

$$Q^+_{12} = \left(- \left(H_1^3\ G_x \frac{\partial P}{\partial \theta} \right)_{12} P_{12} + \Lambda\ H_1\ P_{12} \right) DZ_i/2 \tag{2-76}$$

$$\frac{\partial p}{\partial \theta} \Big|_{12} = \left(P_{i,j+1} - P_{i,j} \right) / \Delta\theta_j \tag{2-77}$$

$$P_{12} = \left(P_{i,j} + P_{i,j+1} \right) / 2.0 \tag{2-78}$$

The remaining flow components are similarly computed and Q_C (I, J) determined.

At J = 1, $\partial P/\partial\theta|_{34}$ is computed by forward difference and is equal to $\partial P/\partial\theta|_{12}$.

The pressure $P_{34}+ = P_{12}+$.

The clearance H_4 is not a regular grid point clearance and thus is not included in the grid clearance array. H_4 is computed as the average of $H_{i,j}$ and $H_{i+i,j}$.

The grid line mass flows are accumulated to obtain the total flow across the grid line.

Similar procedures are used for computing flows across axial lines (see Figure 16).

2.7 Frequency-Dependent Spring and Damping Coefficients

Discretization has been carried out with the use of the cell method[4], which involves a flow balance about each grid point.

$$\int \bar{\nabla}\cdot\bar{Q}\,dA = \oint \bar{Q}\cdot\bar{n}\,dS = -\frac{\partial}{\partial T}\int (1+P)\,H\,dA \tag{2-79}$$

where Q = the mass flow vector per unit length.

The equality of the first two terms comes from the divergence theorem.

In numerical format, the right-hand side becomes:

$$-\frac{\partial}{\partial T}\left[(1+P_{ij})\,H_{ij}A_{ij}\right] \tag{2-80}$$

where,

$$A_{ij} = \frac{1}{4}(\Delta\theta_j + \Delta\theta_{j-1})\,(\Delta Z_i + \Delta Z_{i-1}) \tag{2-81}$$

Generally, a small perturbation analysis is used for determining frequency-dependent spring and damping coefficients and solving the complete equation (2-79). A small perturbation analysis, however, is generally limited to concentric operation and produces complex expressions for the perturbation coefficients. Identical results can be achieved by direct numerical perturbation of the difference equations used in the column matrix solution approach. This method, which is described below, avoids algebraic error in determining the perturbation coefficients and may be used in complex situations where analytical determination of the perturbation coefficients is not feasible.

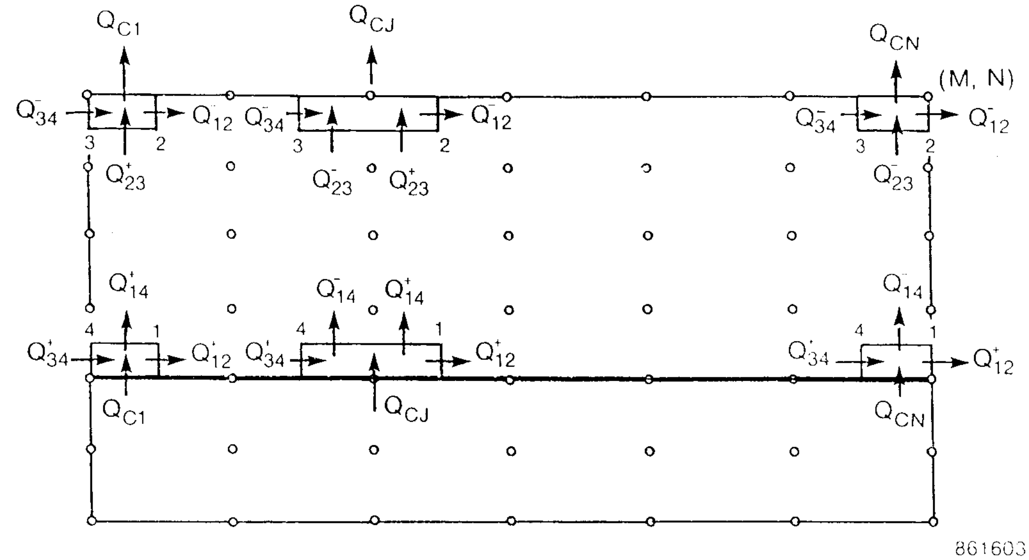

Figure 15. Flow Across Circumferential Line

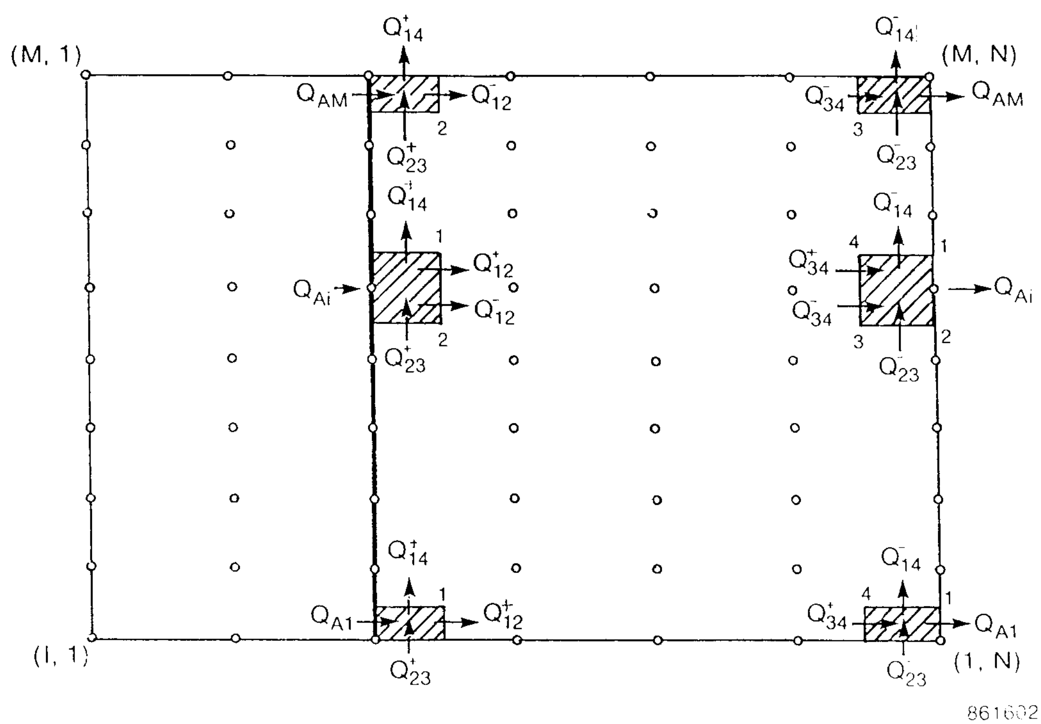

Figure 16. Flow Across Axial Line

After desired convergence of the Newton-Raphson process has been achieved under steady (unperturbed) conditions, the resulting steady-state pressure vectors are denoted as $\{\hat{P}\}$ and the coefficient matrices as $[\hat{C}^j]$, etc. and, as before, the steady state becomes:

$$[\hat{C}^j]\{\hat{P}_j\} + [\hat{E}^j]\{\hat{P}_{j-1}\} + [\hat{D}^j]\{\hat{P}_{j+1}\} = \{\hat{R}^j\} \tag{2-82}$$

The eccentricity components can be perturbed individually by an amount, η, and the matrix $[\hat{C}^j]$ recalculated at the new film thickness (but old pressure distribution, $\hat{P}$); then subtract $[\hat{C}^j]$ at the old film thickness and divide the difference by η to numerically obtain the partial derivative of $[\hat{C}^j]$ with respect to the eccentricity perturbation. This partial derivative will be denoted by $[\hat{C}^{j,k}]$.

Thus,

$$[\hat{C}^{j,k}] = \frac{[\hat{C}^j]|_{\varepsilon_k+\eta} - [\hat{C}^j]|_{\varepsilon_k}}{\eta} \tag{2-83}$$

The matrices $[\hat{E}^{j,k}]$, $[\hat{D}^{j,k}]$ and $[\hat{R}^{j,k}\}$ are obtained in a similar manner. Equation (2-78) may now formally be differentiated with respect to ε_k to obtain the expression:

$$[\hat{C}^j]\{\hat{P}_j^{,k}\}+[\hat{E}^j]\{\hat{P}_{j-1}^{,k}\}+[\hat{D}^j]\{\hat{P}_{j+1}^{,k}\} = \{\hat{R}^{j,k}\}-[\hat{C}^{j,k}]\{\hat{P}_j\}-[\hat{E}^{j,k}]\{\hat{P}_{j-1}\}-[\hat{D}^{j,k}]\{\hat{P}_{j+1}\} \tag{2-84}$$

where $\{\hat{P}_j^{,k}\} = \partial\{\hat{P}_j\}/\partial\varepsilon_k$ is the zero-frequency stiffness pressure. This expression does not yet contain the time-dependent terms found on the right-hand side of Equation (2-75). It is assumed that a sinusoidal disturbance is applied to the shaft, such that the clearance and pressure derivatives are affected as follows:

$$H = e^{i\sigma\bar{t}};\ \hat{P}_j^{,k} = P_j^{,k} e^{i\sigma\bar{t}} \tag{2-85}$$

To complete the process, the right-hand side of Equation (2-75) is differentiated with respect to ε_k and the results added to the right-hand side of Equation (2-80) with $\partial/\partial t$ replaced by $i\sigma$. The terms to be added to the right-hand side of Equation (2-80) in this manner are $-i\sigma\ [\bar{C}^j](\hat{P}_j^{,k})-i\sigma\{\bar{R}^{j,k}\}$ where $[\bar{C}^j]$ are diagonal matrices whose components are

$$\bar{C}_{ii}^{j} = H_{ij}A_{ij} \tag{2-86}$$

Because a cell can have clearance discontinuities, such as a step, it is advantageous to partition the cell into four components as indicated on Figure 7, and then sum the components to obtain $[\bar{C}^j]$. Thus, Equation (2-82) becomes:

$$\bar{C}^j_{ii} = HC_1A_1 + HC_2A_2 + HC_3A_3 + HC_4A_4 \tag{2-87}$$

where HC_1 is the clearance at the corner point 1 of the cell and

$$A_1 = \frac{(\Delta\theta_j)(\Delta Z_i)}{4}$$
$$A_2 = \frac{(\Delta\theta_j)(\Delta Z_{i-1})}{4} \; ; \; etc. \tag{2-88}$$

and $\{\bar{R}^{j,k}\}$ are column vectors whose components are

$$\bar{R}^{j,k}_i = A_{ij}\frac{\partial H_{ij}}{\partial \varepsilon_k}(1 + P_{ij}) \tag{2-89}$$

By combining terms, the final set of linear difference equations for the complex stiffness pressure derivatives ($\acute{P}^k_j$) are obtained

$$[C^{*j}]\{\acute{P}^k_j\} + [\hat{E}^j]\{\acute{P}^k_{j-1}\} + [\hat{D}^j]\{\acute{P}^k_{j+1}\} = \{R^{j,k}\} - [\hat{C}^{j,k}]\{\hat{P}_j\} - [\hat{E}^{j,k}]\{\hat{P}_{j-1}\} - [\hat{D}^{j,k}]\{\hat{P}_{j+1}\} \tag{2-90}$$

where,

$$[C^{*j}] = [\hat{C}^j] + i\sigma[\bar{C}^j] \; ; \; \{R^{j,k}\} = \{\hat{R}^{j,k}\} - i\sigma\{\bar{R}^{j,k}\} \tag{2-91}$$

The system of equations given by Equation (2-86) is solved by the column method in a directly analogous manner to that used in solving the steady-state equation. The principal difference is that all the matrix operations are performed using complex arithmetic. Integration of the real part of the pressure derivatives yields the stiffness; and the complex parts, when integrated and divided by σ, yield damping.

2.8 Critical Mass and Frequency

A critical mass routine was also added to the turbulent version of GCYLT.

For incompressible theory, a closed-form solution exists for the condition of neutral stability for a two-degree-of-freedom, point mass supported by cross-coupled springs and dampers[7]. The so-called critical mass and frequency are obtained, which provides a measure of the stability margin. If the mass attributable to a seal or bearing exceeds the critical mass, then an instability may occur at the orbital frequency calculated. A similar analysis, including the effects of compressibility, is complicated by the frequency dependence of the coefficients. A solution exists when the computed frequency of the point mass is equal to the excitation frequency used to compute the stiffness and damping coefficients. The critical mass and the orbital frequency are given by the following equations:

$$M_c = \frac{BED}{E^2 + AED + CD^2} \tag{2-92}$$

$$\omega_c = \sqrt{\frac{-(AED + E^2 + CD^2)}{ED^2}}$$

$$\text{where } A = K_{yy} + K_{xx},\ B = D_{yx}D_{xy} - D_{xx}D_{yy} \tag{2-93}$$

$$C = K_{xx}K_{yy} - K_{xy}K_{yx};\ D = D_{yy} + D_{xx}$$

$$E = D_{xy}K_{yx} + D_{yx}K_{xy} - D_{xx}K_{yy} - D_{yy}K_{xx}$$

A Newton-Raphson algorithm was utilized. For convergence, the frequency assumed in computing stiffness and damping, ω_a, should equal the frequency computed by the critical mass equations, ω_c. Initially there will be an error, δ.

$$\omega_a - \omega_c = \delta \tag{2-94}$$

To compute the incremental change in ω_a, the following equations apply:

$$\delta^{old} + \frac{\partial \delta}{\partial \omega_a} \Delta\omega_a = 0 \tag{2-95}$$

but from Equation (2-94)

$$\frac{\partial \delta}{\partial \omega_a} = 1 - \frac{\partial \omega_c}{\partial \omega_a} = 1 - \sum_{i=1}^{2}\sum_{j=1}^{2}\left(\frac{\partial \omega_c}{\partial K_{ij}}\frac{\partial K_{ij}}{\partial \omega_a} + \frac{\partial \omega_c}{\partial D_{ij}}\frac{\partial D_{ij}}{\partial \omega_a}\right) \tag{2-96}$$

The partial derivatives, $\frac{\partial \omega_c}{\partial \omega_{ij}}$ and $\frac{\partial \omega_c}{\partial \omega_{ij}}$, can be computed directly from Equation (2-99).

The derivatives $\frac{\partial K_{ij}}{\partial \omega_2}$ and $\frac{\partial D_{ij}}{\partial \omega_2}$ are explicitly determined by computing the gas seal stiffnesses at two incremental frequencies and computing $\frac{\Delta K_{ij}}{\Delta \omega_2}$ and $\frac{\Delta D_{ij}}{\Delta \omega_2}$, respectively;

and from Equation (2-95)

$$\Delta\omega_a = \frac{\dfrac{-\delta^{old}}{\partial\delta}}{\partial\omega_a} \tag{2-97}$$

The new value of ω_2 for the next iteration is obtained from:

$$\omega_a^{new} = \omega_a^{old} + \Delta\omega_a \tag{2-98}$$

At times, the computed frequency, ω_c, was insensitive to variations in the assumed frequency, ω_a. In such cases, successive substitution was found to converge very rapidly.

The critical mass as defined above applies to a two-degree-of-freedom system. It does not include cross-coupling moments. Thus, it would not have application to seals with pressure gradients where moment cross-coupling may be significant.

2.9 Force Balance

Newton-Raphson algorithms are used to produce journal displacements to balance given loads, if this option of the code is applied. The requirements are that:

$$F_{XR} - F_{XC} = 0 \tag{2-99}$$

$$F_{YR} - F_{YC} = 0 \tag{2-100}$$

where,

F_{XR} = required load in X direction

F_{YR} = required load in Y direction

F_{XC} = calculated load in X direction

F_{YC} = calculated load in Y direction

but,

$$F_{XC} = F_{Xold} + \Delta F_X = F_{Xold} + \frac{\partial F_X}{\partial X}\Delta X + \frac{\partial F_X}{\partial Y}\Delta Y \tag{2-101}$$

$$F_{YC} = F_{Yold} + \Delta F_{Y} = F_{Yold} + \frac{\partial F_{Y}}{\partial X}\Delta X + \frac{\partial F_{X}}{\partial Y}\Delta Y \qquad \textbf{(2-102)}$$

The partial derivatives are stiffnesses which are obtained by incrementing X and Y displacements. Equations (2-101) and (2-102) are substituted into Equations (2-99) and (2-100). The system of equations are solved for ΔX and ΔY which provides the new displacements for the next iteration. The process continues until the calculated load equals the required load within the convergence criteria.

3.0 SAMPLE PROBLEMS FOR CODE GCYLT

3.1 Sample Problem 1 - Rayleigh-Step Seal

A four-pad Rayleigh-step seal, without pressure differential, was analyzed (refer to Figure 17). The geometry, operating conditions, and input features were as follows:

- Number of pads = 4
- The seal position was prespecified
- Seal length = 3.852 in.; the symmetry option was used
- Variable grid was used in the axial and circumferential directions. Since symmetry has been applied in the axial direction, the variable grid length equals half the actual length, and is equal to 1.926 in.
- The grid was made finer at the step boundaries where sharp pressure gradients are expected to occur
- Seal diameter = 1.9685 in.
- Step height = 0.00165 in. deep, located at the leading edge of the pad, 5° from the x axis; the lower left corner of the step is 0.655 in. from the left axial boundary. The end of the step is 70.6° from the x axis, and since symmetry has been invoked, the axial end of the step as represented on the grid is 1.926 in. from the inlet end, or at the end of the grid.
- Specific heat ratio of the lubricant = 1.4
- Gas constant = 250,000 $in^2/(s^2\text{-}°R)$
- Absolute temperature = 530°R
- Absolute viscosity = 3.0×10^{-9} $lb\text{-}s/in^2$
- Eccentricity ratio = 0.4
- Eccentricity angle = 270°
- Shaft speed = 70,000 rpm
- Reference pressure = 200 psig
- Boundary pressures are all 0 psig, or 200 psia.

Summary results are shown on Table 1. Figures 18 and 19 show the clearance distribution and the pressure distribution produced by the plotting programs. These plots clearly show the highly loaded pad, which is pad number 3 (highest pressure level and lowest film thickness level).

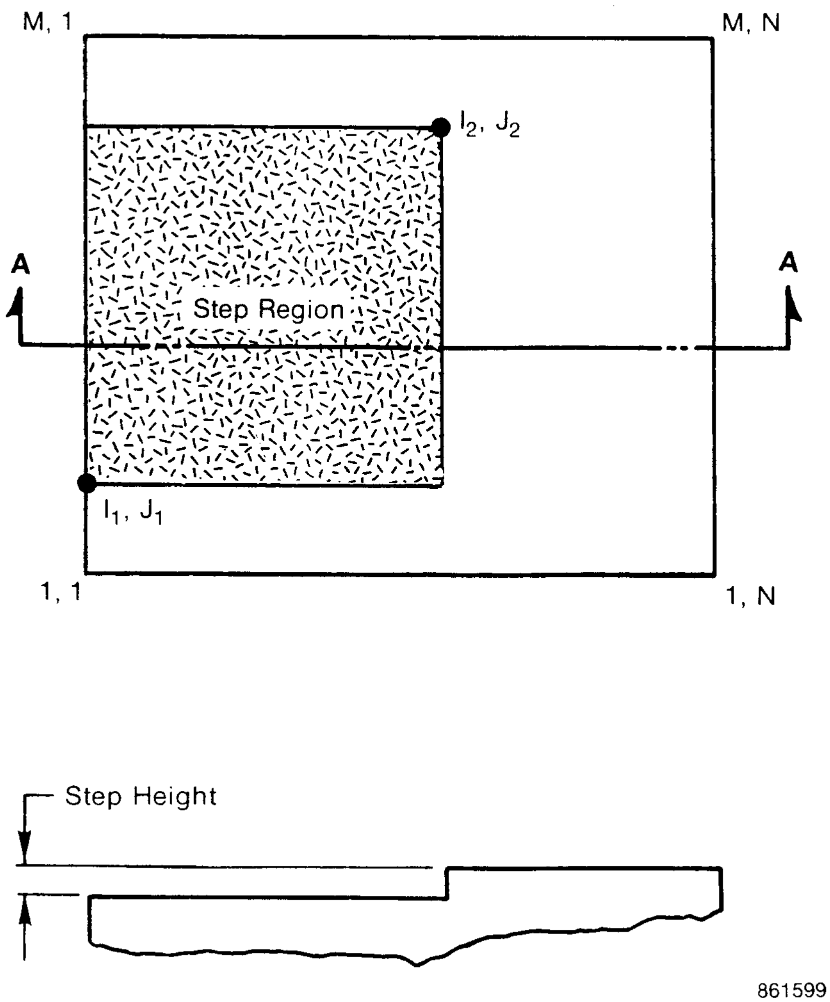

Figure 17. Rayleigh-Step Geometry

Table 1. Sample Case 1: Raleigh Step Seal

Journal & Load Position		
Eccentricity	=	0.4000
Eccentricity Angle	=	-90.00°
Minimum Film	=	0.0006015 in.
Load	=	131.5 lb
Load Angle	=	58.49°
Power Loss	=	2.308 hp
Leakage at I = 1	=	0.10191 E-02 lb/s

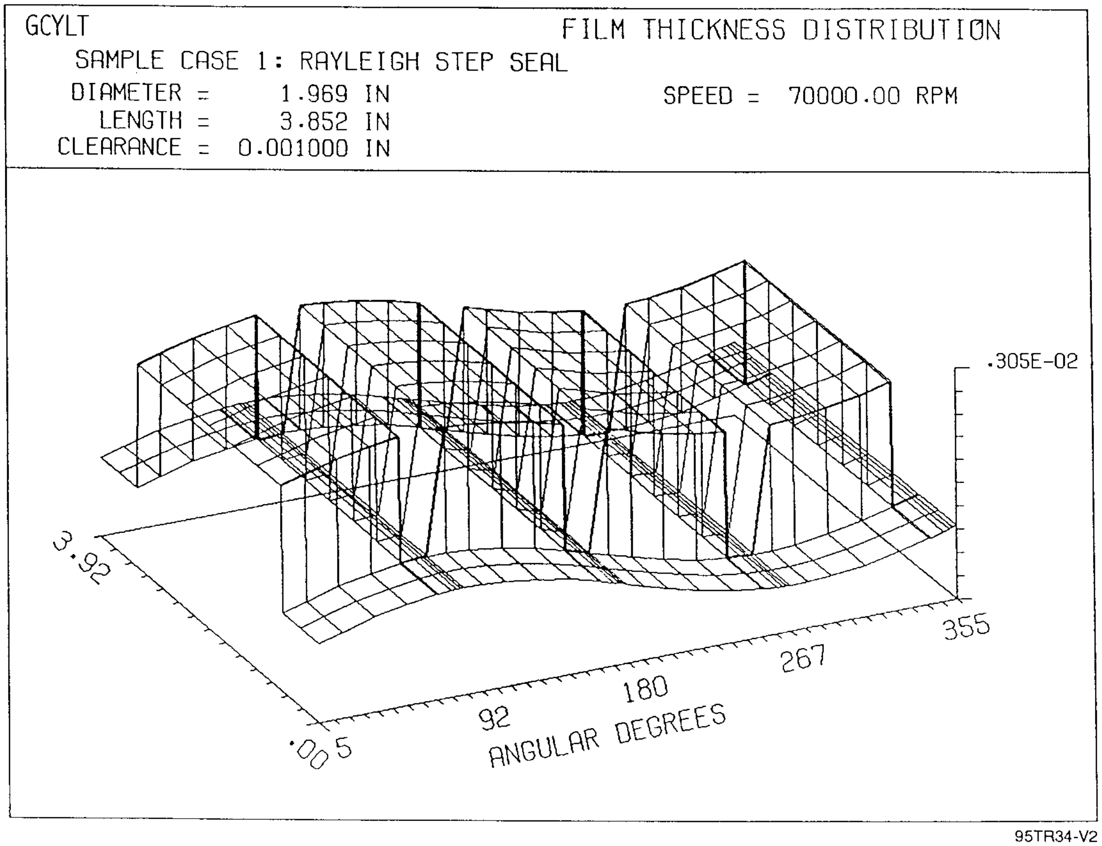

Figure 18. Rayleigh-Step Seal Clearance Distribution

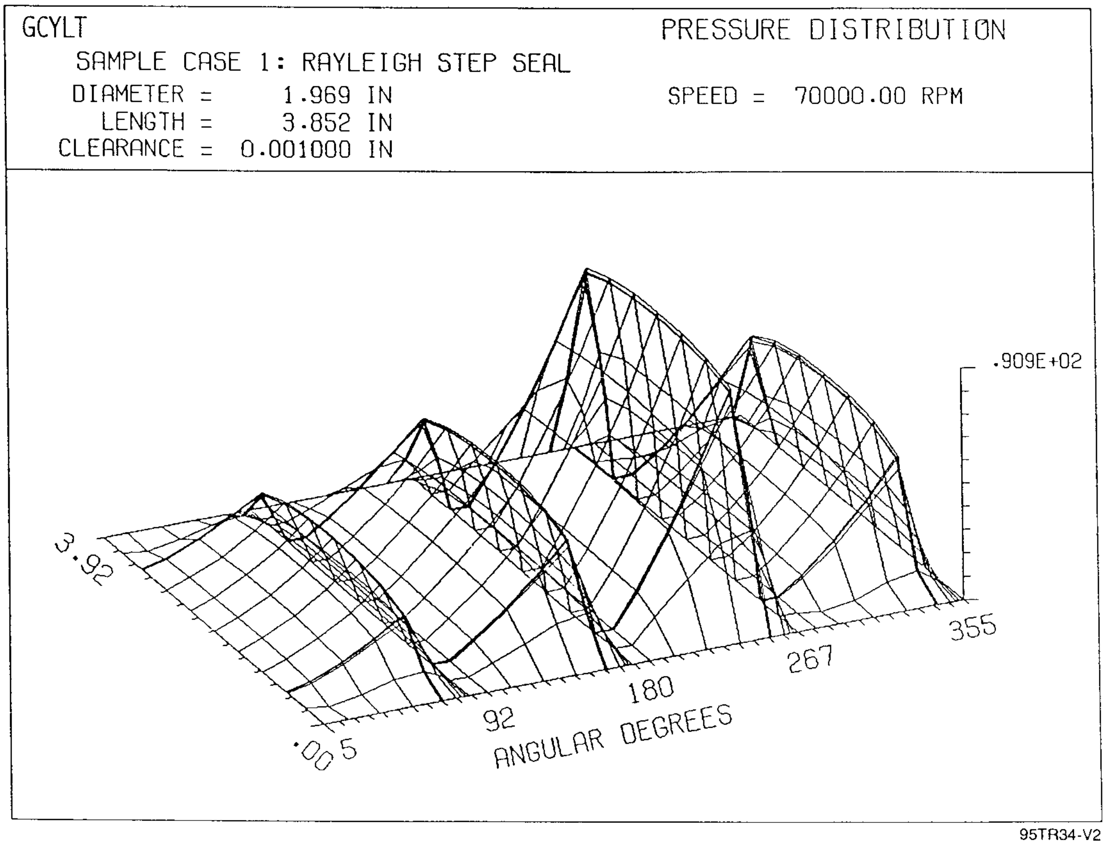

Figure 19. Rayleigh-Step Seal Pressure Distribution

3.2 Sample Problem 2 - Nongrooved Lobe Seal

The nongrooved lobe seal is characterized by offset lobes that are joined at their appexes in a continuous fashion as opposed to a lobe seal where the lobes are separated by axial grooves. Such a seal is depicted on Figure 20; it would be manufactured by a broaching process. For this example, a lobe hydrodynamic geometry was combined with external pressurization through source points at the mid-plane of the seal. The geometry and operating conditions are as follows:

- Seal Diameter = 2.25 in.
- Seal Length = 1.625 in.
- Seal reference clearance (the clearance prior to preload) = 0.0005 in.
- Preload on each lobe is 0.5, which means the lobe is eccentric toward the shaft by a distance of one-half of the reference clearance
- Viscosity of the gas = 3 x 10^{-9} lb-s/in.^{2}
- Gas constant = 2.5 x 10^5 in^2/(s^2-°R)
- Ambient temperature = 510°R
- Total number of orifices = 27, 9 in each sector, located at the mid-plane of each sector; 1 orifice is located at each interior grid point at the mid-plane of the bearing
- Orifice diameter = 0.015 in.
- Coefficient of discharge of each orifice = 0.9
- Supply pressure to the source orifices = 120 psig
- Operating speed = 70,000 rpm
- Reference pressure = 14.7 psig
- Pressure along the boundaries = 0 psig.

An output summary is shown on Table 2. and the clearance and pressure plots are shown on Figures 21 and 22. Notice the discontinuities in the clearance distribution because of the lobed geometry. The proximity of the source points to each other makes the pressure distribution appear as a line source.

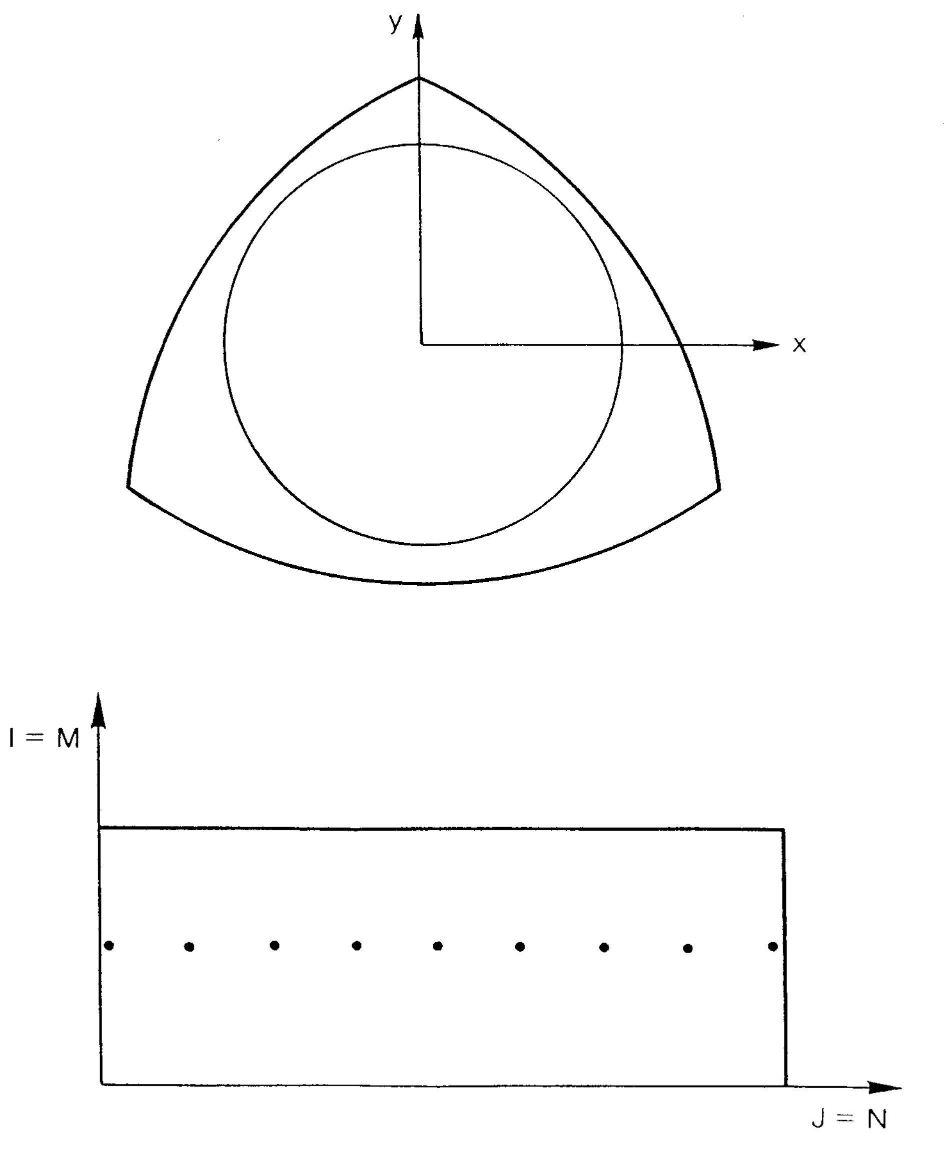

Figure 20. Sectored Lobe Seal

__Table 2. Sample Case 2: Sectored Seal__

Journal & Load Position

Eccentricity	=	0.00000
Eccentricity Angle	=	0.00°
Minimum Film	=	0.0002500 in.
Load	=	0 lb
Load Angle	=	-54.45°
Power Loss	=	1.251 hp
Leakage at I = 1	=	0.14815 E-03 lb/s
Leakage at I = 1	=	0.14815 E-03 lb/s

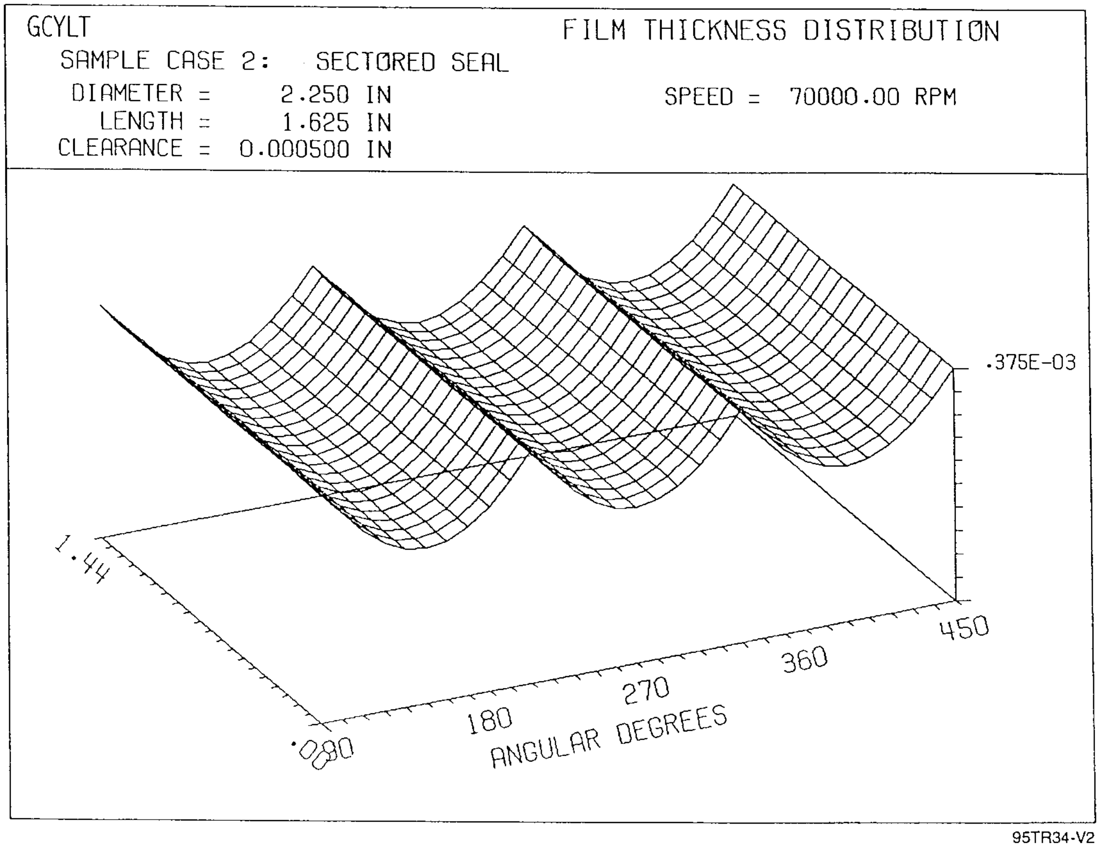

Figure 21. Clearance Distribution, Sectored Lobe Seal

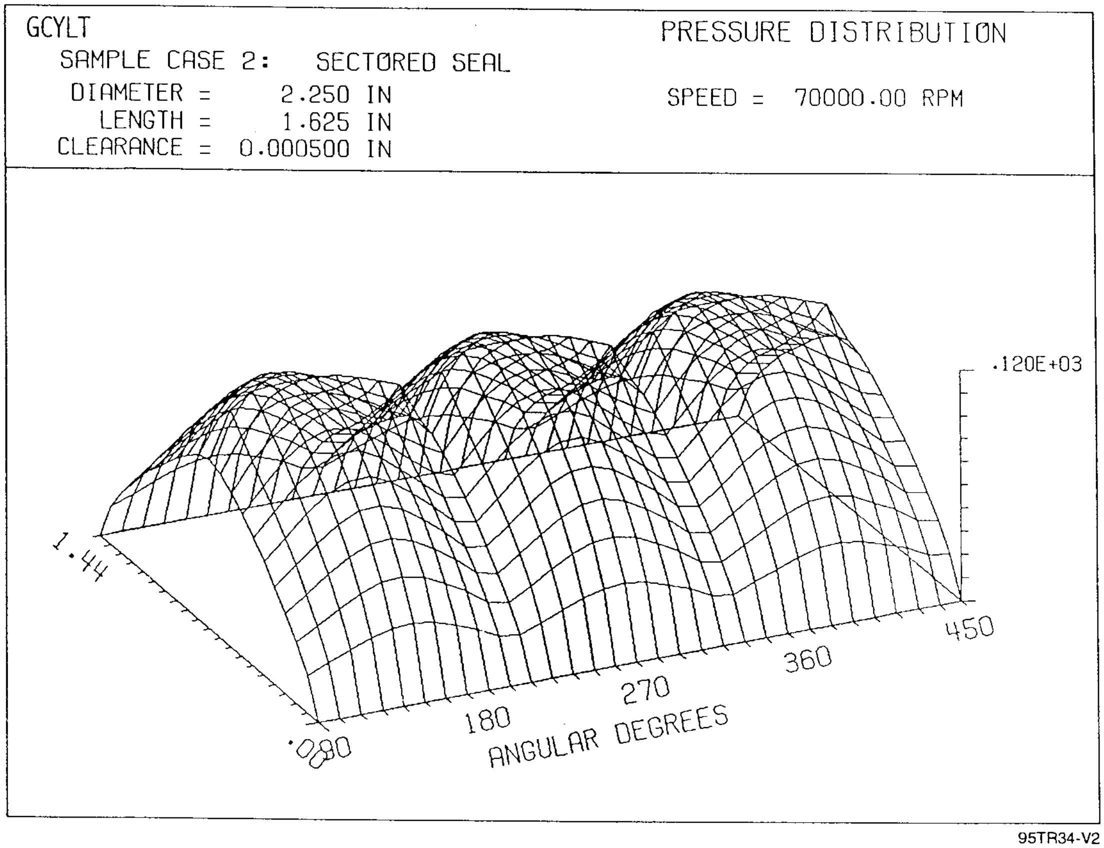

Figure 22. Pressure Distribution, Sectored Lobe Seal

3.3 Sample Problem 3 - Three-Lobe Seal

This problem deals with the hydrodynamic portion of a three-lobe seal where the lobes are separated by axial grooves. Figure 23 shows the general geometry and key parameters. The principal parameters are the preload and pivot angle. The following are geometry and operating conditions:

- The position of the seal to satisfy a given load was to be determined
- International units were invoked
- Stiffness and damping was to be calculated in two degrees of freedom, x and y, at an imposed frequency equal to running speed of 50,000 rpm
- Number of pads = 3
- Start of the first pad is at 100°; the pad extent is 100°
- Pad preload is 50% of the reference clearance, and the preload for the first pad occurs 150° from the x-axis, which means the preload is in the center of the pad
- Shaft diameter = 0.0508 m
- Hydrodynamic length = 0.0254 m
- Reference clearance or machined pad clearance = 1.27×10^{-5} m
- Lubricant viscosity = 2.07×10^{-5} N-s/m^2
- Absolute temperature = 283°K
- Ratio of specific heat of the gas = 1.4
- Gas constant = 290.32 m^3/(s^2-°R)
- Symmetry is applied in the axial direction
- Load to be supported = 200.16 N
- Angle at which the load is applied was 270° from the x-axis
- Initial eccentricity guess is 0.2; initial displacement angle guess is 270° from the x-axis
- Shaft speed = 50,000 rpm
- Reference pressure = 8.274×10^5 Pa.
- Boundary pressures are all 0 gage.

Summary results including stiffness and damping coefficients are shown on Table 3. Graphical representation of the clearance distribution and pressure distribution are shown on Figures 24 and 25, respectively. Figure 26 shows the pressure distribution viewing along an axial direction. The negative pressures are induced by divergent clearance regions. The final eccentricity ratio to balance the applied load was 0.22, and the eccentricity angle was 129.42°.

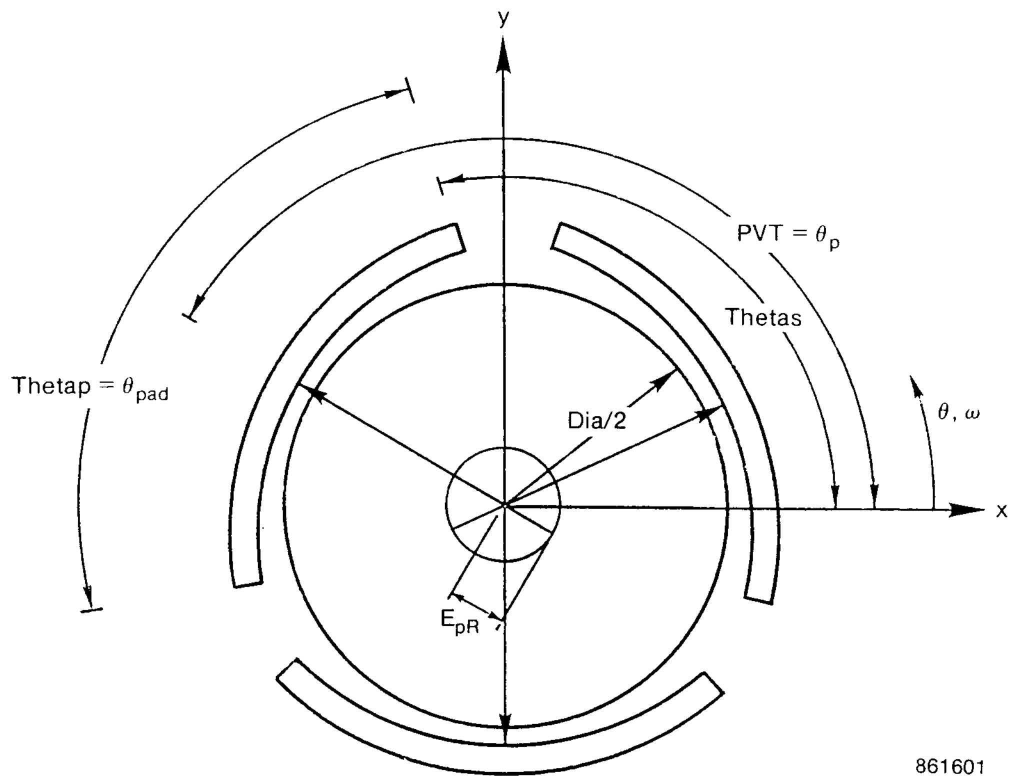

Keyword	Variable	Description
START	THETAS	Pad Start Angle
PADANGLE	THETAP	Pad Angle
PIVOT	PVT	Pivot Angle
PRELOAD	EPR	Offset/Clearance

Figure 23. Three-Lobe Seal

Table 3. Sample Case 3: Three-Lobe Gas Seal

```
-JOURNAL & LOAD POSITION
  ECCENTRICITY          =      0.22087
  ECCENTRICITY ANGLE    =       129.42 DEG
  MINIMUM FILM          =    0.0000037 M
  LOAD                  =    200.2     N
  LOAD ANGLE            =       -90.00 DEG

  POWER LOSS            =    186.2     W

  LEAKAGE AT I = 1      =-0.12904E-04 KG/S

-STIFFNESS COEFFICIENTS
  PRINCIPAL  X      KXX =  0.1459E+09 N/M
  CROSS-COUPLED     KXY = -0.2373E+08 N/M
  CROSS-COUPLED     KXA =  0.0000E+00 N/RAD
  CROSS-COUPLED     KXB =  0.0000E+00 N/RAD
  CROSS-COUPLED     KYX = -0.3890E+08 N/M
  PRINCIPAL  Y      KYY =  0.1003E+09 N/M
  CROSS-COUPLED     KYA =  0.0000E+00 N/RAD
  CROSS-COUPLED     KYB =  0.0000E+00 N/RAD
  CROSS-COUPLED     KAX =  0.0000E+00 N-M/M
  CROSS-COUPLED     KAY =  0.0000E+00 N-M/M
  PRINCIPAL  A      KAA =  0.0000E+00 N-M/RAD
  CROSS-COUPLED     KAB =  0.0000E+00 N-M/RAD
  CROSS-COUPLED     KBX =  0.0000E+00 N-M/M
  CROSS-COUPLED     KBY =  0.0000E+00 N-M/M
  CROSS-COUPLED     KBA =  0.0000E+00 N-M/RAD
  PRINCIPAL  B      KBB =  0.0000E+00 N-M/RAD

-DAMPING COEFFICIENTS
  PRINCIPAL  X      DXX =   9977.     N-S/M
  CROSS-COUPLED     DXY = -0.1090E+05 N-S/M
  CROSS-COUPLED     DXA =  0.0000E+00 N-S/M
  CROSS-COUPLED     DXB =  0.0000E+00 N-S/RAD
  CROSS-COUPLED     DYX =   5162.     N-S/M
  PRINCIPAL  Y      DYY =  0.1392E+05 N-S/M
  CROSS-COUPLED     DYA =  0.0000E+00 N-S/RAD
  CROSS-COUPLED     DYB =  0.0000E+00 N-S/RAD
  CROSS-COUPLED     DAX =  0.0000E+00 N-M-S/M
  CROSS-COUPLED     DAY =  0.0000E+00 N-M-S/M
  PRINCIPAL  A      DAA =  0.0000E+00 N-M-S/RAD
  CROSS-COUPLED     DAB =  0.0000E+00 N-M-S/RAD
  CROSS-COUPLED     DBX =  0.0000E+00 N-M-S/M
  CROSS-COUPLED     DBY =  0.0000E+00 N-M-S/M
  CROSS-COUPLED     DBA =  0.0000E+00 N-M-S/RAD
  PRINCIPAL  B      DBB =  0.0000E+00 N-M-S/RAD
```

95TR34-V2

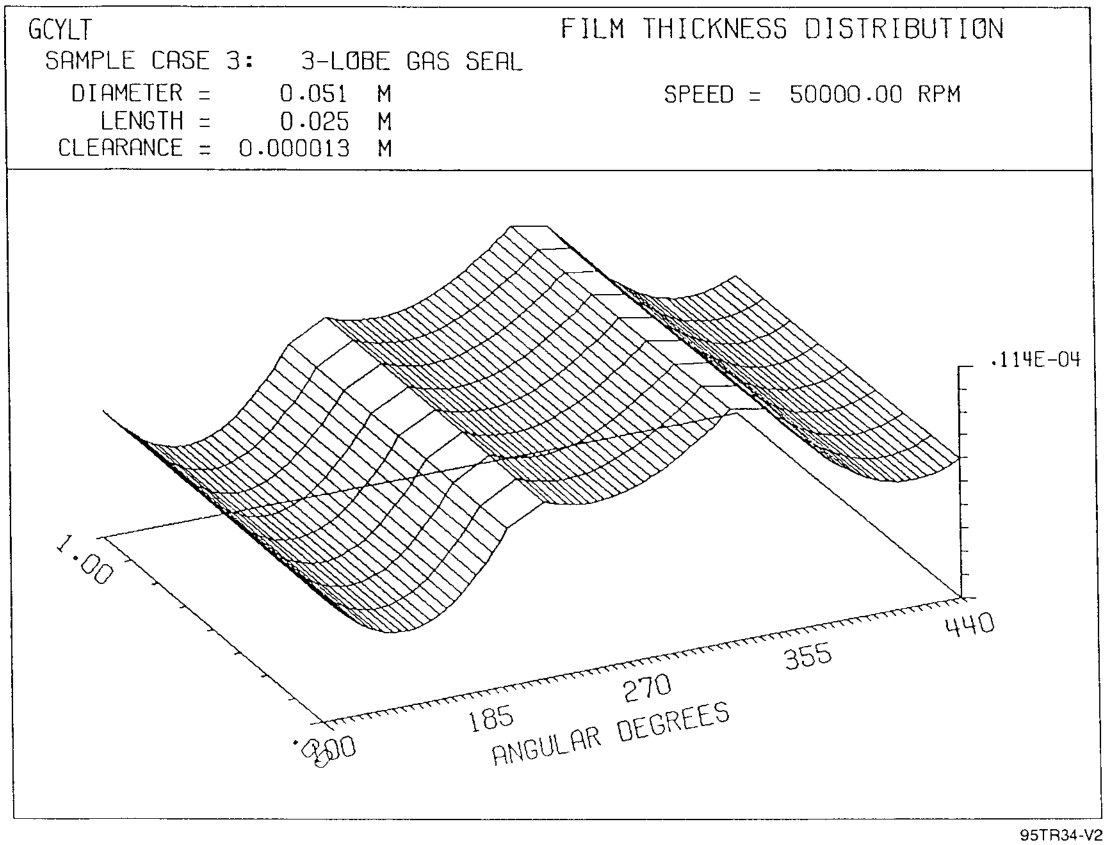

Figure 24. Clearance Distribution, Three-Lobe Seal

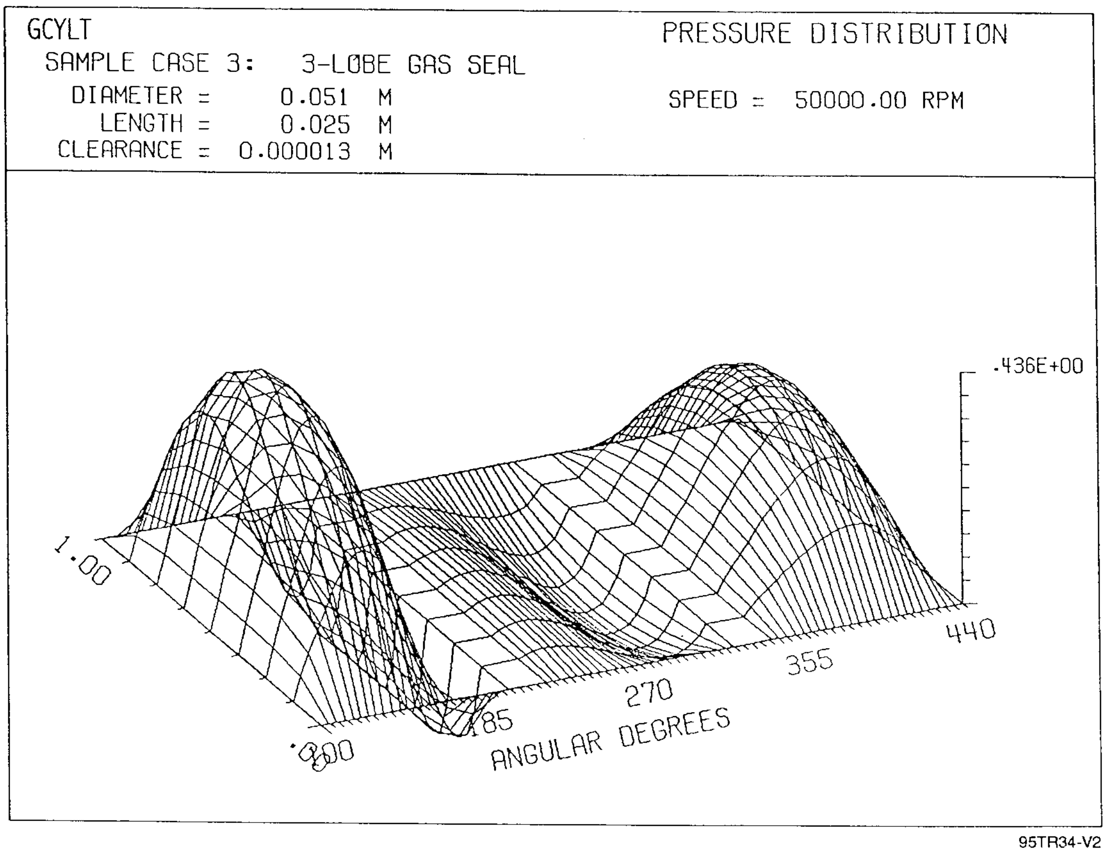

Figure 25. Pressure Distribution, Three-Lobe Seal

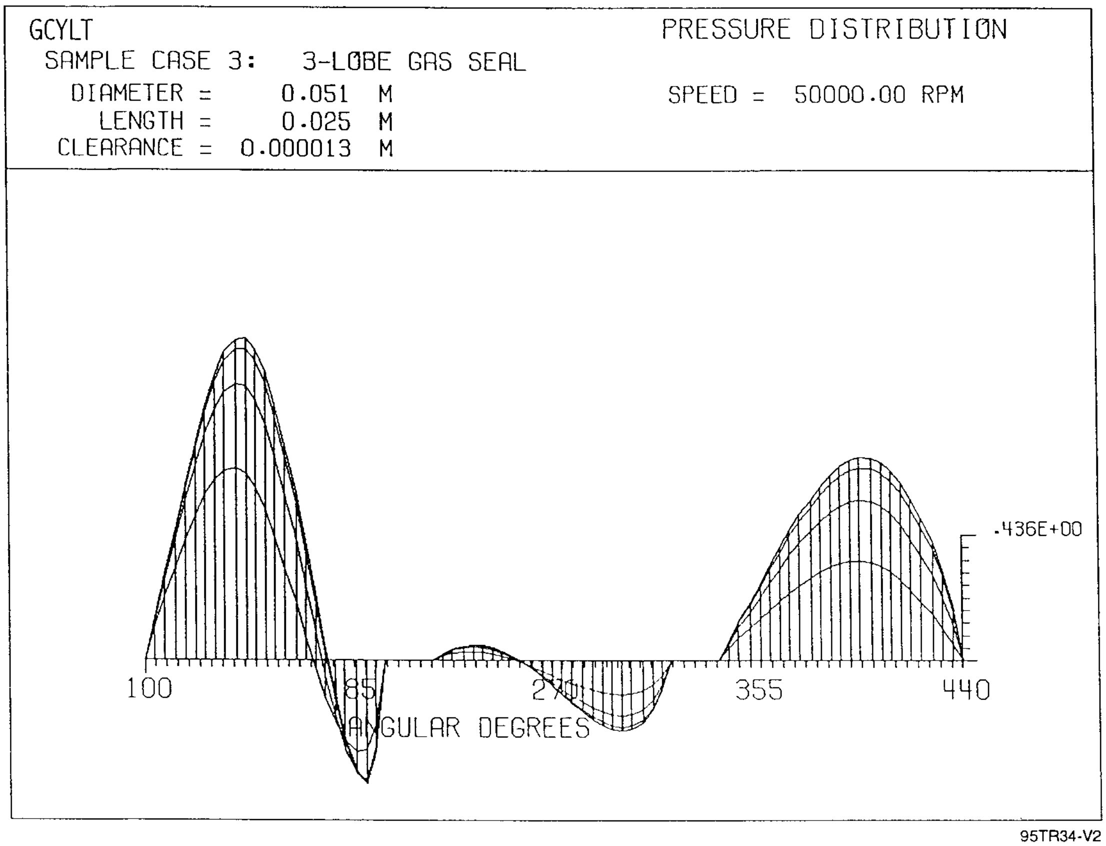

Figure 26. Pressure Distribution, Viewing in Axial Direction

3.4 Sample Problem 4 - T-Shaped Sectored Seal

This problem deals with an actual helium buffered seal analysis and design (for SSME) that was accomplished for NASA. A design that incorporates a self-adjusting clearance that can accommodate thermal and centrifugal distortions and shaft dynamic excursions avoids many of the problems associated with captured clearance configurations. The sectored ring seal provides the desired self-adjusting clearance features. The general configuration of the sectored seal is shown on Figure 27. The sectors consist of T-shaped sections mated to each other at each end with sealed joints. The sectors can move relative to each other circumferentially and that is how the seal accommodates variations in the sleeve dimensions due to thermal expansions and contractions and centrifugal growths. The T-shaped sector was chosen because it is a symmetrical shape, and the various fluid and friction forces can be designed to avoid upsetting moments on the individual sectors. An overlapping V joint prevents a direct clearance path between the hydrogen and oxygen ends of the seal. Each sector is supported by a hydrostatic fluid-film on its inner circumference and along the side walls which forms a friction-free secondary seal to permit free radial motion of the sectors in response to sleeve movements. The fluid films are predominantly hydrostatic to avoid any pitching tendencies introduced by the hydrodynamic effects. The hydrostatic bearings are fed by the buffer pressure on the outside diameter of the seal. Figure 28 shows the pressure distribution and force balance on the individual sectors.

This sample problem describes one case conducted in the analysis of the circumferential hydrostatic seal on one of the sectors. The geometry and operating conditions are as follows:

- Number of pads to be analyzed = 1
- The position of the sector to satisfy a given load was to be determined
- Load applied = 370 lb
- Load angle from the x-axis = 270°
- Initial guess on the eccentricity of the seal = 0.5
- Initial guess on the eccentricity angle = 90°
- Variable grids were used in both the axial and circumferential directions. The grid is made very fine around the source points. The starting angle of the sector is 30° from the x-axis and its angular extent is 120°. The axial length of the seal is 1.627 in.
- Shaft diameter = 2.6798 in.
- Reference clearance = 0.001 in.
- Ratio of specific heat of the gas = 1.66
- Gas constant = 1,790,000 $in^2/(s^2\text{-}°R)$
- Absolute temperature = 528°R
- Gas viscosity = 2.9×10^{-9} $lb\text{-}s/in^2$
- Shaft speed = 0 rpm
- Reference pressure = 14.7 psig
- Boundary pressure surrounding the seal = 50 psig
- Cross-coupled stiffness and damping were to be computed at an excitation frequency of 0 rpm

- There are 6 discrete, inherently compensated source points in the sector of diameter = 0.020 in. The location of these orifices was determined from the design layout of the sector. The coefficient of discharge of each orifice is unity.
- Buffer pressure = 200 psig
- Flow is to be determined along four paths that make up the periphery of the seal.

As indicated on the summary output (Table 4), the eccentricity of the sector to support the load is 0.6345 and the eccentricity angle is 90°. Plots of the clearance and pressure distribution are shown on Figures 29 and 30, respectively. Note on the plots the fine grid work surrounding the orifice locations.

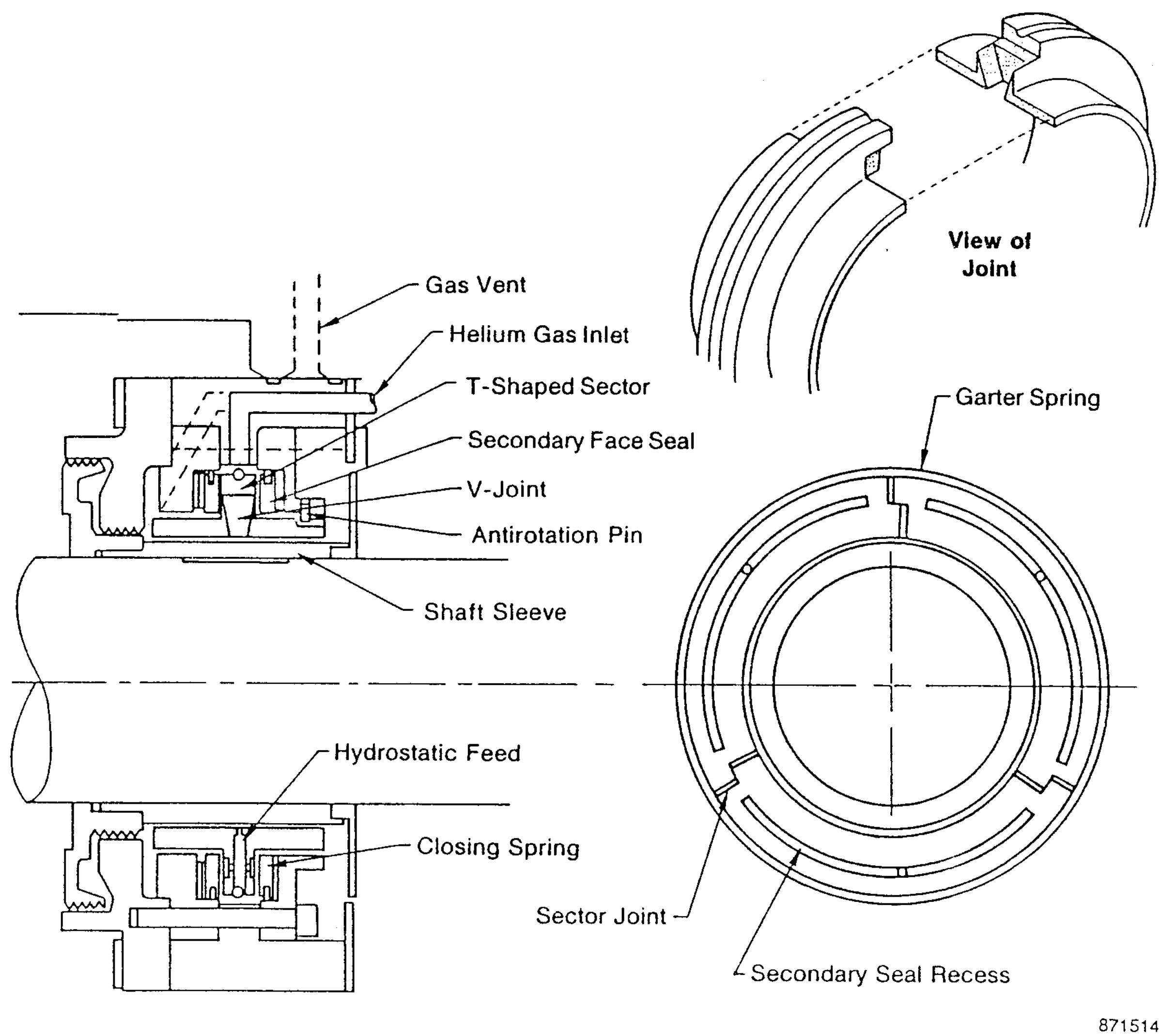

Figure 27. T-Shaped Sectored Ring Seal

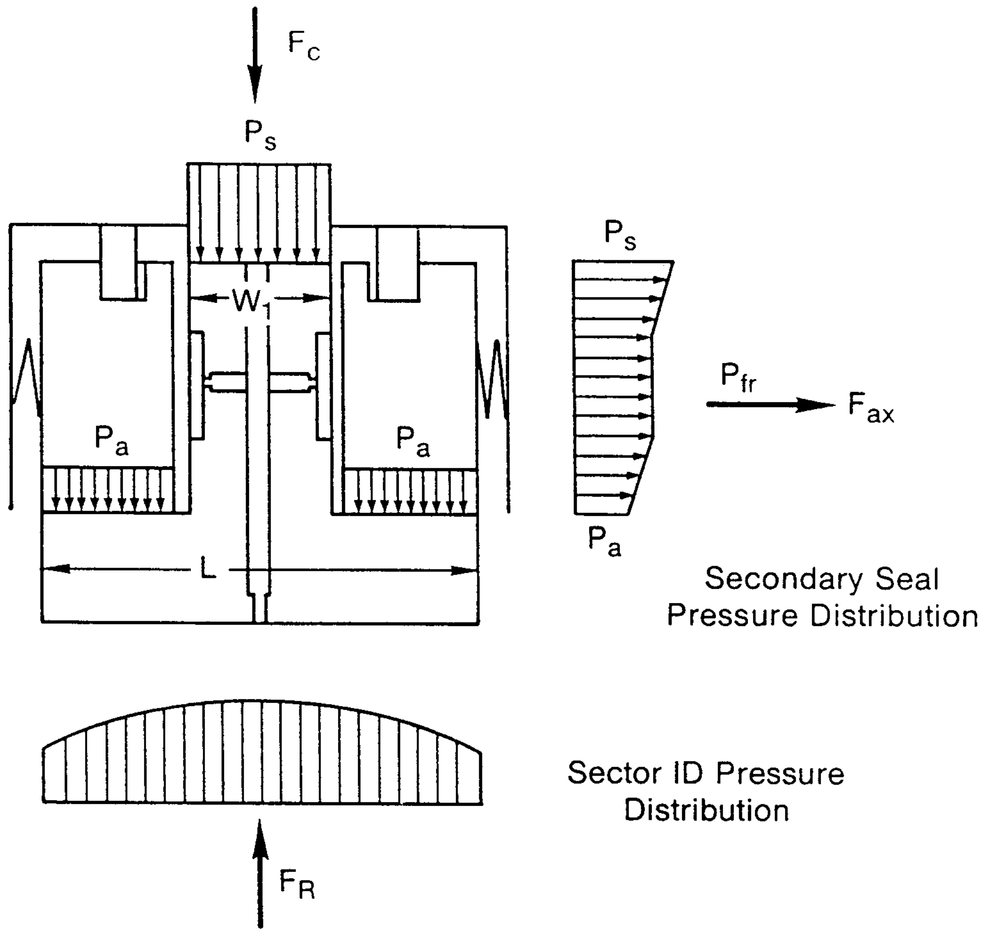

$$F_c = P_s A_s + P_a A_a$$

Radial Force Balance

$$F_R - F_c \pm F_f \pm F_r = 0$$

Axial Force Balance

$$F_{ax} - F_p - k_s \delta_a = 0$$

871511-1

Figure 28. Pressure Distribution and Force Balance, Sectored Seal

Table 4. Sectored Buffer Seal Sample Problem

```
-JOURNAL & LOAD POSITION
  ECCENTRICITY            =      0.63453
  ECCENTRICITY ANGLE      =        90.00 DEG
  MINIMUM FILM            =    0.0003663 IN
  LOAD                    =    370.0     LB
  LOAD ANGLE              =       -90.00 DEG

  POWER LOSS              =  0.0000E+00 HP

  LEAKAGE AT I = 1        =-0.25673E-04 LB/S

  LEAKAGE AT I = M        = 0.25673E-04 LB/S

-STIFFNESS COEFFICIENTS
  PRINCIPAL  X       KXX =  0.4032E+05 LB/IN
  CROSS-COUPLED      KXY = -0.2428E-07 LB/IN
  CROSS-COUPLED      KXA = -0.2531E-07 LB/RAD
  CROSS-COUPLED      KXB =  0.2009E-02 LB/RAD
  CROSS-COUPLED      KYX =  -141.6     LB/IN
  PRINCIPAL  Y       KYY =  0.2429E+05 LB/IN
  CROSS-COUPLED      KYA =  -391.7     LB/RAD
  CROSS-COUPLED      KYB =  -74.14     LB/RAD
  CROSS-COUPLED      KAX =  0.8476E-06 IN-LB/IN
  CROSS-COUPLED      KAY = -0.4463E-02 IN-LB/IN
  PRINCIPAL  A       KAA =  0.5055E+05 IN-LB/RAD
  CROSS-COUPLED      KAB = -0.5231E-06 IN-LB/RAD
  CROSS-COUPLED      KBX =  0.1525E-02 IN-LB/IN
  CROSS-COUPLED      KBY =  0.1127E-07 IN-LB/IN
  CROSS-COUPLED      KBA = -0.4153E-08 IN-LB/RAD
  PRINCIPAL  B       KBB =  0.1099E+05 IN-LB/RAD

-DAMPING COEFFICIENTS
  PRINCIPAL  X       DXX =   15.89     LB-S/IN
  CROSS-COUPLED      DXY =  0.3707E-10 LB-S/IN
  CROSS-COUPLED      DXA =  0.3617E-11 LB-S/RAD
  CROSS-COUPLED      DXB =  0.5322E-06 LB-S/RAD
  CROSS-COUPLED      DYX =  0.2025E-01 LB-S/IN
  PRINCIPAL  Y       DYY =   128.5     LB-S/IN
  CROSS-COUPLED      DYA =  0.6261E-01 LB-S/RAD
  CROSS-COUPLED      DYB =  0.1058E-01 LB-S/RAD
  CROSS-COUPLED      DAX =  0.9535E-10 IN-LB-S/IN
  CROSS-COUPLED      DAY =  0.1738E-05 IN-LB-S/IN
  PRINCIPAL  A       DAA =   7.329     IN-LB-S/RAD
  CROSS-COUPLED      DAB = -0.5647E-09 IN-LB-S/RAD
  CROSS-COUPLED      DBX = -0.4686E-06 IN-LB-S/IN
  CROSS-COUPLED      DBY = -0.5672E-12 IN-LB-S/IN
  CROSS-COUPLED      DBA = -0.2274E-11 IN-LB-S/RAD
  PRINCIPAL  B       DBB =   1.288     IN-LB-S/RAD

-RIGHTING MOMENT
  ABOUT X-X           MX =  0.2995E-05 LB-IN
  ABOUT Y-Y           MY =  0.2342E-14 LB-IN


-FLOW THRU SPECIFIED GRID LINE
 FROM   1   1  TO  27   1    FLOW= -0.4651E-04 LB/S


-FLOW THRU SPECIFIED GRID LINE
 FROM   1  34  TO  27  34    FLOW=  0.4651E-04 LB/S


-FLOW THRU SPECIFIED GRID LINE
 FROM   1   1  TO   1  34    FLOW= -0.2567E-04 LB/S


-FLOW THRU SPECIFIED GRID LINE
 FROM  27   1  TO  27  34    FLOW=  0.2567E-04 LB/S
```

95TR34-V2

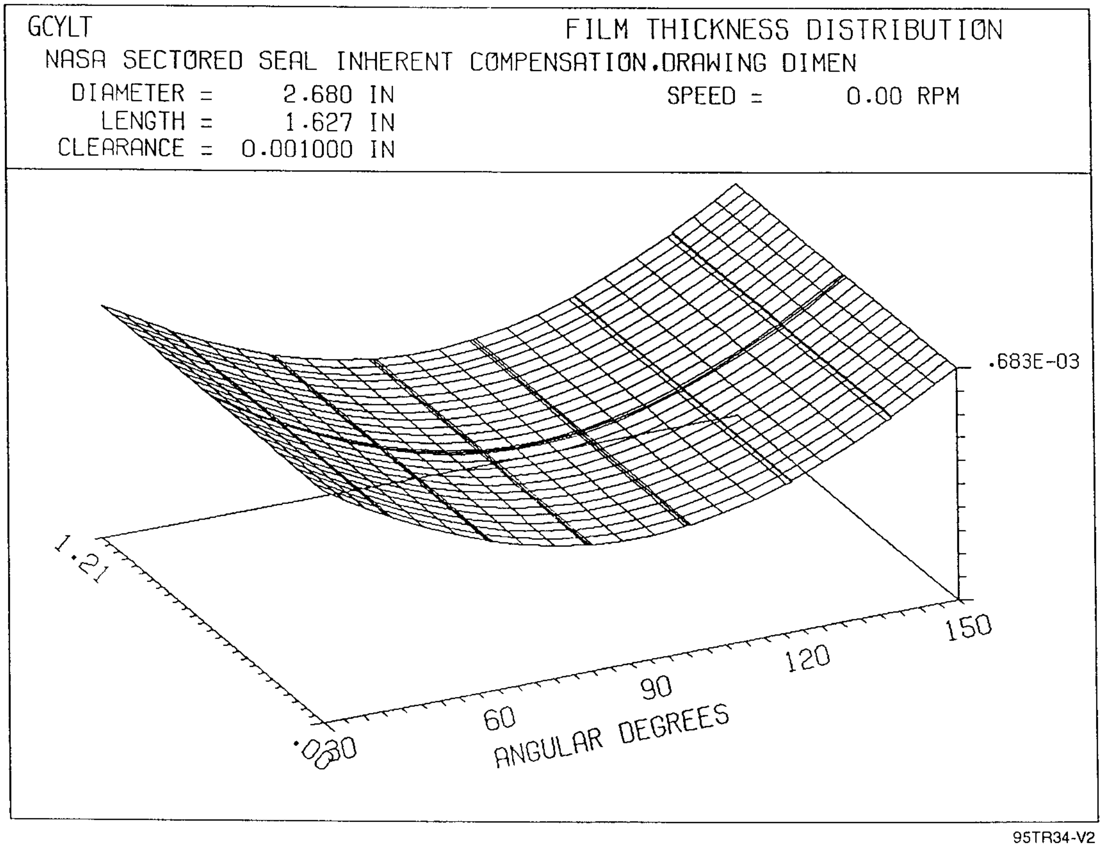

Figure 29. Clearance Distribution, Sectored Seal

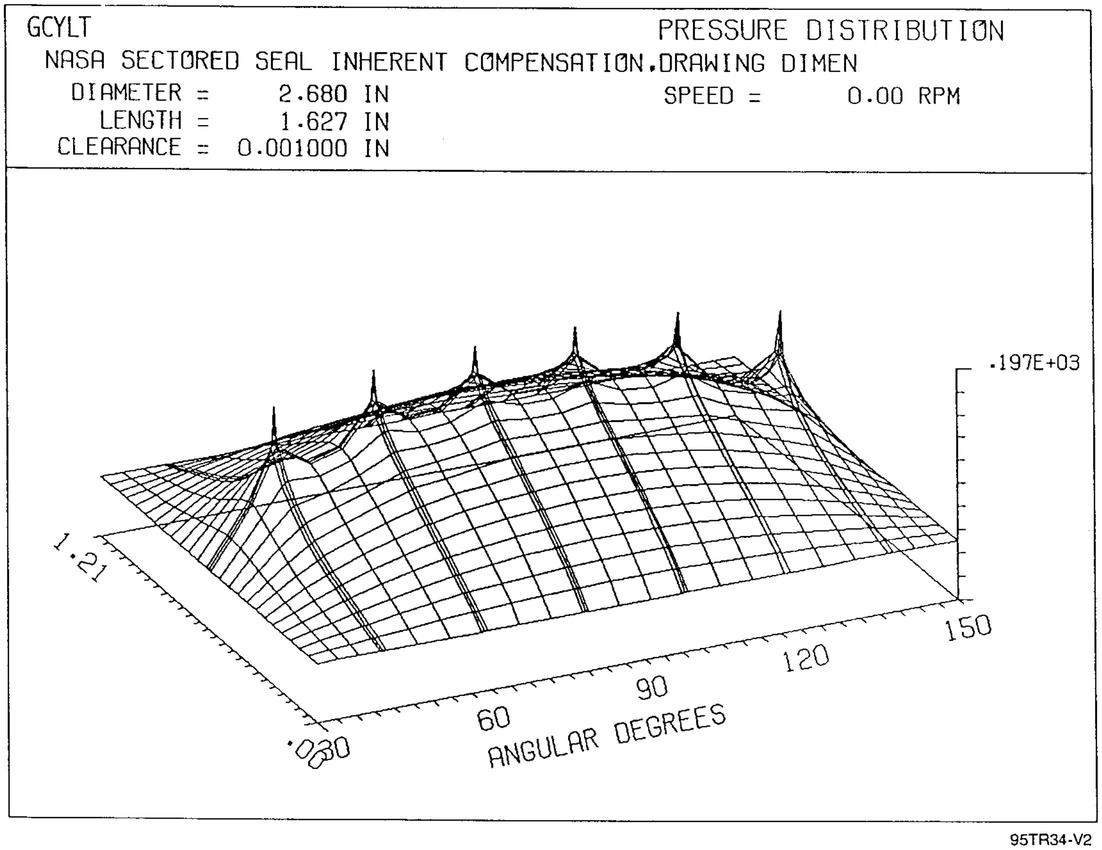

Figure 30. Pressure Distribution, Sectored Seal

3.5 Sample Problem 5 - Rayleigh-Step, Floating-Ring Seal

This example represents another buffer fluid seal that was designed for use in the SSME. The principle of operation of a hydrodynamic, lift-pad, floating-ring seal is illustrated on Figure 31. The seal consists of two rings that are mounted back-to-back. The buffer fluid enters between the rings and forces the rings up against the stationary housing. The buffer fluid leaks into the clearance annulus between the shaft and the seal and prevents ingress of exterior fluid on either side of the floating-ring assembly. The rings are held in equilibrium by a number of forces, as shown on Figure 31. F_c is a pressure force from the inlet buffer fluid that forces the rings up against the housings. This pressure force is partially balanced on the housing sides of the rings by undercutting and exposing the housing sides of the rings to buffer pressure. The balance force is identified as F_B. F_H represents a hydrodynamic force that is generated by rotation between the shaft and ring. The net hydrodynamic force is zero when the shaft and rings are in the concentric position. However, when the ring becomes eccentric with respect to the shaft, a hydrodynamic force is built up that opposes the eccentricity. There is also a normal force, F_N, acting on the ring at the contact area between the ring and the housing. In addition to the equilibrium forces mentioned above, there is a friction force, F_f, between the seal ring and housing. Seal tracking requires that the hydrodynamic force is strong enough to overcome the friction force.

Figure 32 shows the hydrodynamic geometry that is incorporated into the bore of the seal rings. A portion of the length of the bore is segregated into sectors, and these sectors are separated from one another by axial grooves. A circumferential groove that goes completely around the bore is installed upstream of the final seal dam region. At the interior of the sectors, Rayleigh-step pockets are machined. The velocity direction of the shaft is such that it produces hydrodynamic pressures due to pumping of the fluid over the Rayleigh-step. The sealing occurs across the dam which is a narrow annulus of low clearance exposed to high pressure at its interior circumferential groove and to lower pressure at its outboard end. The shaded regions on Figure 32 indicate depressions from grooves and Rayleigh-step pockets.

In this example, one pad of the Rayleigh-step interface was examined from the high-pressure interior end to the low-pressure exterior end. Geometric and operating parameters are as follows:

- International units are to be used
- Because the performance of one pad was examined, the grid represented a 90° arc from the center of one axial groove to the next. The boundary conditions at the circumferential ends of the single pad must be periodic, i.e., all pads will act identically, which will occur when the shaft is in the concentric position. The periodicity option of the code was invoked.
- Shaft diameter = 0.05 m
- Total seal length = 0.0123 m
- Seal clearance = 1.27×10^{-5} m
- Step height = 2.54×10^{-5} m
- Gas viscosity = 2.19×10^{-5} N-s/m^2
- Absolute temperature = 338.6°K
- Ratio of specific heat = 1.66

- Gas constant = 1154.8364 m^2 $m^2/(s^2\text{-}°K)$
- Shaft speed = 70,000 rpm
- Reference pressure = 101,352.93 Pa
- The high pressure to be sealed is 1.37895 x 10^6 Pa, which would be at the bottom of the grid. The remaining boundaries are at 0 psig.

In this example, advantage was taken of inputting constant pressure regions for the inlet grooves of sequential pads and the circumferential exterior grooves.

Summary output for the single pad is shown on Table 5. Each individual pad load is 571.6 N. The leakage at the low-pressure end (I = M) exceeds that at the high-pressure end I = l, because of the groove leakage.

Following the output are the 3-D plots of the clearance and pressure distribution (Figures 33 and 34, respectively). Note on Figure 33 that the high ambient pressures in the groove regions overshadow the contribution from the Rayleigh-step.

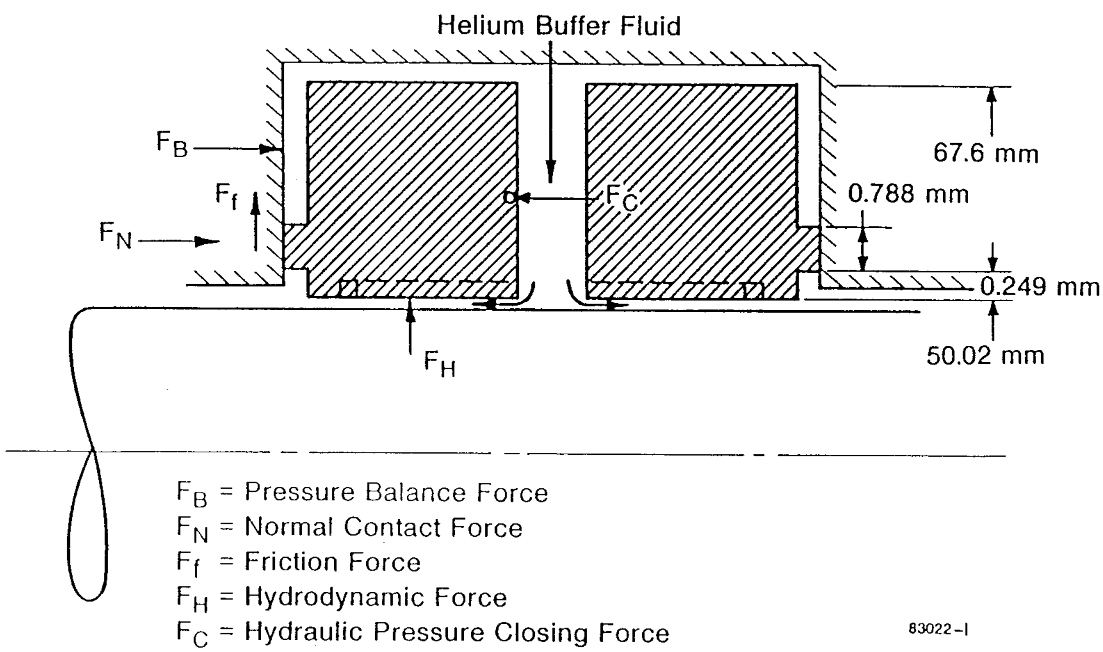

Figure 31. Rayleigh-Step, Floating Ring Seal

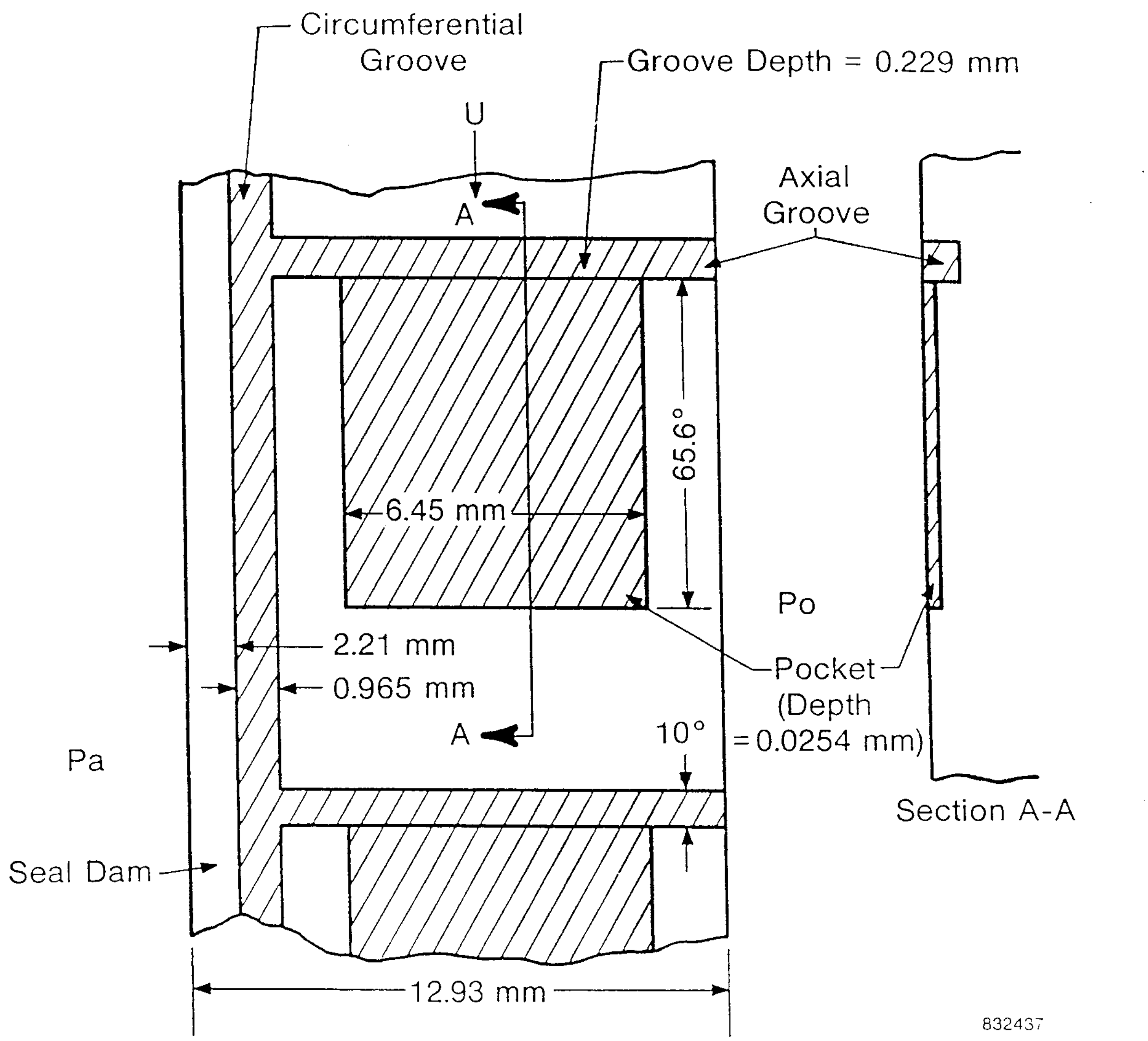

Figure 32. Developed View of 50-mm Rayleigh-Step Pad

Table 5. Single-Pad Rayleigh-Step Seal Problem

```
-JOURNAL & LOAD POSITION
  ECCENTRICITY             =      0.00000
  ECCENTRICITY ANGLE       =         0.00 DEG
  MINIMUM FILM             =    0.0000127 M
  LOAD                     =    571.6     N
  LOAD ANGLE               =      -134.73 DEG

  POWER LOSS               =    26.27     W

  LEAKAGE AT I = 1         =-0.23044E-04 KG/S

  LEAKAGE AT I = M         = 0.33187E-03 KG/S

-RIGHTING MOMENT
  ABOUT X-X             MX = -0.1609      N-M
  ABOUT Y-Y             MY =  0.1552      N-M
```

95TR34-V2

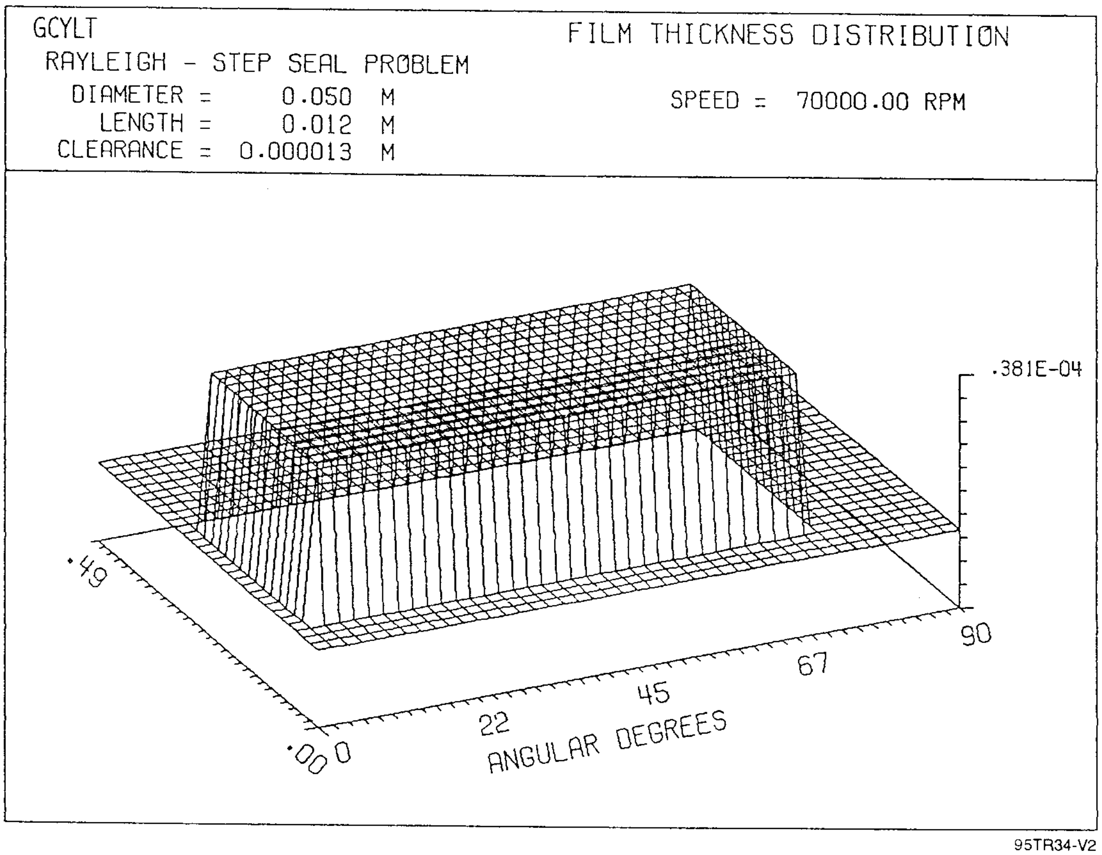

Figure 33. Clearance Distribution, Rayleigh-Step Pad

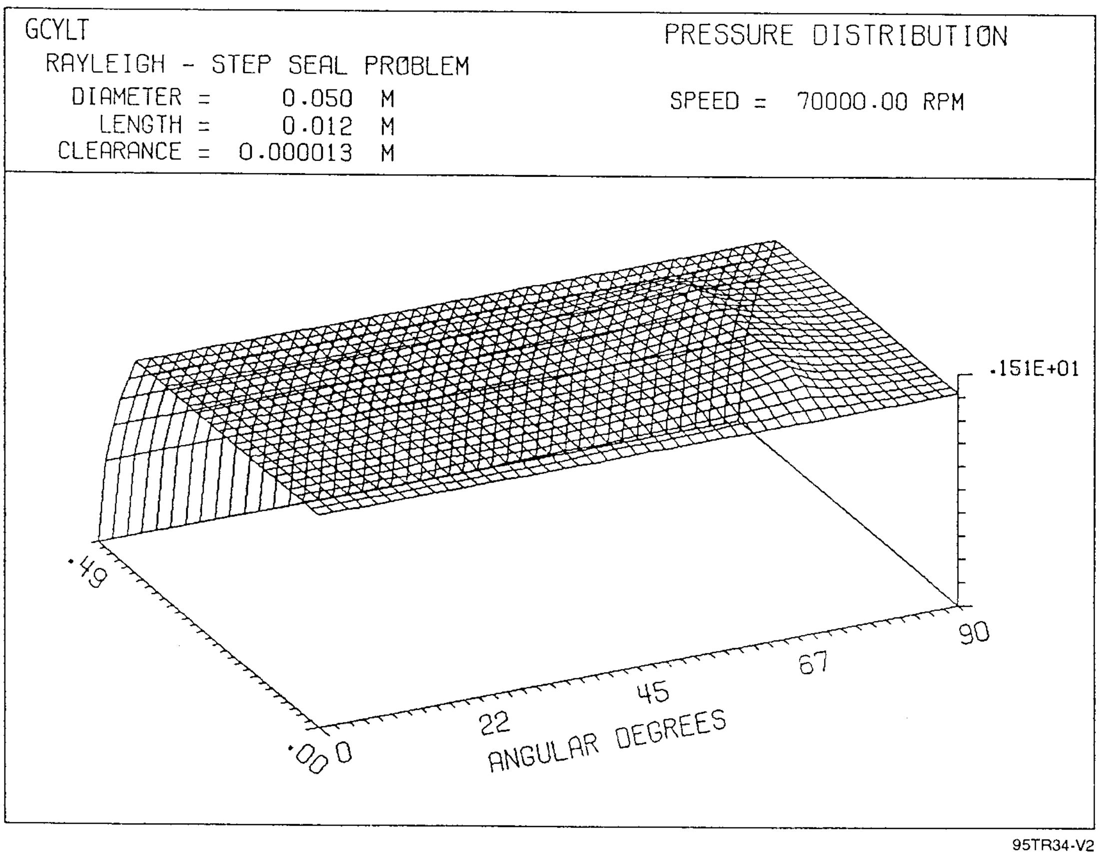

Figure 34. Pressure Distribution, Rayleigh-Step Pad

3.6 Sample Problem 6 - Rayleigh-Step Seal with Eccentricity

This problem will be similar to Problem 5 except the shaft is to be eccentric with respect to the seal ring. In this case, periodic boundary conditions cannot be used and to conserve grid space, one hydrodynamic pad will be modeled and the number of pads will be four. To model separate pads, however, requires that the boundary conditions be known on all extremities of the pad. The seal dam region is not a separate pad problem but is a single 360° pad. Thus, the problem resolves into two separate problems; one that treats the separate Rayleigh pads and one that treats the seal dam. For this particular example, only the Rayleigh-Step hydrodynamic region is considered. The following geometric and operating parameters have been applied:

- International units were invoked
- The shaft position relative to the seal ring was specified
- Stiffness is calculated in four degrees of freedom at a 70,000 rpm excitation frequency
- Number of pads is 4; each pad has an extent of 90°
- Shaft diameter = 0.05 m
- Shaft length = 0.0123 m
- Reference clearance = 1.27×10^{-5} m
- Gas viscosity = 2.19×10^{-5} N-s/m^2
- Absolute temperature = 338.6°K
- Ratio of specific heat = 1.66
- Gas constant = 1154.84 m^2/(s^2-°K)
- Shaft eccentricity ratio = 0.5
- Eccentricity angle = 270°
- Shaft speed = 70,000 rpm
- Reference pressure = 1.01353×10^5 Pa
- Pad boundary pressures are 1.37895×10^6 Pa.

To include the groove pressures, two constant pressure regions were specified.

As shown on Table 6, at the specified position, the load capacity of the seal is 69.73 N and the load angle is 69.47° from the x-axis. The minimum film thickness is 6.4×10^{-6} m. The clearance and pressure distributions are shown on Figures 35 and 36, respectively.

Table 6. Multipad Rayleigh-Step Seal Problem

```
-JOURNAL & LOAD POSITION
  ECCENTRICITY              =      0.50000
  ECCENTRICITY ANGLE        =       -90.00 DEG
  MINIMUM FILM              =    0.0000064 M
  LOAD                      =    69.73     N
  LOAD ANGLE                =        69.47 DEG

  POWER LOSS                =    116.0     W

  LEAKAGE AT I = 1          =-0.99207E-04 KG/S

  LEAKAGE AT I = M          = 0.99207E-04 KG/S

-STIFFNESS COEFFICIENTS
  PRINCIPAL  X      KXX =  0.1298E+08 N/M
  CROSS-COUPLED     KXY =  0.5795E+07 N/M
  CROSS-COUPLED     KXA =   25.55     N/RAD
  CROSS-COUPLED     KXB =   2.247     N/RAD
  CROSS-COUPLED     KYX =  0.2313E+06 N/M
  PRINCIPAL  Y      KYY =  0.1616E+08 N/M
  CROSS-COUPLED     KYA =   59.29     N/RAD
  CROSS-COUPLED     KYB =   30.28     N/RAD
  CROSS-COUPLED     KAX =  0.2214E-07 N-M/M
  CROSS-COUPLED     KAY = -0.9859E-08 N-M/M
  PRINCIPAL  A      KAA =   36.49     N-M/RAD
  CROSS-COUPLED     KAB =  0.2037     N-M/RAD
  CROSS-COUPLED     KBX =  0.1360E-07 N-M/M
  CROSS-COUPLED     KBY = -0.5505E-07 N-M/M
  CROSS-COUPLED     KBA =  -12.66     N-M/RAD
  PRINCIPAL  B      KBB =   19.24     N-M/RAD

-DAMPING COEFFICIENTS
  PRINCIPAL  X      DXX =   753.6     N-S/M
  CROSS-COUPLED     DXY =  -303.8     N-S/M
  CROSS-COUPLED     DXA = -0.1023E-02 N-S/M
  CROSS-COUPLED     DXB = -0.5204E-04 N-S/RAD
  CROSS-COUPLED     DYX =   163.4     N-S/M
  PRINCIPAL  Y      DYY =   815.2     N-S/M
  CROSS-COUPLED     DYA = -0.2082E-02 N-S/RAD
  CROSS-COUPLED     DYB = -0.1277E-02 N-S/RAD
  CROSS-COUPLED     DAX = -0.2680E-14 N-M-S/M
  CROSS-COUPLED     DAY =  0.3079E-13 N-M-S/M
  PRINCIPAL  A      DAA =  0.3602E-02 N-M-S/RAD
  CROSS-COUPLED     DAB = -0.1509E-03 N-M-S/RAD
  CROSS-COUPLED     DBX = -0.2348E-13 N-M-S/M
  CROSS-COUPLED     DBY =  0.8120E-13 N-M-S/M
  CROSS-COUPLED     DBA = -0.5116E-04 N-M-S/RAD
  PRINCIPAL  B      DBB =  0.2658E-02 N-M-S/RAD

-RIGHTING MOMENT
  ABOUT X-X          MX = -0.1978E-15 N-M
  ABOUT Y-Y          MY =  0.6593E-16 N-M
```

95TR34-V2

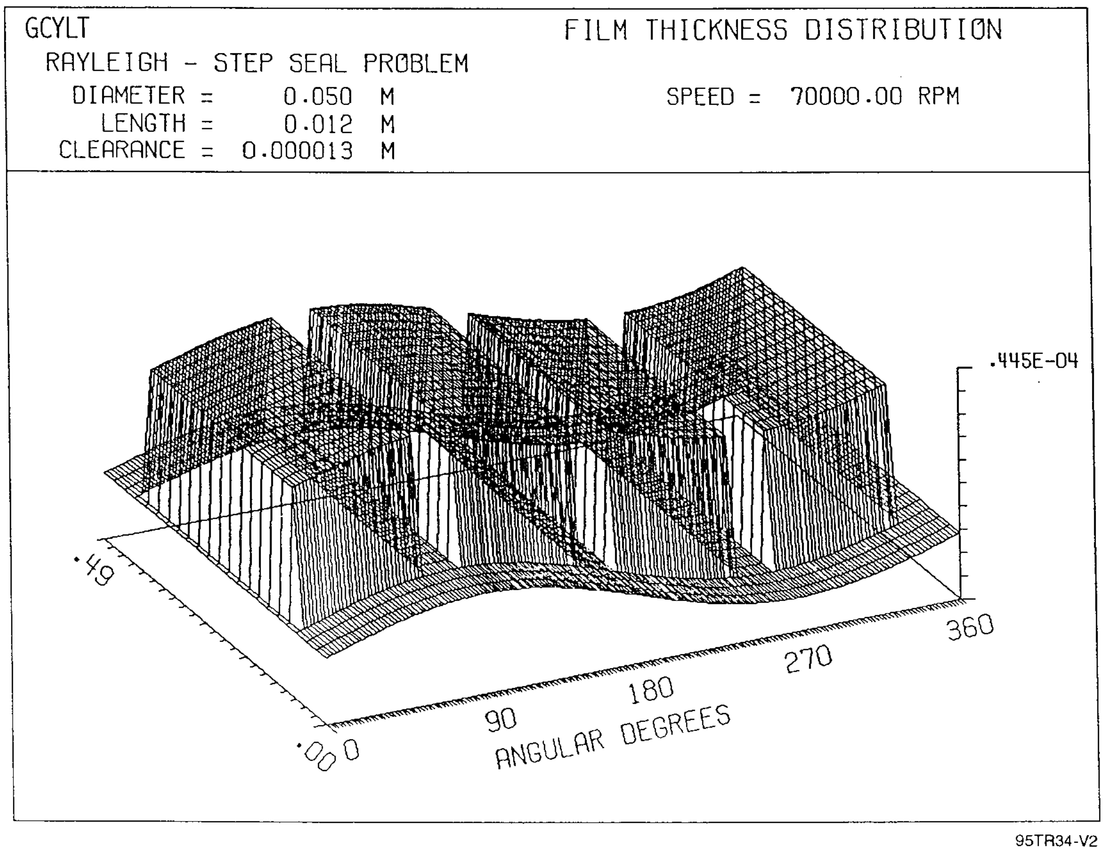

Figure 35. Clearance Distribution, Rayleigh-Step Seal with Eccentricity

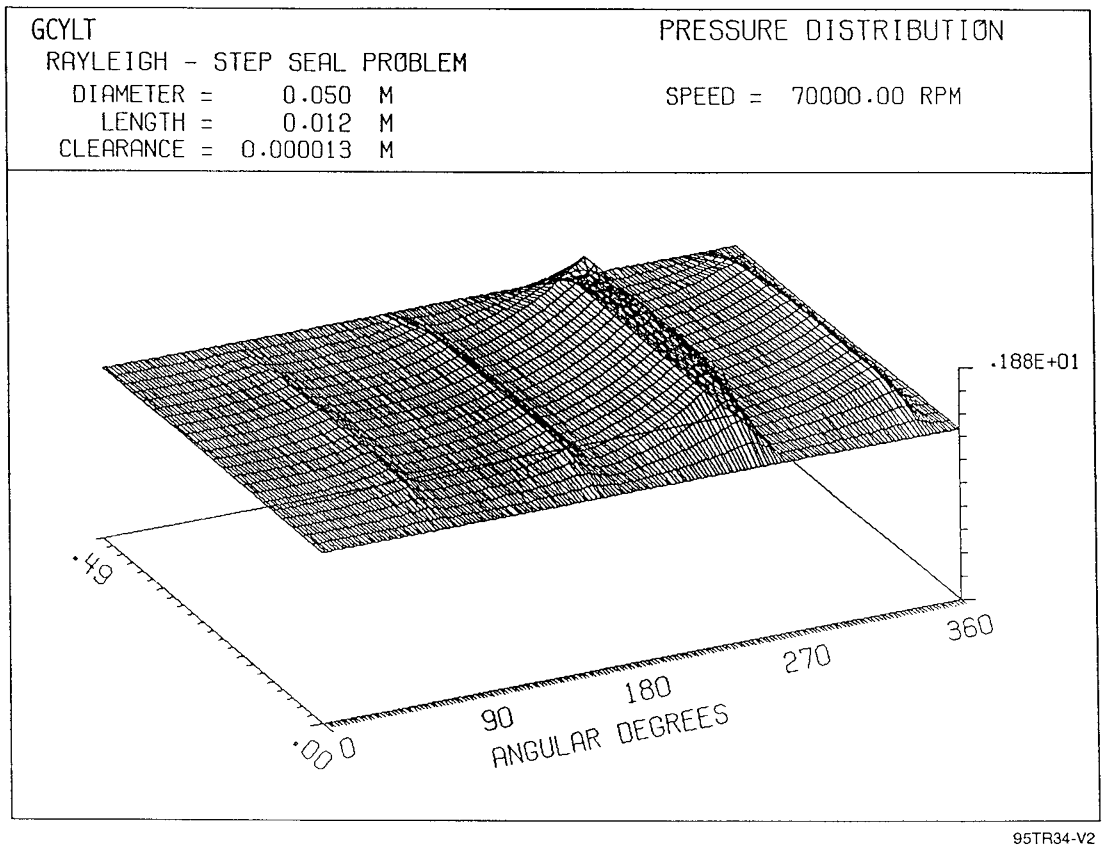

Figure 36. Pressure Distribution, Rayleigh-Step Seal with Eccentricity

3.7 Critical Mass - Sample Problem

The Rayleigh-Step Seal problem (see Sections 3.5 and 3.6) was further analyzed to determine critical mass and frequency as a function of speed and operating clearance.

Figure 37 shows critical mass as a function of speed and operating clearance. If the mass attributable to the seal or bearing exceeds the critical mass, then an instability can occur. The usefulness of the critical mass parameter is that it provides a comparative measure of the stability characteristics of different configurations. Clearly from Figure 37, the low clearance seal would have superior stability characteristics. The critical frequencies are shown on Figure 38. For both clearances, a constant ratio exists between the critical orbital frequency and the operating speed. The ratios are slightly less than 0.5.

Critical mass problems should be confined to small axial pressure gradient cases, because the angular modes are not considered.

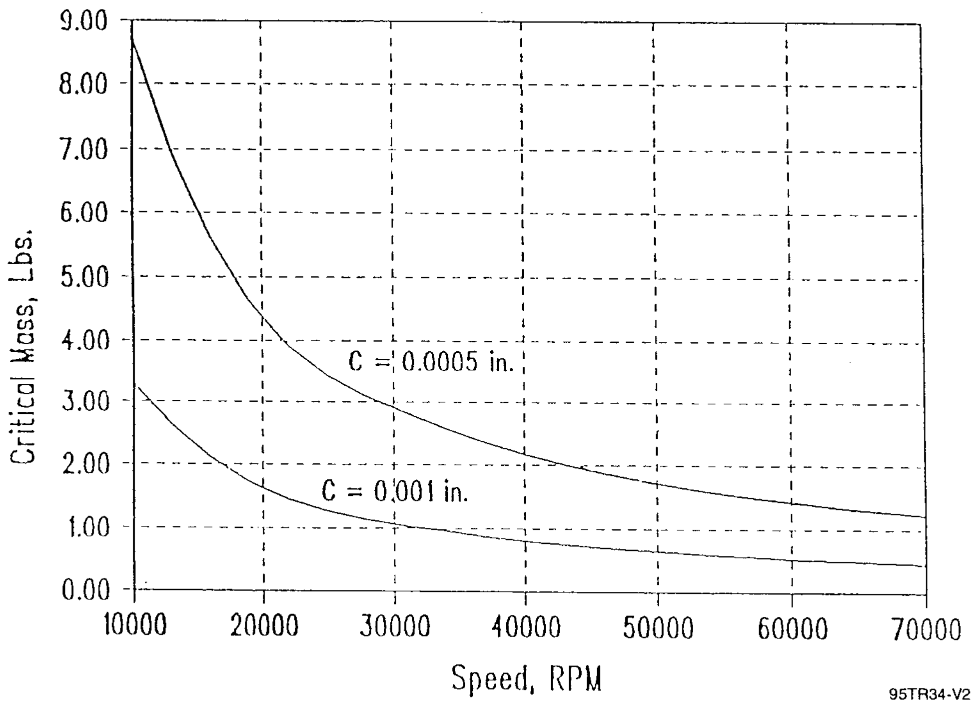

Figure 37. Rayleigh-Step Seal, Critical Mass versus Speed

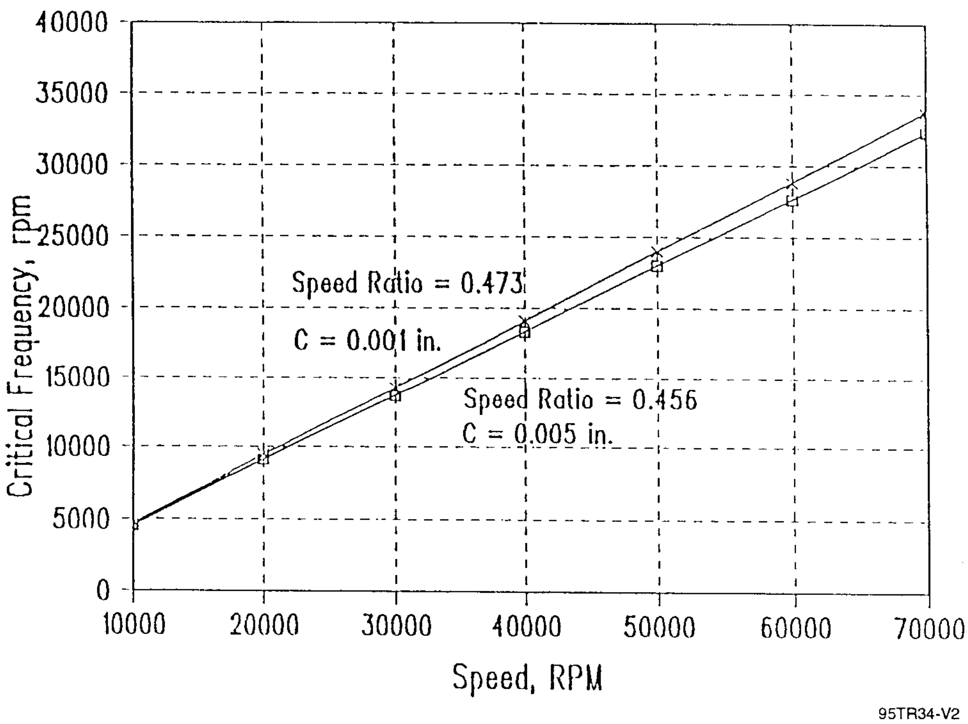

Figure 38. Rayleigh-Step Seal, Critical Frequency versus Speed

4.0 COMPARISONS OF GCYLT WITH GCYL

It is informative to determine the effects of turbulence on seal performance. Comparisons were made between the laminar code GCYL and the revised turbulent code GCYLT to establish the significance of turbulence. The sample problems previously described were run for each of the codes and the results are shown in Tables 7 through 12.

Table 7 shows the variation for the single Rayleigh-Step problem described by Sample Problem 1. The Couette Reynolds number for this case is

$$R_e = \frac{PVh}{\mu} = \frac{p_o R\omega C}{G_c T_a \mu}$$

$$= \frac{214.7\ x \left(\frac{1.9685}{2}\right)\left(\frac{70{,}000 x 2\pi}{60}\right)(.001)}{(250{,}000)(530)(3x10^{-9})}$$

$$= 3896$$

Thus, the problem is clearly in the turbulent regime (R_e>1000) and accounts for the variation in performance. In particular, note the higher load capacity of the turbulent model. The flow is also greater because of the higher pressure generated.

Table 7. Rayleigh-Step Seal Comparison

	GCYLT	GCYL
ε	.40	0.4
γ, deg	-90	-90
h_{min}, in.	0.0006015	0.0006015
W, lb	131.5	27.54
α_L deg	58.49	61.44
HP, hp	2.308	0.4555
Q_1, lb/s	-0.10191 x 10^{-2}	-0.44783 x 10^{-3}
P_{max}, lb/in^2	54.325	12.209

ε = eccentricity ratio
γ = eccentricity angle
h_{min} = minimum film thickness
W = load
α_L = load angle
HP = power loss
Q_1 = leakage at I =1
P_{max} = maximum film pressure

Table 8 shows the comparison for the three-pad sectored seal. In this case, the Couette Reynolds number of 158 is definitely laminar. However, the externally pressurized orifices introduce high pressure gradients which cause Poiseuille turbulence to occur and cause a slight variation in results.

The three-lobe seal comparisons are shown on Table 9. The Couette Reynolds number is 841, which is in the transition zone and which will cause a slight variation with the laminar results.

The hydrostatic sector comparison (Sample Problem 4) is shown on Table 10. Since this is a zero speed case, Couette turbulence could not enter. Poiseuille turbulence, however, is present and was confirmed by a temporary flag inserted into the code. The turbulence occurs at the orifice locations, where high pressure gradients occur and cause the variation in performance outlined in the tabulation.

The last two examples (Tables 11, 12) were for Rayleigh-step seals operating under similar conditions. The Couette Reynolds number for the step region is 384 and is, thus, laminar. The variation between the laminar and turbulent cases is due to Poiseuille turbulence occurring in the step region where high pressure gradients occur.

Table 8. Three-Pad Sectored Seal Comparison

	GCYLT	GCYL
ε	0	0
γ, deg	0	0
h_{min}, in.	0.000250	0.000250
W, lb	--	--
α_L, deg	-54.45	-57.19
HP, hp	1.251	1.233
Q_I, lb/s	-0.14815×10^{-3}	-0.14924×10^{-3}
P_{max}, lb/in.^{2}	119.77	119.78

$$R_e = \frac{\rho v h}{\mu} = \frac{14.7}{250{,}000\ (510)} \frac{(1.125) \times (70{,}000 \times \pi/30)\ (.0005)}{3 \times 10^{-9}} = 158.4656$$

ε = eccentricity ratio
γ = eccentricity angle
h_{min} = minimum film thickness
W = load
α_L = load angle
HP = power loss
Q_I = leakage at I=1
P_{max} = maximum film pressure

Table 9. Three-Lobe Seal Comparison

	GCYLT	GCYL
ε	.22088	.22103
γ, deg	129.42	129.38
h_{min}, in.	0.0000037	0.0000037
W, lb	200.2	200.2
α_L, deg	-90	-90
HP, hp	186.2	186.1
Q_1, lb/s	$.12898 \times 10^{-4}$	$.12875 \times 10^{-4}$
K_{xx}, lb/in.	$.152 \times 10^{9}$	$.146 \times 10^{9}$
K_{xy}, lb/in.	$-.2103 \times 10^{8}$	$-.2379 \times 10^{8}$
K_{yx}, lb/in.	$-.3595 \times 10^{8}$	$-.3890 \times 10^{8}$
K_{yy}, lb/in.	$.8662 \times 10^{8}$	$.1002 \times 10^{9}$
D_{xx}, lb-s/in.	$.1165 \times 10^{5}$	9939
D_{xy}, lb-s/in.	$-.1510 \times 10^{5}$	$-.1089 \times 10^{5}$
D_{yx}, lb-s/in.	5204	5140
D_{yy}, lb-s/in.	$.1653 \times 10^{5}$	$.1393 \times 10^{5}$

K_{ij} = Stiffness in i direction due to j displacement
D_{ij} = Damping in i direction due to j velocity
ε = eccentricity ratio
γ = eccentricity angle
h_{min} = minimum film thickness
W = load
α_L = load angle
HP = power loss
Q_1 = leakage at I=1
P_{max} = maximum film pressure

Table 10. Hydrostatic Sector Comparison

	GCYLT	GCYL
ε	0.6345	0.55932
γ, deg	90	90
h_{min}, in.	0.000366	0.0004414
W, lb	370	369.6
α_L, deg	-90	-90
HP, hp	0	0
Q_1, lb-s	-0.25673×10^{-4}	-0.39586×10^{-4}
Q_M, lb-s	0.25673×10^{-4}	0.39586×10^{-4}
K_{xx}, lb/in.	.40320	43020
K_{yx}, lb/in.	-141.6	-126.9
K_{yy}, lb/in.	24290	48580
K_{ya}, lb/rad	-391.7	-298.6
K_{yb}, lb/rad	-74.14	-59.98
K_{AA}, in.-lb/rad	50550	43,890
K_{BB}, in.-lb/rad	10990	10,000
D_{xx}, lb-s/in.	15.89	10.98
D_{yx}, lb-s/in.	0.0202	0.0143
D_{yy}, lb-s/in.	128.5	81.68
D_{YA}, lb-s/rad	0.063	0.0367
D_{YB}, lb-s/rad	0.0106	0.0067
D_{AA}, in.-lb-s/rad	7.329	4.599
D_{BB}, in.-lb-s/rad	1.288	0.9138
P_1, lb/in^2	178	170*
P_2, lb/in^2	193	188*
P_3, lb/in^2	197	194*
P_4, lb/in^2	197	194*
P_5, lb/in^2	193	188*
P_6, lb/in^2	178	170*

*Pressures downstream of orifices

ε = eccentricity ratio
α_L = load angle
γ = eccentricity angle
HP = power loss
h_{min} = minimum film thickness
Q_1 = leakage at I=1
W = load
Q_M = leakage at I=M
P_{max} = maximum film pressure

Table 11. Rayleigh-Step Seal, Single Pad Comparison

	GCYLT	GCYL
ε	0	0
γ, deg	0	0
h_{min}, m	1.27×10^{-5}	1.27×10^{-5}
W, N	571.6	571
α_L, deg.	-134.73	-134.78
HP, hp	26.27	21.79
Q_1, kg/s	-0.23×10^{-4}	$-.217 \times 10^{-4}$
Q_M, kg/s	$.332 \times 10^{-3}$	$.403 \times 10^{-3}$

ε = eccentricity ratio
γ = eccentricity angle
h_{min} = minimum film thickness
W = load
α_L = load angle
HP = power loss
Q_i = leakage at I=1
P_{min} = maximum film pressure

Table 12. Four-Pad Rayleigh-Step Seal Comparison

	GCYLT	GCYL
ε	0.5	0.5
γ, deg	-90	-90
h_{min}, in.	6.4×10^{-6}	6.4×10^{-6}
W, N	69.73	52.96
α_L, deg	69.47	71.63
HP, hp	116	95.08
Q_I, kg/s	$-.99207 \times 10^{-4}$	$-.88483 \times 10^{-4}$
Q_M, kg/s	$.99207 \times 10^{-4}$	$.88483 \times 10^{-4}$
K_{xx}, N/in.	12,980,000	10,160,000
K_{xy}, N/in.	5,795,000	3,371,000
K_{XA}, N/rad	25.55	14.33
K_{XB}, N/rad	2.47	-.3405
K_{yx}, N/in.	23.130	-61,600
K_{yy}, N/in.	16,160	11,690
K_{YA}, N/rad	59.29	37.51
K_{YB}, N/rad	30.28	20.59
K_{AA}, N-m/rad	36.49	27.53
K_{AB}, N-m/rad	0.2307	1.657
K_{BA}, N-m/rad	-12.66	-10.32
K_{BB}, N-m/rad	19.24	14.46
D_{xx}, N-s/in.	753.6	786.4
D_{xy}, N-s/in.	-303.8	-216.6
D_{yx}, N-s/in.	163.4	192.7
D_{yy}, N-s/in	815.2	901.7

ε = eccentricity ratio
α_L = load angle
γ = eccentricity angle
HP = power loss
h_{min} = minimum film thickness
Q_I = leakage at I=1
W = load
P_{max} = maximum film pressure

5.0 VERIFICATION

Several mechanisms were used to conduct verification of the code. Results of the code were compared against information in the public domain literature, and comparisons were made against the results of other codes and against manual computations.

Although simple in concept, extensive changes were implemented to the original laminar code to accommodate turbulence. A first check on the turbulent code was to run a laminar case to see if it compared precisely against the original code.

Most of the comparison cases involved a 360° plain seal with the parameters shown on Table 13.

Table 13. 360° Plain Seal Parameters

Diameter	=	1 in.
Length	=	2 in.
Clearance	=	0.0005 in.
Viscosity	=	3×10^{-9} lb-s/in^2
Absolute Temperature	=	530°R
Specific Heat Ratio	=	1.4
Gas Constant	=	247,000 in^2/S^2/°R
Eccentricity Ratio	=	0.5
Eccentricity Angle	=	270°
Ambient Pressure	=	Pa = Variable (psia)
Pressure Difference	=	Pd = Variable (psi)
Speed	=	N = Variable (rpm)
W	=	Load Capacity (lb)
γ	=	Attitude Angle (deg)
HP	=	Power Loss (hp)
K_{ij}	=	Stiffness in i direction due to j displacement
D_{ij}	=	Damping in i direction due to j velocity

Laminar comparisons were made against the original codes and against another code, SPIRALG, that was run with the smooth surface option. Results are shown on Table 14. The turbulent code GCYLT compared exactly against GCYL and comparisons with SPIRALG were excellent.

The original code GCYL was also compared against information in the literature. Figure 39 shows the pressure distribution in an infinitely long Rayleigh-Step slider at various values of the compressibility parameter Λ., For this case, closed-form solutions are available. Turbulence would show some variation at high values of Λ.

Table 14. Laminar Check of GCYLT

		GCYL	GCYLT	SPIRALG
h_{min},	mils	0.000252	0.000252	.00025
W,	lb	1.695	1.695	1.672
γ	deg	7.76	7.76	7.47
HP	hp	$.214 \times 10^{-4}$	$.214 \times 10^{-4}$	$.214 \times 10^{-4}$
K_{xx}	lb/in.	921	921	869
K_{xy}	lb/in.	8572	8572	8437
$K_{x\alpha}$	lb/rad	2.163	2.163	--
$K_{x\beta}$	lb/rad	2.431	2.431	--
K_{yx}	lb/in.	-6715	-6715	-6630
K_{yy}	lb/in.	2301	2301	2166
$K_{y\alpha}$	lb/rad	1.072	1.072	--
$K_{y\beta}$	lb/rad	0.5987	0.5987	--
$K_{\alpha x}$	in.-lb/in.	--	--	--
$K_{\alpha y}$	in.-lb/in.	--	--	--
$K_{\alpha\alpha}$	in.-lb/rad	329.4	329.4	293
$K_{\alpha\beta}$	in.-lb/rad	819.3	819.3	804
$K_{\beta x}$	in.-lb/in.	--	--	--
$K_{\beta y}$	in.-lb/in.	--	--	--
$K_{\beta\alpha}$	in.-lb/rad	-1399	-1399	1369
$K_{\beta\beta}$	in.-lb/rad	97.87	97.87	86.33
D_{xx}	lb-s/in.	125.2	125.2	124
D_{xy}	lb-s/in.	-30.16	-30.16	-29
$D_{x\alpha}$	lb-s/rad	--	--	--
$D_{x\beta}$	lb-s/rad	--	--	--
D_{yx}	lb-s/in.	34.73	34.73	33.87
D_{yy}	lb-s/in.	205.1	205.1	202.9
$D_{y\alpha}$	lb-s/rad	--	--	--
$D_{y\beta}$	lb-s/rad	--	--	--
$D_{\alpha x}$	in^2-lb/s	--	--	--
$D_{\alpha y}$	in^2-lb/s	--	--	--
$D_{\alpha\alpha}$	in.-lb-s/rad	30.76	30.76	30.31
$D_{\alpha\beta}$	in.-lb-s/rad	-2.787	-2.787	-2.58
$D_{\beta x}$	in^2-lb-s	--	--	--
$D_{\beta y}$	in^2-lb-s	--	--	--
$D_{\beta\alpha}$	in.-lb-s/rad	2.698	2.698	2.48
$D_{\beta\beta}$	in.-lb-s/rad	16.99	16.99	16.75

P_a = 14.7 psia P_d = 0.0   N = 1000 rpm   Excitation Frequency = 0

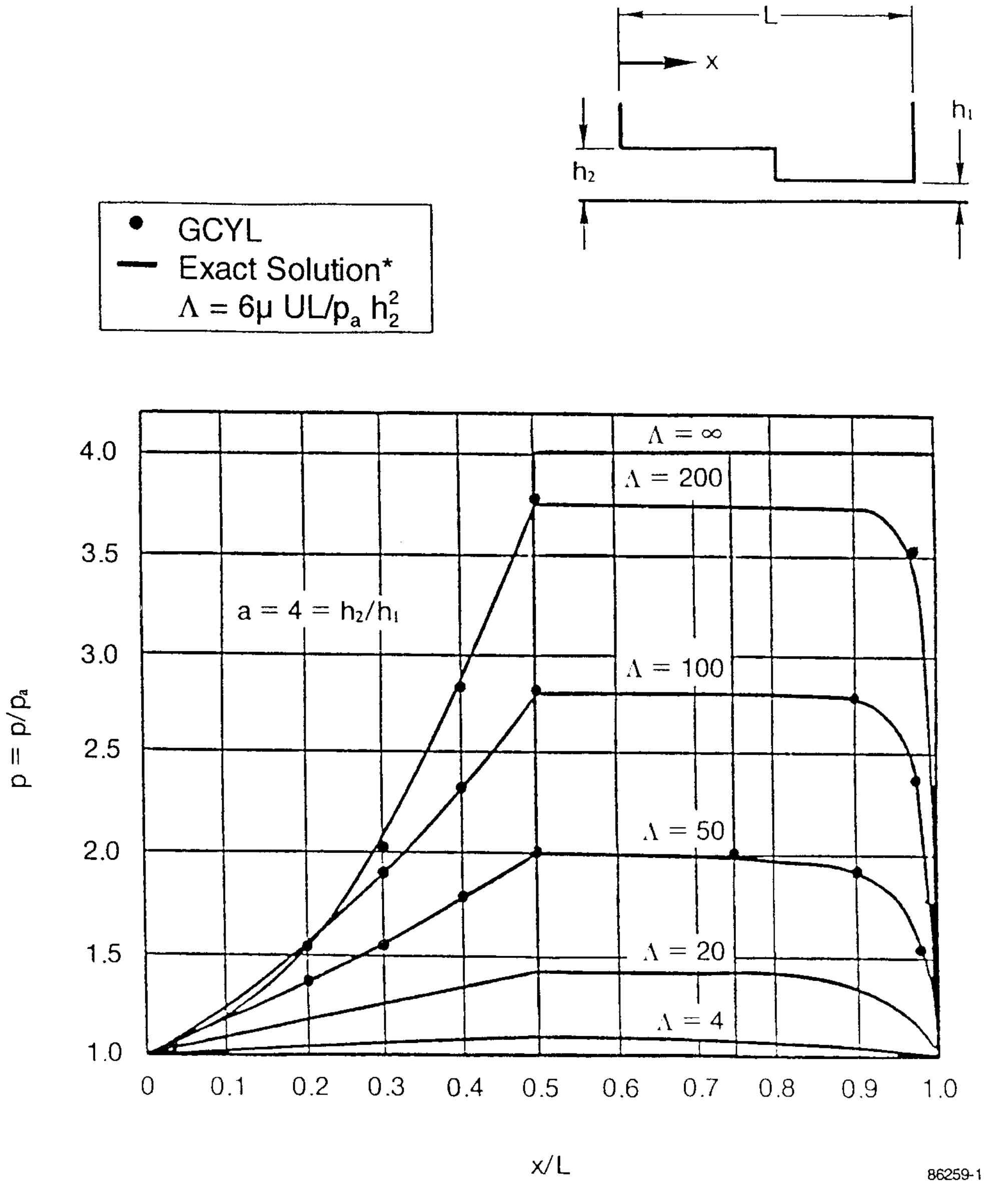

*"Theory of Hydrodynamic Lubrication", O. Pinkus, R. Sternlicht, McGraw-Hill, N.Y. 1961

Figure 39. Rayleigh-Step, Program Verification

Further comparisons were made for a plain cylindrical seal with an L/D ratio of 1 with information from Reference 8. Computations were made at two different eccentricity ratios, $\varepsilon = 0.6$ and 0.8. Nondimensional load capacity and attitude angles are shown in Figures 40 and 41, respectively. Excellent correlation is demonstrated. Again, these comparisons were made with the earlier laminar version of the code.

To validate Couette and Poiseuille turbulence, GCYLT was run against another code available at MTI called GBEAR. The GBEAR code accurately predicts Couette turbulence for gases, but not Poiseuille turbulence.

Table 15 shows comparative results for Couette turbulence with a Reynolds number of 48,995. The comparative results are very good for all parameters.

A Poiseuille turbulence check was made by running at a low speed, with a high pressure gradient and a high ambient pressure. By using a high value of ambient pressure, the compressibility parameter, Λ, is reduced to a low value. Then the liquid and gas cases nearly correspond. Comparative results are shown on Table 16. Again, the comparative results are very good.

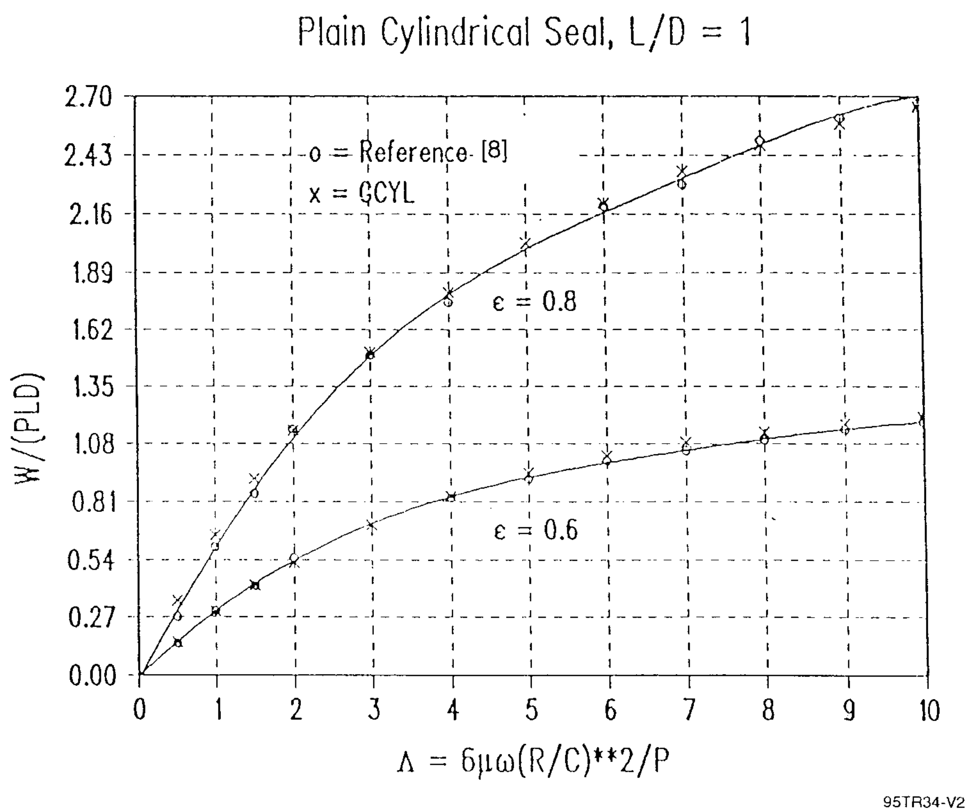

Figure 40. Dimensionless Load Capacity versus Λ

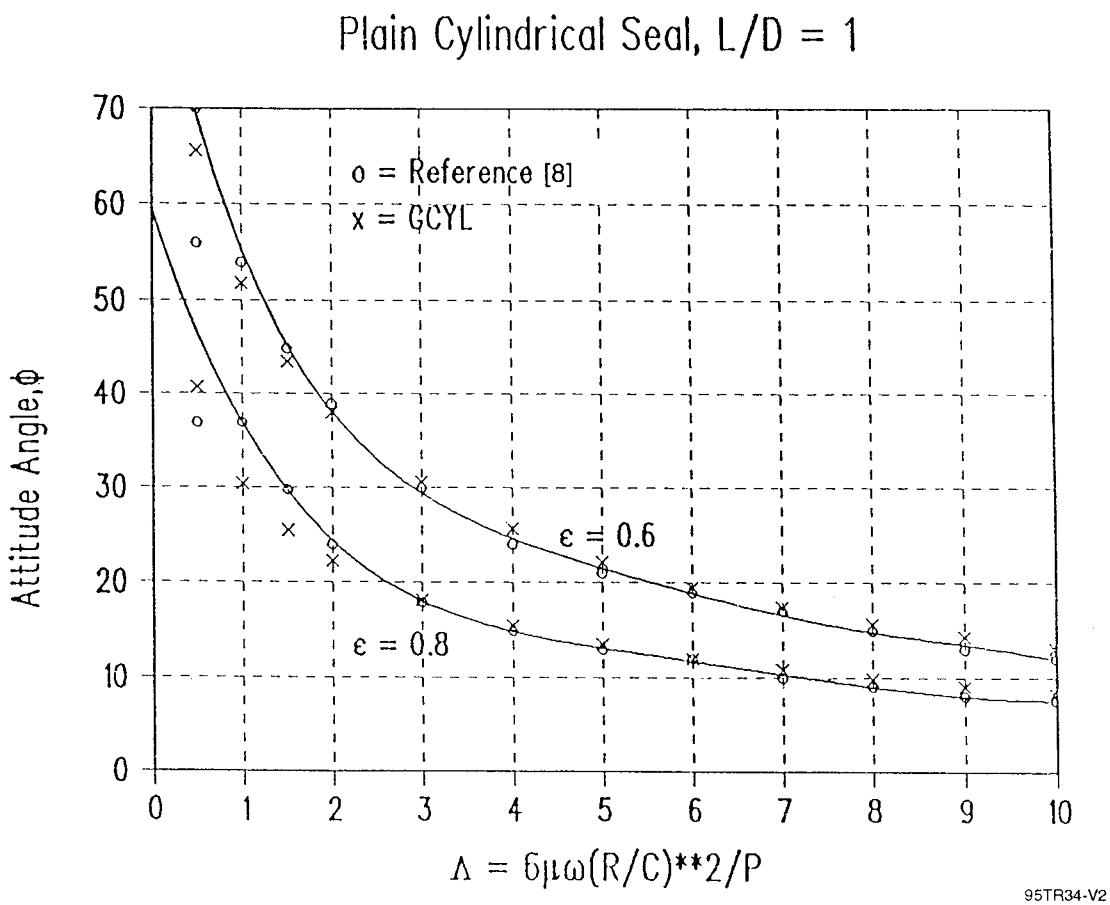

Figure 41. Attitude Angle versus Λ

Table 15. Couette Turbulence Comparison

		GCYLT	GBEAR
h_{min}	mils	0.252	0.252
W	lb	1270	1269
γ	deg	4.92	4.63
HP	hp	1.2	1.2
Q	lb/s	--	--
K_{xx}	lb/in.	43,740	40,917
K_{xy}	lb/in.	6,458,000	6,443,64
K_{yx}	lb/in.	-5,062,000	5,058,81
K_{yy}	lb/in.	919,000	813,689
D_{xx}	lb-s/in.	1920	1936
D_{xy}	lb-s/in.	-270.7	-166
D_{yx}	lb-s/in.	334.3	-147
D_{yy}	lb-s/in.	2649	2650
M_c	lb	16	12
ω_c	rpm	23,987	24,064

N = 50,000 rpm P_a = 14,700 psig
R_{ec} = 48,995   Excitation Frequency = 0

Table 16. Poiseuille Turbulence Comparison

		GCYLT	GBEAR
h_{min}	mils	0.25	0.25
W	lb	9.513	9.449
γ	deg	0.03	0
HP	hp	9.48×10^{-5}	9.43×10^{-5}
Q_1	lb/s	.0270	.0267
K_{xx}	lb/in.	10.05	--
K_{xy}	lb/in.	46,170	47,271
K_{yx}	lb/in.	-38,860	-37,188
K_{yy}	lb/in.	23.16	0.78
D_{xx}	lb-s/in.	728.7	739
D_{xy}	lb-s/in.	-0.60	--
D_{yx}	lb-s/in.	0.82	0.88
D_{yy}	lb-s/in.	862.7	875
M_c	lb	-.35	-2.8
ω_c	rpm	511	497

N = 1000 rpm P_a = 14,700 psig
P_d = 500 psig   Excitation Frequency = 0

An internal check of the code was made by analyzing a recessed hydrostatic bearing. With the flow path option, the net flow around the periphery of a hydrostatic pad can be determined and compared against the inflow to the recess. For flow continuity, the sum of the peripheral flows should equal the inlet flow. The following geometry and operating parameters were considered.

- A single pad with grid dimension of 15 x 37 (M x N)
- The pad diameter is 2 inches
- The pad length is 2 inches
- The pad clearance is 0.001 in.
- The pad angle is 180° and the starting angle is at 180°
- There is one recess located in the pad, and the grid corner points are as follows:
  Left bottom corner, M = 3, N = 22
  Right top corner, M = 13, N = 27
- The specific heat of the gas is 1.4
- The gas constant is 250,000 $in^2/(s^2$-°R)
- The absolute temperature is 530°R
- The absolute viscosity is 3 x 10^{-9} lb-s/in^2
- The inlet orifice diameter to the recess is 0.020 in. and the coefficient of discharge is 1.0. The orifice is located in the grid at M = 8, N = 24.
- The supply pressure to the orifice is 150 psig. The pressure surrounding the pad is at 0 psig. The reference ambient pressure is 14.7 psia.
- Several eccentricities and speeds were examined and are defined in the subsequent discussions.

The output from the code supplies the total flow from the peripheral flow path and the pressure in the recess. A manual computation can then be made for calculating the inlet flow through the orifice using the following equation:

$$f_o = 386.4\, A_o C_D G_1 P_s \left\{ \left(\frac{p_r}{p_s}\right)^{\frac{2}{\gamma}} \left[1 - \left(\frac{p_r}{p_s}\right)^{\frac{\gamma-1}{\gamma}} \right] \right\}^{\frac{1}{2}} \qquad \textbf{(5-1)}$$

where

$$G_1 = \sqrt{\frac{2\gamma}{G_c \theta (\gamma - 1)}} \qquad \textbf{(5-2)}$$

f_o = inlet flow, lb/s	A_o = orifice area, in^2
C_D = discharge coefficient	p_s = supply pressure, psia
p_r = recess pressure, psia	γ = ratio of specific heats
G_c = gas constant, $in^2/(s^2$-°R)	θ = absolute temperature, °R

Table 17 provides the results of several cases:

Table 17. Recessed Pad Flow Comparisons

ε	N rpm	Q_p lb/s	P_r psig	Q_o lb/s	Δ %
0.0	0.0	0.001188	46.6*	0.001189	0.08
0.4	0.0	0.001162	88.6	0.001163	0.09
0.0	70,000	0.001188	37.7*	0.001189	0.08

* = choked flow
N = shaft speed
P_r = recess pressure
Δ = percent variation
ε = eccentricity ratio
Q_p = peripheral flow
Q_o = orifice flow

Note that the peripheral and orifice flows differ by less than 0.1%.

When using the source points or spot recess options of the code, it is important to surround the source point with a fine grid to obtain an accurate result and a computation in which pressures will converge. Studies were made of varying grid sizes for a source problem. The variable grid option was applied and varied. A single pad with a central row of orifices were analyzed (see Sample Problem Number 4). The following information is pertinent:

- Number of pads = 1
- Pad angle = 120°
- Start angle = 30°
- Number of grid points in circumferential direction = 34
- Number of grid points in axial direction = 27
- Diameter = 2.6798 in.
- Length = 1.627 in.
- Specific heat ratio = 1.66
- Gas constant = 1,790,000 $in^2/(s^2\text{-}°R)$
- Absolute temperature = 528°R
- Viscosity = 2.9 x 10^{-9} $lb\text{-}s/in^2$
- Shaft speed = 0 rpm
- Reference pressure = 14.7 psia
- Boundary pressure = 50 psig
- Supply pressure to inherently compensated orifices = 200 psig
- Preload = 50% located at the center of the pad

- Stiffness is to be determined
- Six source points are located along a circumferential line in the axial center of the pad at circumferential grid locations 5, 10, 15, 20, 25, 30.

The hole diameter is 0.020, and the coefficient of discharge is 1.0.

Table 18 indicates the effect of grid width around the source point in both the axial and circumferential directions. As the grid width is changed, the source pressures remain relatively unaffected until the grid width is 6 to 8X the orifice hole size. A similar conclusion can be drawn for the other performance parameters of load, flow, stiffness and damping. The recommended grid width from the source point to a neighboring grid line is twice the orifice diameter.

Table 18. Comparative Studies - Discrete Orifices versus Grid Size A (Orifice Size = 0.015 in.)

Comparison of Source Pressures

A in	P_1 psig	P_2 psig	P_3 psig	P_4 psig	P_5 psig	P_6 psig
0.015	166	187	192	192	187	174
0.030	170	185	191	191	185	170
0.060	166	184	190	190	184	166
0.120	160	182	188	189	182	160

Comparison of Performance

A in.	W lb	Q_1 lb/s x 10^4	Q_M lb/s x 10^4	K_{xx} lb/in. x 10^{-6}	K_{yy} lb/in. x 10^{-6}	D_{xx} (lb-s)/in.	D_{yy} (lb-s)/in.
0.015	356.9	0.48753	0.48753	0.0462	0.0858	8.506	60.67
0.030	361.7	0.50539	0.50539	0.0457	0.0842	8.494	59.79
0.060	368.2	0.5305	0.5305	0.0475	0.0817	8.360	58.70
0.120	377.3	0.5651	0.5651	0.0522	0.0967	8.072	55.97

A = grid width in both circumferential and axial directions
W = load capacity
Q_1 = flow out of grid line M=1
Q_M = flow out of grid line M=M
K_{xx} and K_{yy} = stiffness in x and y directions, respectively
D_{xx} and D_{yy} = damping in x and y directions, respectively

6.0 THEORETICAL DESCRIPTION AND NUMERICAL METHODS FOR CODE GFACE

6.1 Governing Equations

Reynolds lubrication equation for compressible flow in polar coordinates is as follows:

$$\frac{\partial}{\partial r}\left(\frac{r\rho h^3}{\mu}\frac{\partial p}{\partial r}\right)+\frac{1}{r}\frac{\partial p}{\partial \theta}\left(\frac{\rho h^3}{\mu}\frac{\partial p}{\partial \theta}\right)=6U\frac{\partial(\rho h)}{\partial \theta}+12r\rho\frac{\partial h}{\partial t} \tag{6-1}$$

The coordinate system used is shown on Figure 42. The equation is made dimensionless with the following definitions. (Upper case variables are dimensionless).

$$R=\frac{r}{r_o};\quad H=\frac{h}{C_o};\quad T=\frac{t}{t_o};\quad P=\frac{p}{p_o}9$$

$$\Lambda=\frac{6\mu\omega r_o^2}{p_o C_O^2};\quad t_o=\frac{12\mu r_o^2}{p_o C_O^2} \tag{6-2}$$

Substituting the dimensionless variables into Reynolds equation produces a dimensionless Reynolds equation:

$$\frac{\partial}{\partial R}\left(RPH^3\frac{\partial P}{\partial R}\right)+\frac{1}{R}\frac{\partial}{\partial \theta}\left(PH^3\frac{\partial P}{\partial \theta}\right)=\Lambda\frac{\partial(PH)}{\partial \theta}+\frac{\partial(PH)}{\partial T} \tag{6-3}$$

For steady-state solutions, the time dependent term on the right-hand side is eliminated.

The method of solutions is equivalent to that described for GCYLT. The grid is portioned into cells and a flow balance is established throughout the cells to determine the pressure distribution utilizing Newton-Raphson in combination with the column-matrix approach for each iteration. Precise details are included in Reference 3.

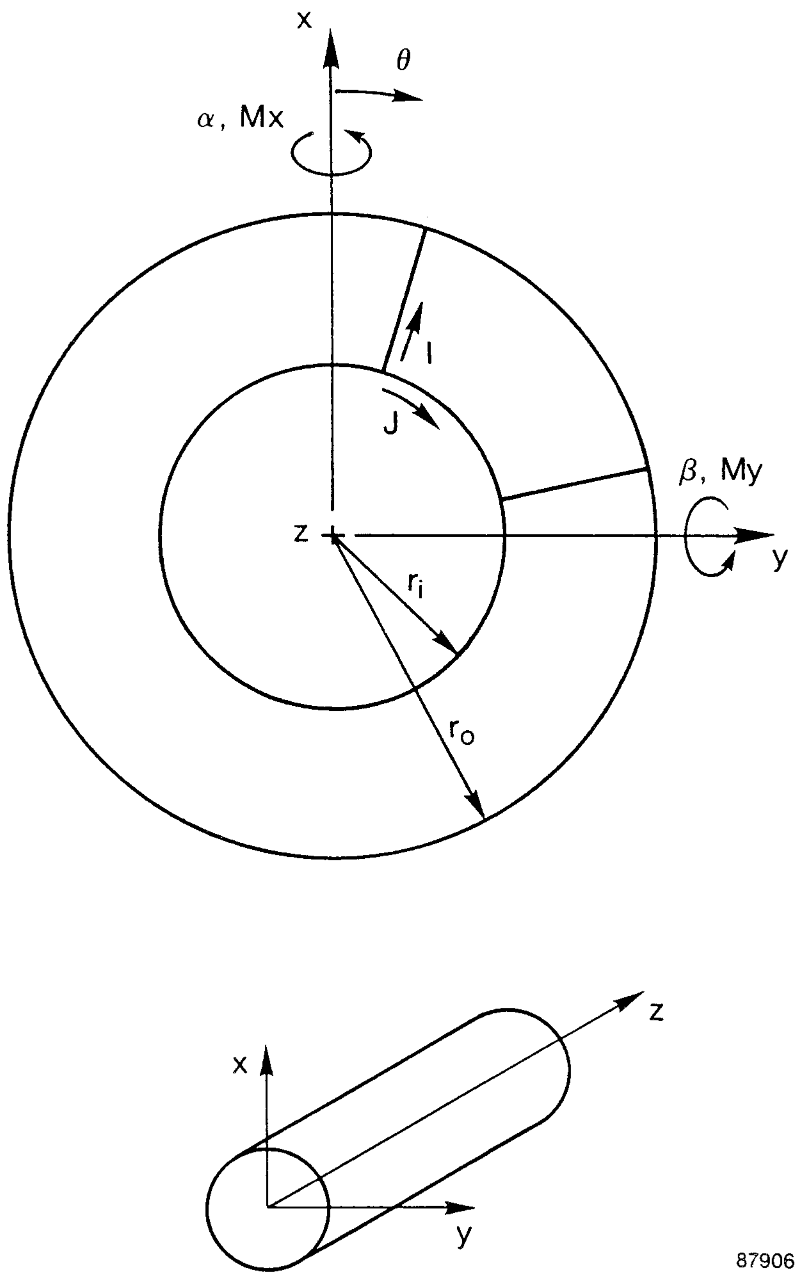

Figure 42. Coordinate System for GFACE

6.2 Film Thickness Distribution and Misalignment

Misalignment occurs through axes in the plane of the bearing. If a thrust collar misaligns an angle α about the x axis and β about the y axis (see Figure 42), the film thickness at any radius r, and angle θ is :

$$H = C_o + e - \alpha r \sin\theta + \beta r \cos\theta \tag{6-4}$$

where C_o = *reference or initial clearance*

e =axial displacement

In non-dimensional form

$$H = 1 + \frac{e}{C_o} - \frac{\alpha R_o}{C_o} R\sin\theta + \frac{\beta R_o}{C_o} R\cos\theta \tag{6-5}$$

In addition to a flat misaligned surface, other geometries can be treated. These are depicted on Figure 43. Included are Rayleigh steps and tapers in both the circumferential and radial directions. The boundaries of circumferential steps and tapers are defined by the i,j grid point values of the lower left and upper right hand corners of the depressed region. Hydrostatic geometries are also included. Inherently compensated orifices can be located in the grid region as well as orifice fed holes and orifice fed recesses. The recess location is defined similarly to steps and tapers.

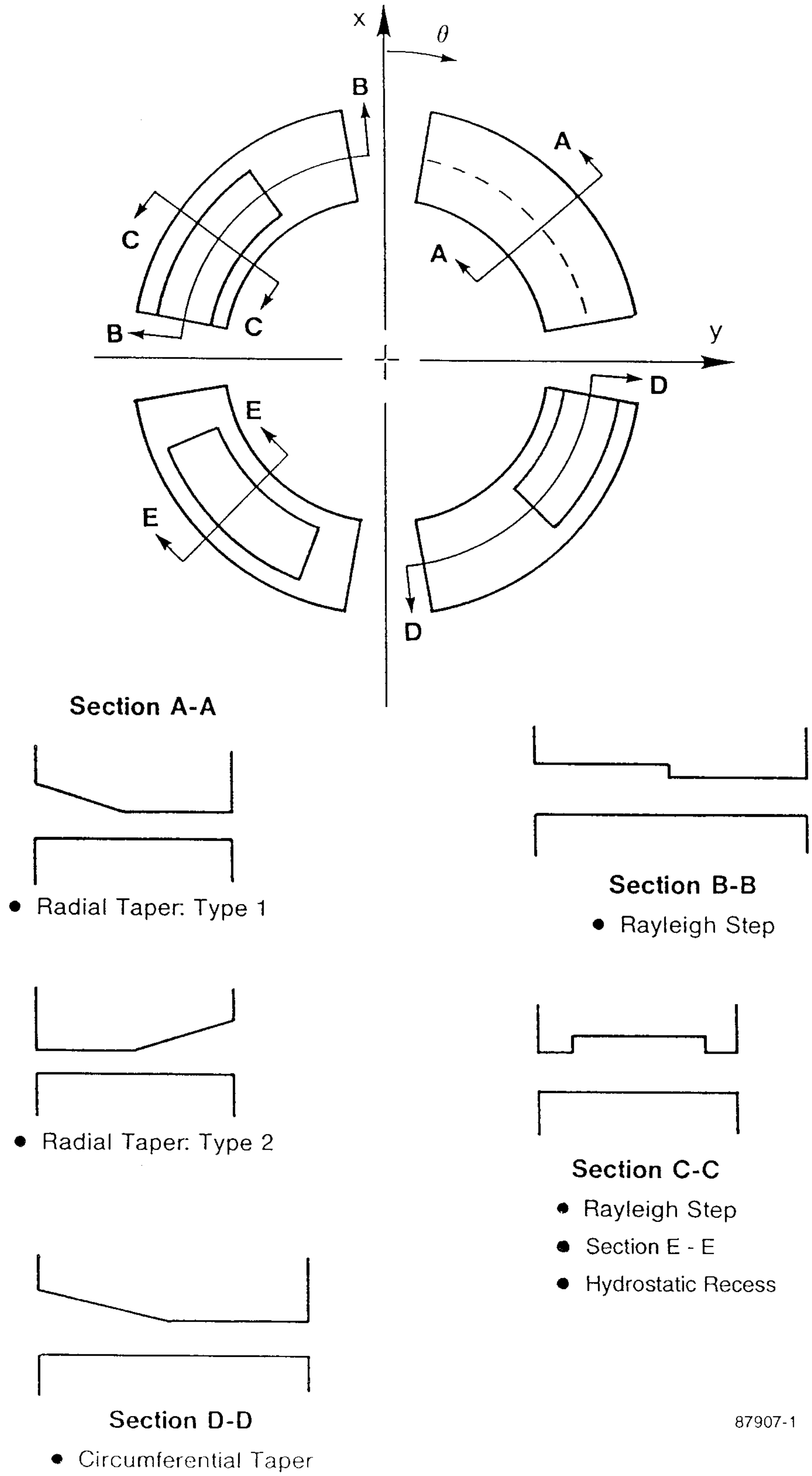

Figure 43. Non-Uniform Clearance Geometries

7.0 SAMPLE PROBLEMS OF CODE GFACE

7.1 Multipad Rayleigh Step Seal

An eight-pad Rayleigh-step seal without pressure gradient, but with misalignment was analyzed. The geometry and operating conditions were as follows:

Number of pads, NPAD	8
Outer diameter	4.0 in.
Inner diameter	2.5 in.
Angular extent of pad	35 degrees
Starting angle of first pad	5 degrees
The displacement was given	
Compute Stiffness at synchronous frequency	5000
Apply variable grid	
Clearance	0.0002 in.
Misalignment angle about the X- axis	-0.001 degrees
Number of steps in grid	1
Step depth	0.0004 in.
Location of step	
Lower left corner	I=5, J=1
Upper right corner	I=8, J=8
Specific heat ratio	1.4
Gas constant	246,900 $in.^2/s^2/^oR$
Absolute temperature	1460^o R
Viscosity	5.35×10^{-9} $lb\text{-}s/in^2$
Speed	5000 rpm
Convergence tolerance	0.01
Ambient (reference) pressure	14.7 psi

Summary output is indicated on Table 19.

Clearance and pressure distribution plots are shown on Figures 44, 45 and 46. Since misalignment is slight, the variation from pad to pad is not very significant.

7.2 Tapered Land Seal

A single sector of a 16 pad tapered land seal was analyzed. Periodic boundary conditions were applied. Figure 47 shows the grid network layout of the pad. High pressure at the top flows through a radial groove into the tapered region and also into a circumferential groove that circumvents the complete seal. The slope of the taper is 0.05209.

- A load of 13 lb was applied and the axial position to support this load was determined. The initial guess for clearance was 0.0002 in.
- Stiffness and damping coefficients were determined at zero speed excitation.
- Periodic boundary conditions were applied to a single pad representation. The start of the pad angle was 67.5 degrees from the x-axis and the pad extent was 22.5 degrees.
- The outer diameter was 4.5 in. and the inner diameter was 3.793 in.
- As shown on Figure 47, the slope of the taper is 0.0509 and its location is indicated on the figure. The radial inlet region and circumferential groove were modeled as constant pressure areas.
- The gas viscosity was 1.75×10^{-9} lb-s/in.^{2} and the gas constant was 423,184 in.^{2}/s^2/°F.
- The operating speed was 50,000 rpm and the pressure differential was 50 psig from OD to ID.

The program output is indicated on Table 20. The computed load is 13.08 lb as compared to the 13 lb specified, which is well within the tolerance. The computed clearance is 0.000296 in. Plots of the clearance and pressure distribution are indicated on Figures 48 and 49.

Table 19. GFACE Multipad Step Seal

```
-JOURNAL POSITION & FORCES

  MINIMUM CLEARANCE      =   0.000165 IN
  LOAD CAPACITY          =  39.43     LB
  MOMENT ABOUT X-X       =   6.680    IN-LB
  MOMENT ABOUT Y-Y       =  -1.503    IN-LB

  POWER LOSS             =  0.1527E-01 HP

  LEAKAGE AT INNER       = -0.6470E-06 LB/S
  LEAKAGE AT OUTER       =  0.1003E-05 LB/S

-STIFFNESS COEFFICIENTS
  PRINCIPAL  Z       KZZ =  0.2805E+06 LB/IN
  CROSS-COUPLED      KZA =  0.5135E+05 LB/RAD
  CROSS-COUPLED      KZB =  -5180.     LB/RAD
  CROSS-COUPLED      KAZ =  0.5199E+05 IN-LB/IN
  PRINCIPAL  A       KAA =  0.3825E+06 IN-LB/RAD
  CROSS-COUPLED      KAB =  0.4896E+05 IN-LB/RAD
  CROSS-COUPLED      KBZ = -0.1025E+05 IN-LB/IN
  CROSS-COUPLED      KBA = -0.5135E+05 IN-LB/RAD
  PRINCIPAL  B       KBB =  0.3771E+06 IN-LB/RAD

-DAMPING COEFFICIENTS
  PRINCIPAL  Z       DZZ =   17.97     LB-S/IN
  CROSS-COUPLED      DZA =  -18.28     LB-S/RAD
  CROSS-COUPLED      DZB =  -6.224     LB-S/RAD
  CROSS-COUPLED      DAZ =  -19.62     IN-LB-S/IN
  PRINCIPAL  A       DAA =   19.59     IN-LB-S/RAD
  CROSS-COUPLED      DAB =  -89.65     IN-LB-S/RAD
  CROSS-COUPLED      DBZ =  0.1520E-02 IN-LB-S/IN
  CROSS-COUPLED      DBA =   90.14     IN-LB-S/RAD
  PRINCIPAL  B       DBB =   24.25     IN-LB-S/RAD
```

95TR34-V2

Table 20. GFACE Single Tapered Land Seal

```
-JOURNAL POSITION & FORCES

  MINIMUM CLEARANCE       =    0.000296 IN
  LOAD CAPACITY           =   13.08     LB
  MOMENT ABOUT X-X        =   26.82     IN-LB
  MOMENT ABOUT Y-Y        =   -5.263    IN-LB

  POWER LOSS              =   0.2926E-01 HP

  LEAKAGE AT INNER        = -0.2327E-04 LB/S
  LEAKAGE AT OUTER        =  0.9632E-05 LB/S

-STIFFNESS COEFFICIENTS

  PRINCIPAL  Z       KZZ =    4719.      LB/IN
  CROSS-COUPLED      KZA =    9396.      LB/RAD
  CROSS-COUPLED      KZB =   -2108.      LB/RAD
  CROSS-COUPLED      KAZ =    9939.      IN-LB/IN
  PRINCIPAL  A       KAA =  0.1990E+05   IN-LB/RAD
  CROSS-COUPLED      KAB =   -4320.      IN-LB/RAD
  CROSS-COUPLED      KBZ =   -1544.      IN-LB/IN
  CROSS-COUPLED      KBA =   -2980.      IN-LB/RAD
  PRINCIPAL  B       KBB =    1237.      IN-LB/RAD

-DAMPING COEFFICIENTS
  PRINCIPAL  Z       DZZ =    1.608      LB-S/IN
  CROSS-COUPLED      DZA =    3.256      LB-S/RAD
  CROSS-COUPLED      DZB =  -0.6525      LB-S/RAD
  CROSS-COUPLED      DAZ =    3.255      IN-LB-S/IN
  PRINCIPAL  A       DAA =    6.599      IN-LB-S/RAD
  CROSS-COUPLED      DAB =   -1.312      IN-LB-S/RAD
  CROSS-COUPLED      DBZ = -0.1294E-03   IN-LB-S/IN
  CROSS-COUPLED      DBA =   -1.299      IN-LB-S/RAD
  PRINCIPAL  B       DBB =   0.3091      IN-LB-S/RAD
```

95TR34-V2

7.3 Hydrostatic Recess Seal

The configuration of the hydrostatic recess seal is shown on Figure 50. It is a four-recess seal and variable grid was used to get a fine grid definition at the recess extremities where large clearance changes occur. Since the entire seal was modeled, a large number of variable grid points must be entered. For this example, 137 entries in the circumferential direction were inputted. For hydrostatic recesses, the additional input variables are the recess depths and locations and the location and sizes of the feeding orifices.

The land clearance is 0.0005 in. and the recess depth is 0.020 in. One orifice feeds each recess at a diameter of 0.010 in. Other important parameters are:

- Supply pressure = 200 psig
- Absolute temperature = 1460° R (1000°F)
- Gas viscosity = 5.35 x 10^{-9} lb-s/in.^{2}
- Speed = 0
- OD pressure = 200 psig
- ID pressure = 0 psig.

The output summary is shown on Table 21. Note that the damping is negative indicating an unstable seal. Hydrostatic gas lubricated seals or bearings are prone to pneumatic hammer or chattering of the opposed surfaces. Generally, recesses should be avoided and gas introduced into the film strictly by the inlet holes. This type of feeding is discussed in the next sample problem. The clearance and pressure distributions are shown on Figures 51 and 52, respectively.

7.4 Inherently Compensated Hydrostatic Seal

A hydrostatic seal with a series of feed holes that enter directly into the film employs inherent compensation which implies that the restrictor area is the curtain area of a cylinder with diameter equal to the hole diameter and length equal to the film height at the hole location. The seal analyzed had an inside diameter of 2 in. and an outside diameter of 4 in. For this example, holes were specified at a radius of 2.4 in and every 10 degrees in the circumferential direction. The hole size was 0.010 in. diameter.

Other parameters are as follows:

- Clearance = 0.0005 in.
- Supply pressure = 200 psig
- Gas constant = 246,900 in.^{2}/s^2/°R
- Absolute temperature = 1460 °R (1000 °F)
- Viscosity = 5.35 x 10^{-9} lb-s/in.^{2}
- Speed = 0
- OD pressure = 200 psig
- ID pressure = 0 psig.

Table 21. GFACE Recess Seal

```
-JOURNAL POSITION & FORCES

  MINIMUM CLEARANCE        =    0.000500 IN
  LOAD CAPACITY            =   6265.     LB
  MOMENT ABOUT X-X         =  0.1421E-06 IN-LB
  MOMENT ABOUT Y-Y         = -0.1740E-06 IN-LB

  POWER LOSS               =  0.0000E+00 HP

  LEAKAGE AT INNER         = -0.8928E-03 LB/S
  LEAKAGE AT OUTER         = -0.2859E-03 LB/S

-STIFFNESS COEFFICIENTS
  PRINCIPAL  Z       KZZ =  0.3003E+07 LB/IN
  CROSS-COUPLED      KZA =   79.56     LB/RAD
  CROSS-COUPLED      KZB =   79.73     LB/RAD
  CROSS-COUPLED      KAZ = -0.1382E-01 IN-LB/IN
  PRINCIPAL  A       KAA =  0.4779E+07 IN-LB/RAD
  CROSS-COUPLED      KAB =  -1.289     IN-LB/RAD
  CROSS-COUPLED      KBZ = -0.3776     IN-LB/IN
  CROSS-COUPLED      KBA = -0.7086     IN-LB/RAD
  PRINCIPAL  B       KBB =  0.4779E+07 IN-LB/RAD

-DAMPING COEFFICIENTS
  PRINCIPAL  Z       DZZ = -0.1258E+05 LB-S/IN
  CROSS-COUPLED      DZA =  -4.177     LB-S/RAD
  CROSS-COUPLED      DZB =  -4.178     LB-S/RAD
  CROSS-COUPLED      DAZ =  0.7818E-04 IN-LB-S/IN
  PRINCIPAL  A       DAA = -0.1440E+05 IN-LB-S/RAD
  CROSS-COUPLED      DAB =  0.7198E-02 IN-LB-S/RAD
  CROSS-COUPLED      DBZ =  0.1054E-05 IN-LB-S/IN
  CROSS-COUPLED      DBA =  0.3959E-02 IN-LB-S/RAD
  PRINCIPAL  B       DBB = -0.1440E+05 IN-LB-S/RAD
```

95TR34-V2

The output summary for this case is shown on Table 22. Notice that the direct damping in the axial direction (DZZ) is a positive number and that this configuration is not unstable as is the prior problem that incorporated recesses. There is no trapped volume that can cause out-of-phase stability problems.

The clearance and pressure distributions are shown on Figures 53 through 55.

7.5 Radial Taper Seal

One of the options in GFACE is the incorporation of a radial taper in the seal face. A tapered seal was analyzed. The following parameters were applied:

- Inner diameter = 1.0 in.
- Outer diameter = 1.5 in.
- Clearance = 0.0004 in.
- Pad angle = 360°
- Specific heat = 1.4
- Gas constant = 255,488 in.^{2}/s^2/°R
- Absolute temperature = 520 °R (60 °F)
- Viscosity = 2.5 x 10^{-9} lb-s/in.^{2}
- Speed = 30,000 rpm
- OD pressure = 0 psig
- ID pressure = 400 psig

An ID taper was incorporated (see Table 23) that extended half way up the face of the seal, and the slope of the taper was 0.1833. Clearance and pressure distributions are indicated on Figures 56 and 57.

Table 22. GFACE Hydrostatic Source Seal

-JOURNAL POSITION & FORCES

MINIMUM CLEARANCE		=	0.000500	IN
LOAD CAPACITY		=	6588.	LB
MOMENT ABOUT X-X		=	0.9286E-09	IN-LB
MOMENT ABOUT Y-Y		=	-0.8015E-09	IN-LB
POWER LOSS		=	0.0000E+00	HP
LEAKAGE AT INNER		=	-0.1165E-02	LB/S
LEAKAGE AT OUTER		=	-0.1727E-03	LB/S
-STIFFNESS COEFFICIENTS				
PRINCIPAL Z	KZZ	=	0.1722E+07	LB/IN
CROSS-COUPLED	KZA	=	410.1	LB/RAD
CROSS-COUPLED	KZB	=	410.1	LB/RAD
CROSS-COUPLED	KAZ	=	-0.2244E-03	IN-LB/IN
PRINCIPAL A	KAA	=	0.2562E+07	IN-LB/RAD
CROSS-COUPLED	KAB	=	0.6152E-03	IN-LB/RAD
CROSS-COUPLED	KBZ	=	-0.1138E-03	IN-LB/IN
CROSS-COUPLED	KBA	=	0.1788E-02	IN-LB/RAD
PRINCIPAL B	KBB	=	0.2562E+07	IN-LB/RAD
-DAMPING COEFFICIENTS				
PRINCIPAL Z	DZZ	=	4538.	LB-S/IN
CROSS-COUPLED	DZA	=	-0.1395	LB-S/RAD
CROSS-COUPLED	DZB	=	-0.1395	LB-S/RAD
CROSS-COUPLED	DAZ	=	0.8589E-07	IN-LB-S/IN
PRINCIPAL A	DAA	=	0.2322E+05	IN-LB-S/RAD
CROSS-COUPLED	DAB	=	-0.2646E-06	IN-LB-S/RAD
CROSS-COUPLED	DBZ	=	0.2733E-10	IN-LB-S/IN
CROSS-COUPLED	DBA	=	-0.7288E-06	IN-LB-S/RAD
PRINCIPAL B	DBB	=	0.2322E+05	IN-LB-S/RAD

95TR34-V2

Table 23. GFACE Inside Radial Tapered Land Seal

-JOURNAL POSITION & FORCES

MINIMUM CLEARANCE		=	0.000400	IN
LOAD CAPACITY		=	277.4	LB
MOMENT ABOUT X-X		=	-0.1214E-12	IN-LB
MOMENT ABOUT Y-Y		=	-0.8861E-13	IN-LB
POWER LOSS		=	0.3356E-02	HP
LEAKAGE AT INNER		=	0.1264E-01	LB/S
LEAKAGE AT OUTER		=	0.1246E-01	LB/S
-STIFFNESS COEFFICIENTS				
PRINCIPAL Z	KZZ	=	0.5404E+05	LB/IN
CROSS-COUPLED	KZA	=	47.84	LB/RAD
CROSS-COUPLED	KZB	=	47.84	LB/RAD
CROSS-COUPLED	KAZ	=	-0.3066E-07	IN-LB/IN
PRINCIPAL A	KAA	=	0.2056E+05	IN-LB/RAD
CROSS-COUPLED	KAB	=	321.0	IN-LB/RAD
CROSS-COUPLED	KBZ	=	0.2232E-07	IN-LB/IN
CROSS-COUPLED	KBA	=	-321.0	IN-LB/RAD
PRINCIPAL B	KBB	=	0.2056E+05	IN-LB/RAD
-DAMPING COEFFICIENTS				
PRINCIPAL Z	DZZ	=	1.088	LB-S/IN
CROSS-COUPLED	DZA	=	-0.1101E-03	LB-S/RAD
CROSS-COUPLED	DZB	=	-0.1101E-03	LB-S/RAD
CROSS-COUPLED	DAZ	=	0.8441E-13	IN-LB-S/IN
PRINCIPAL A	DAA	=	0.2047	IN-LB-S/RAD
CROSS-COUPLED	DAB	=	-0.1491E-02	IN-LB-S/RAD
CROSS-COUPLED	DBZ	=	-0.2549E-16	IN-LB-S/IN
CROSS-COUPLED	DBA	=	0.1491E-02	IN-LB-S/RAD
PRINCIPAL B	DBB	=	0.2047	IN-LB-S/RAD

95TR34-V2

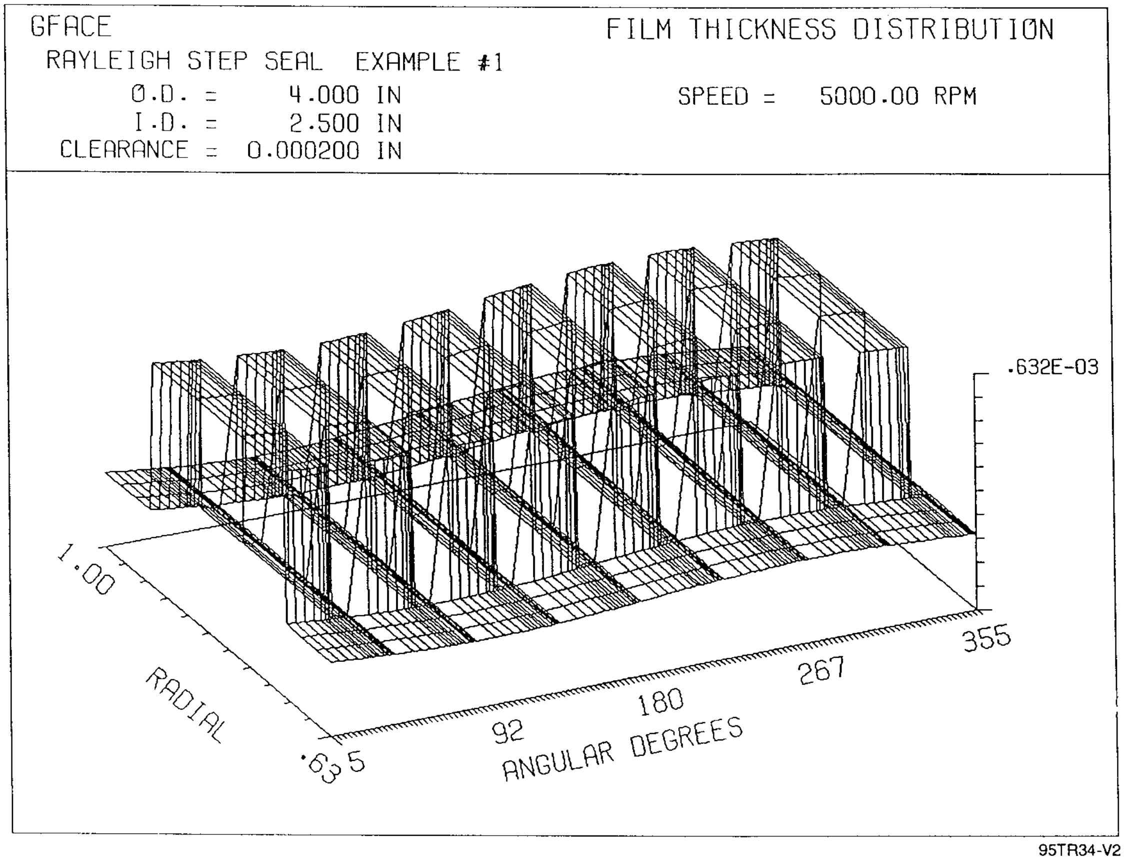

Figure 44. Sample Problem 1, Rayleigh-Step Seal, Clearance Distribution

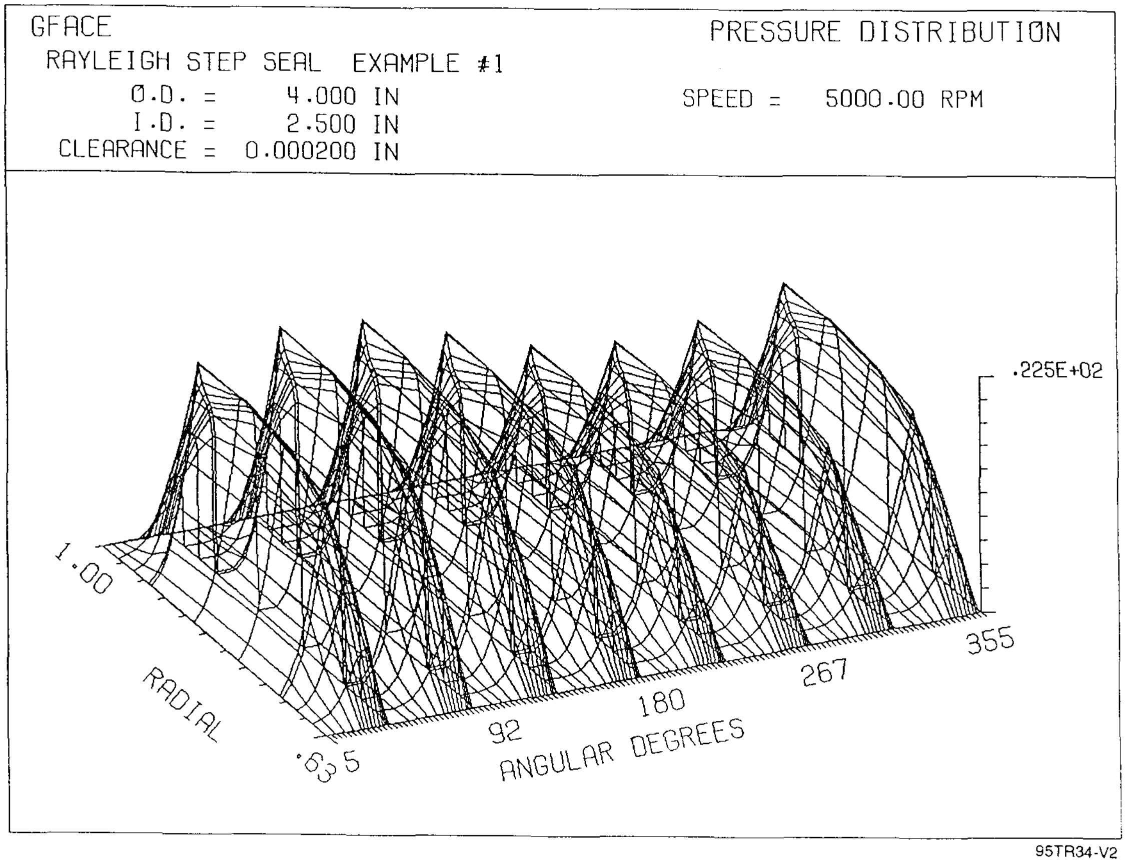

Figure 45. Sample Problem 1, Rayleigh-Step Seal, Pressure Distribution

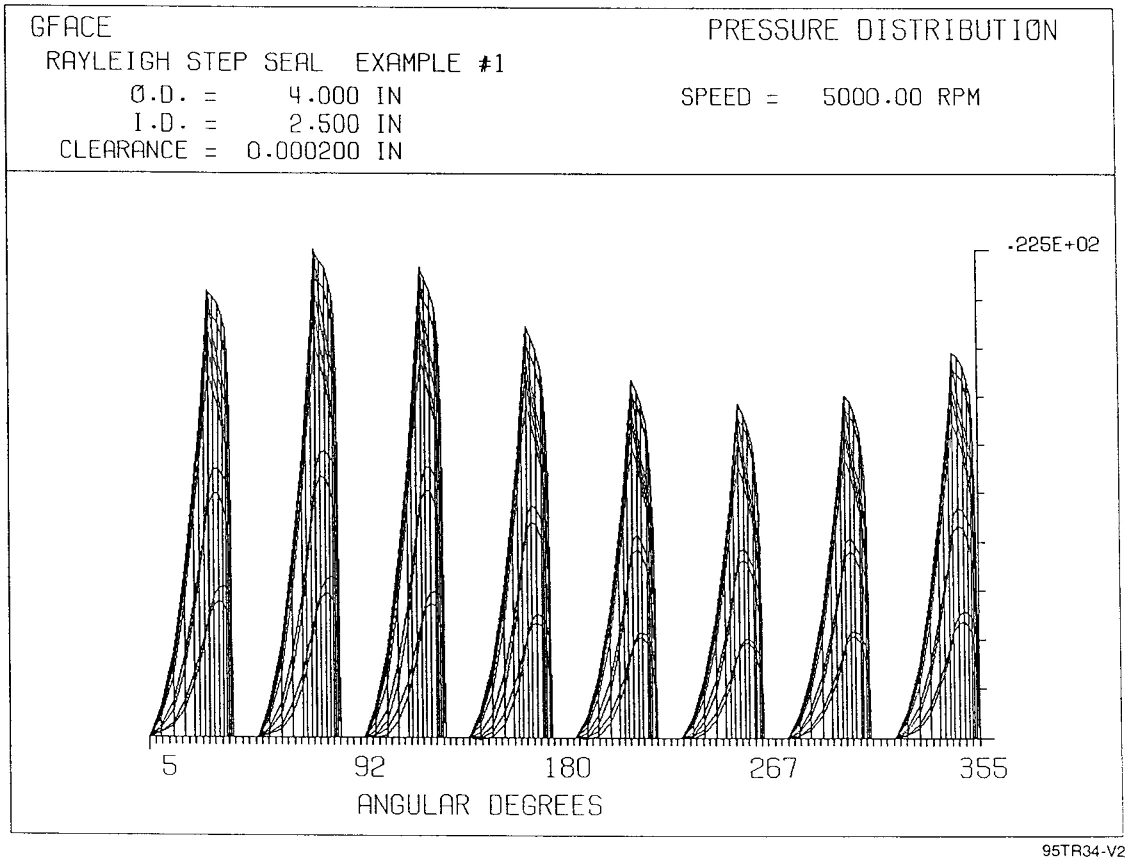

Figure 46. Sample Problem 1, Rayleigh-Step Seal, Pressure Distribution, Looking Along Radius

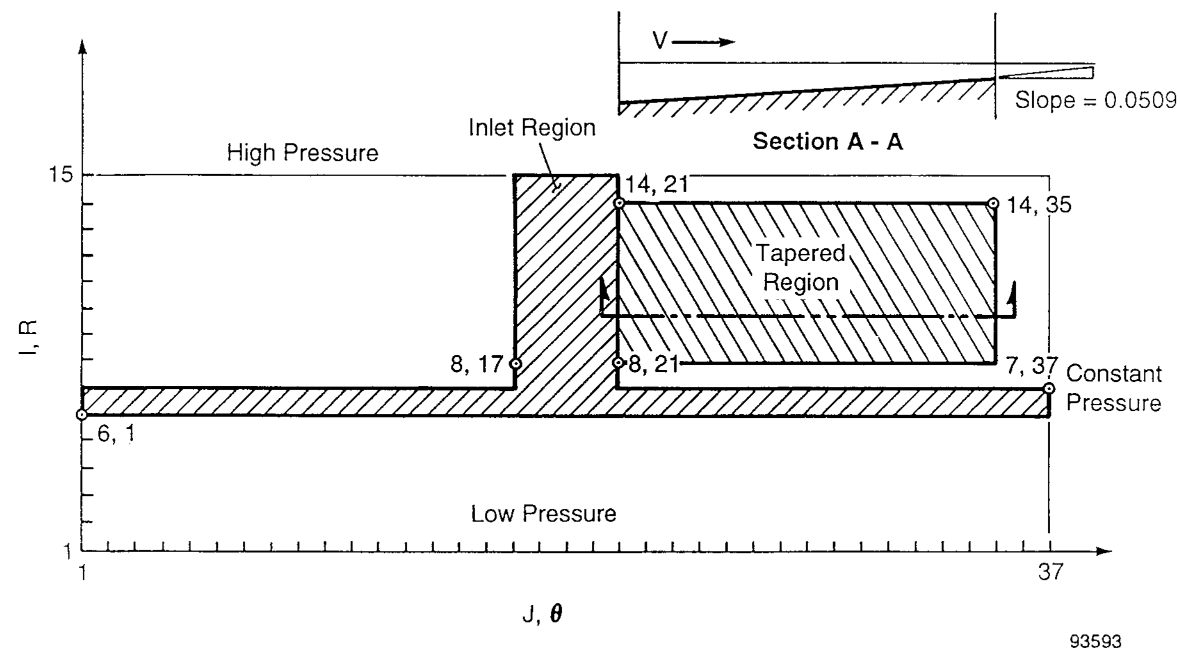

Figure 47. Sample Problem 2, Tapered Land Seal, Grid Regions

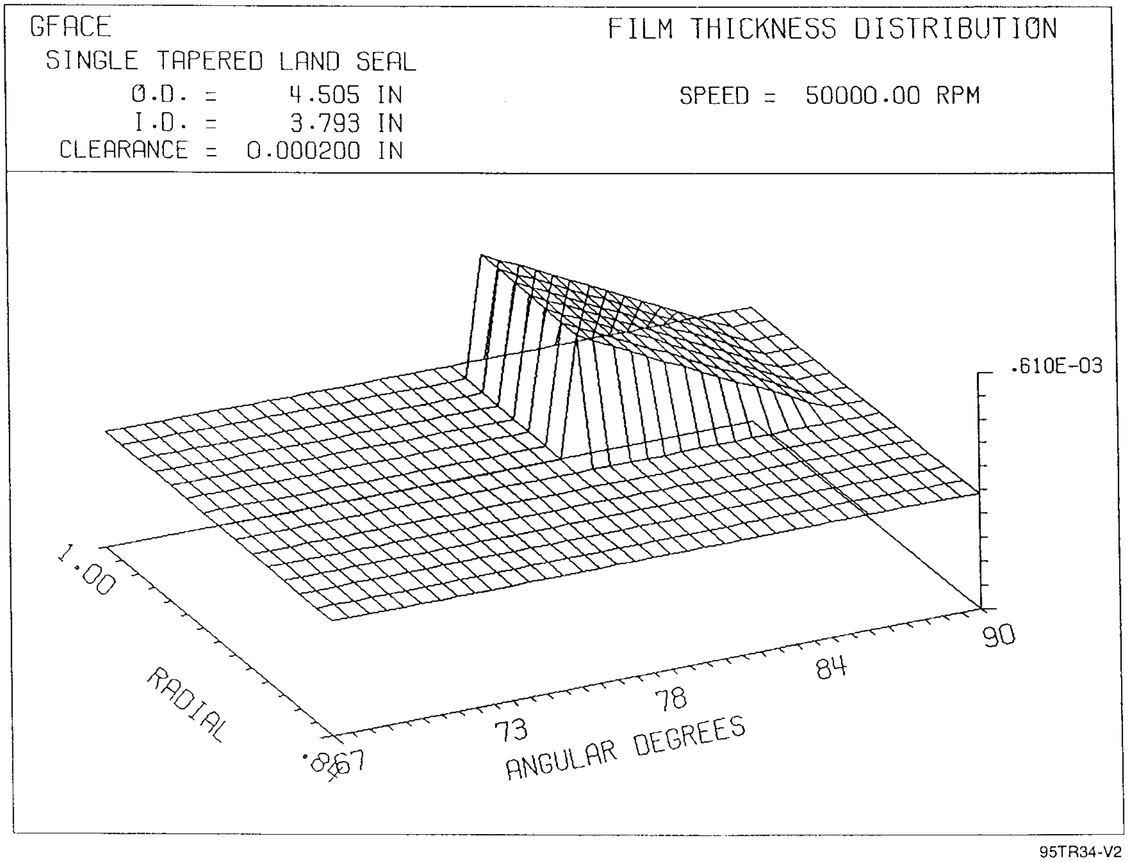

Figure 48. Sample Problem 2, Tapered Land Seal, Clearance Distribution

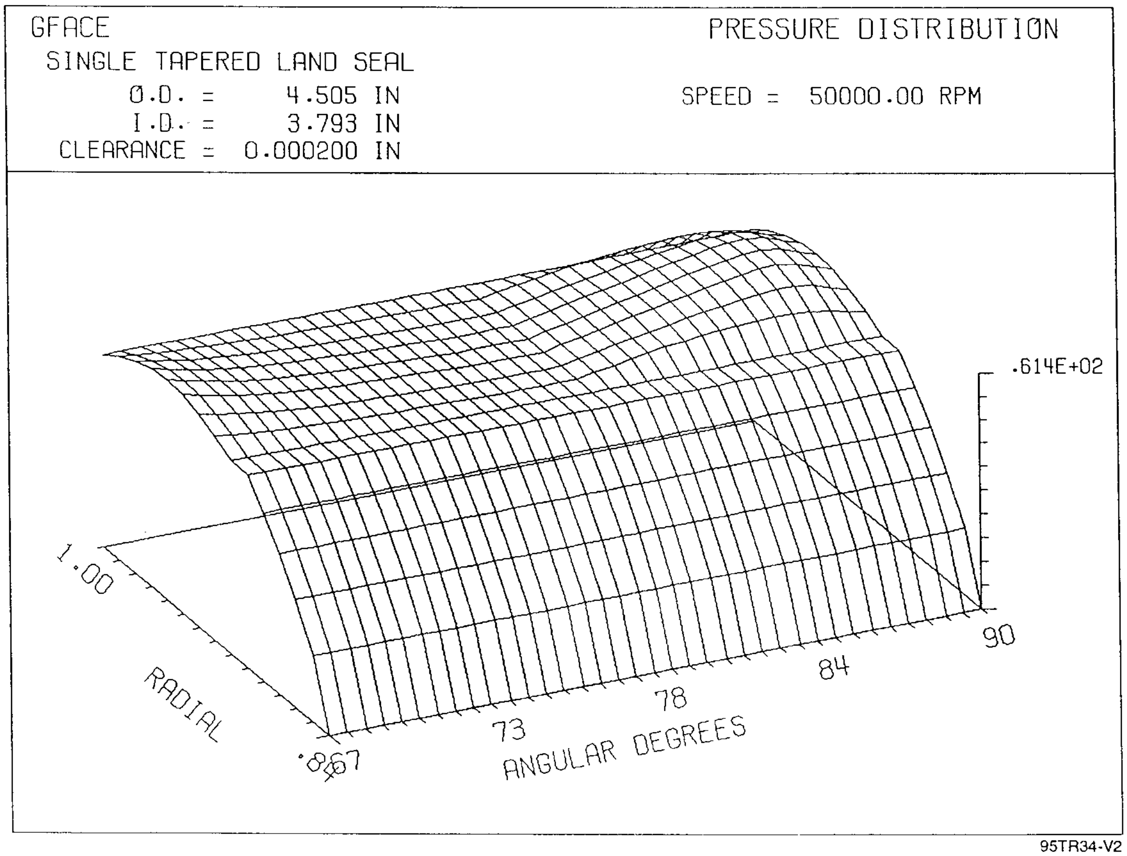

Figure 49. Sample Problem 2, Tapered Land Seal, Pressure Distribution

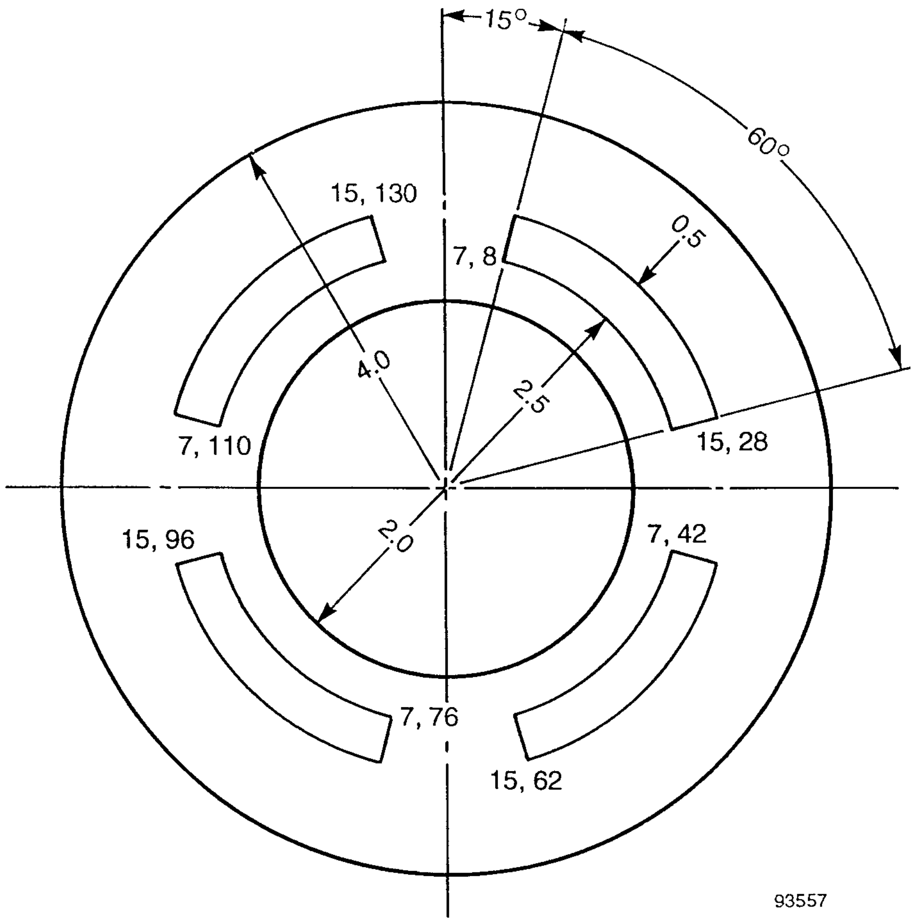

Figure 50. Sample Problem 4, Four-Recess Seal Configuration

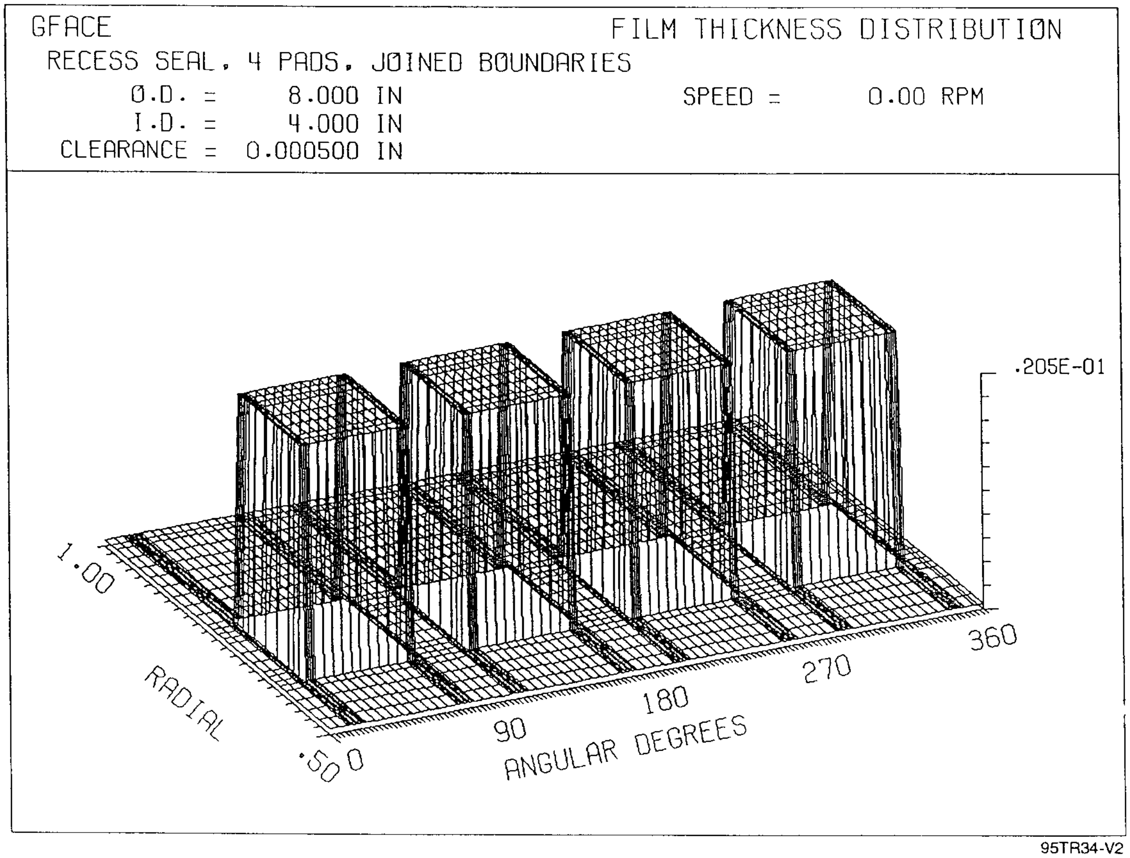

Figure 51. Sample Problem 4, Four-Recess Seal, Clearance Distribution

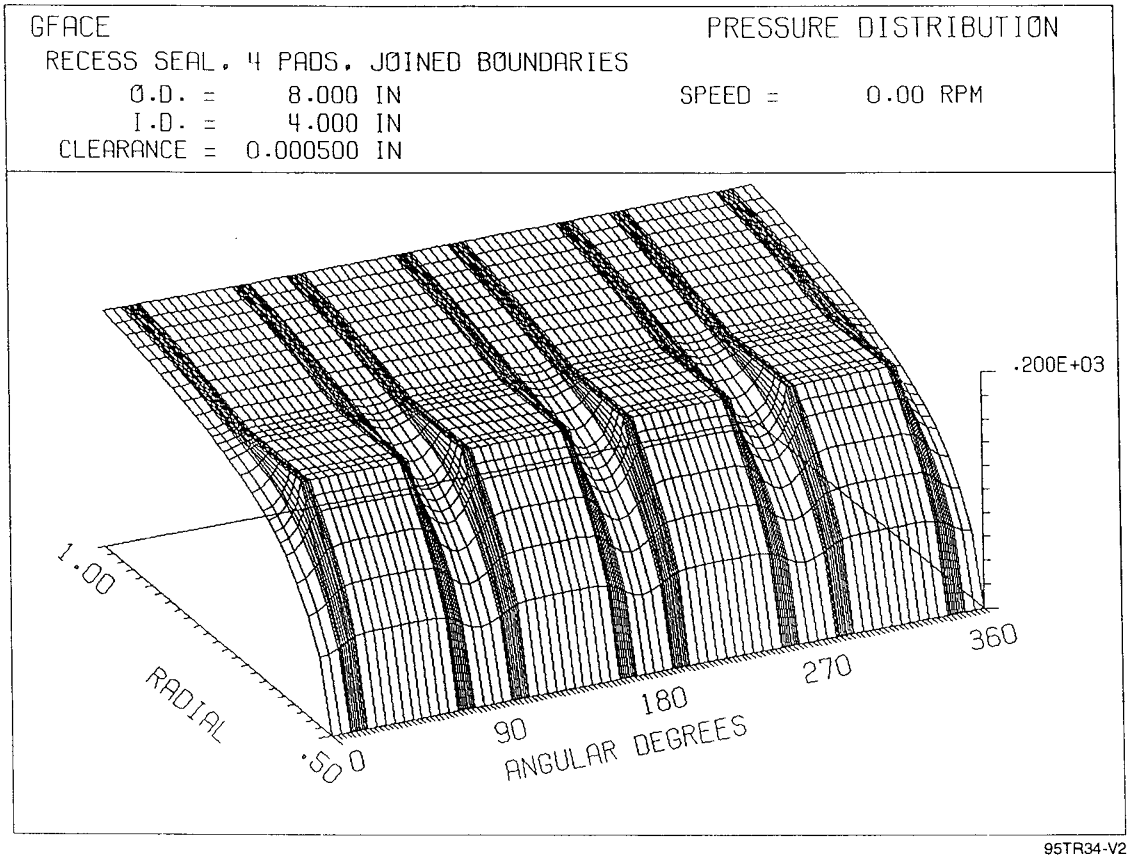

Figure 52. Sample Problem 4, Four-Recess Seal, Pressure Distribution

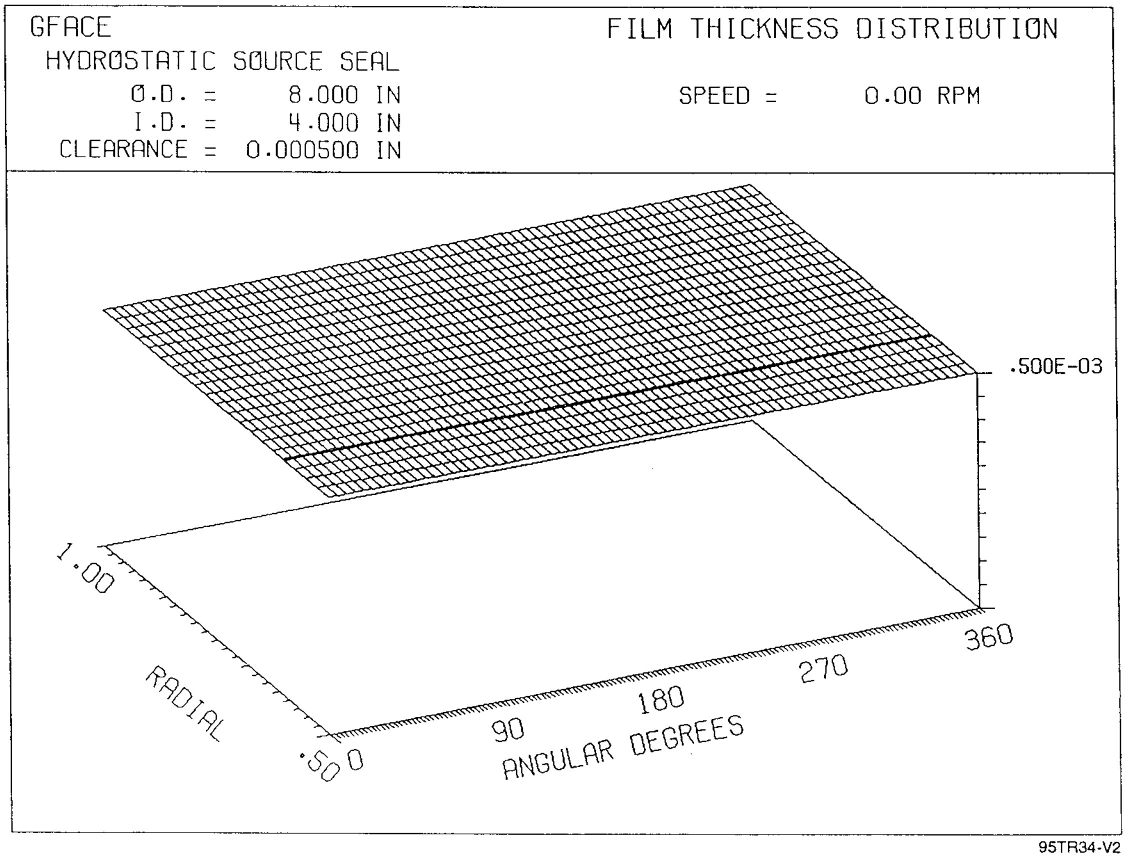

Figure 53. Sample Problem 6, Inherently Compensated Seal, Clearance Distribution

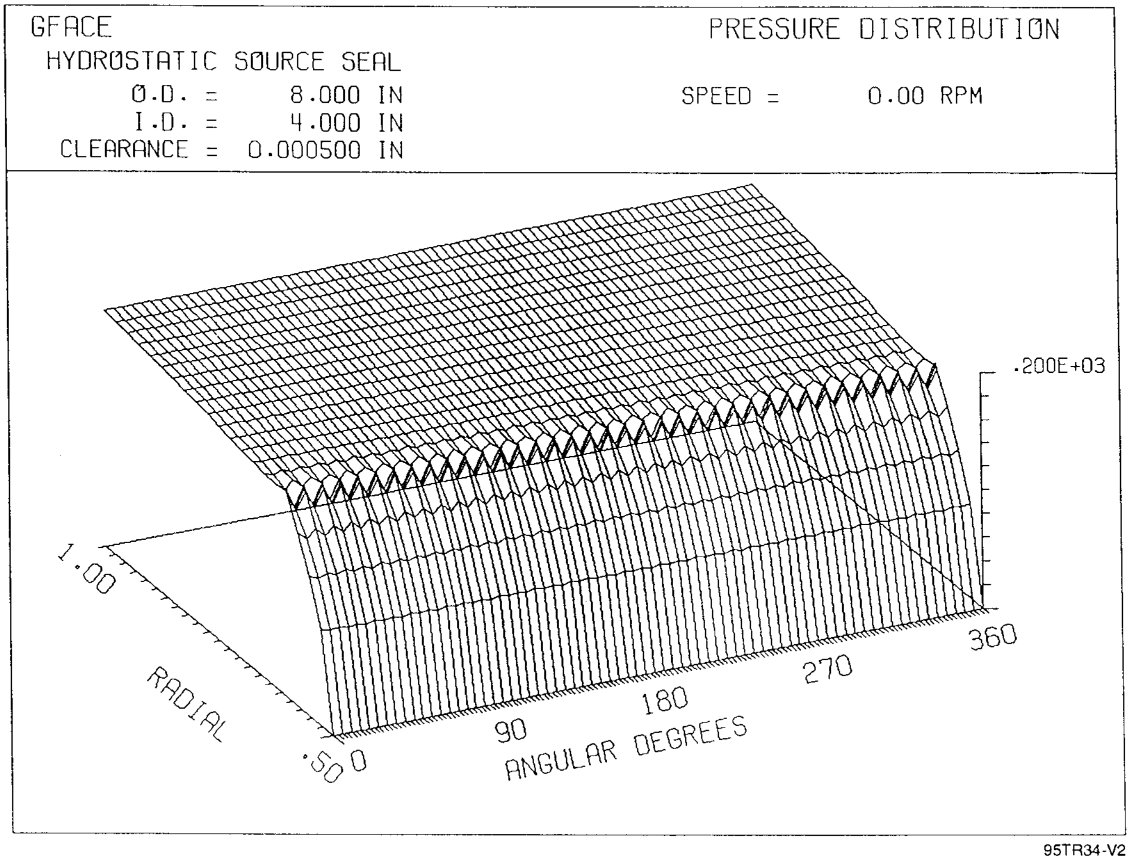

Figure 54. Sample Problem 6, Inherently Compensated Seal, Pressure Distribution

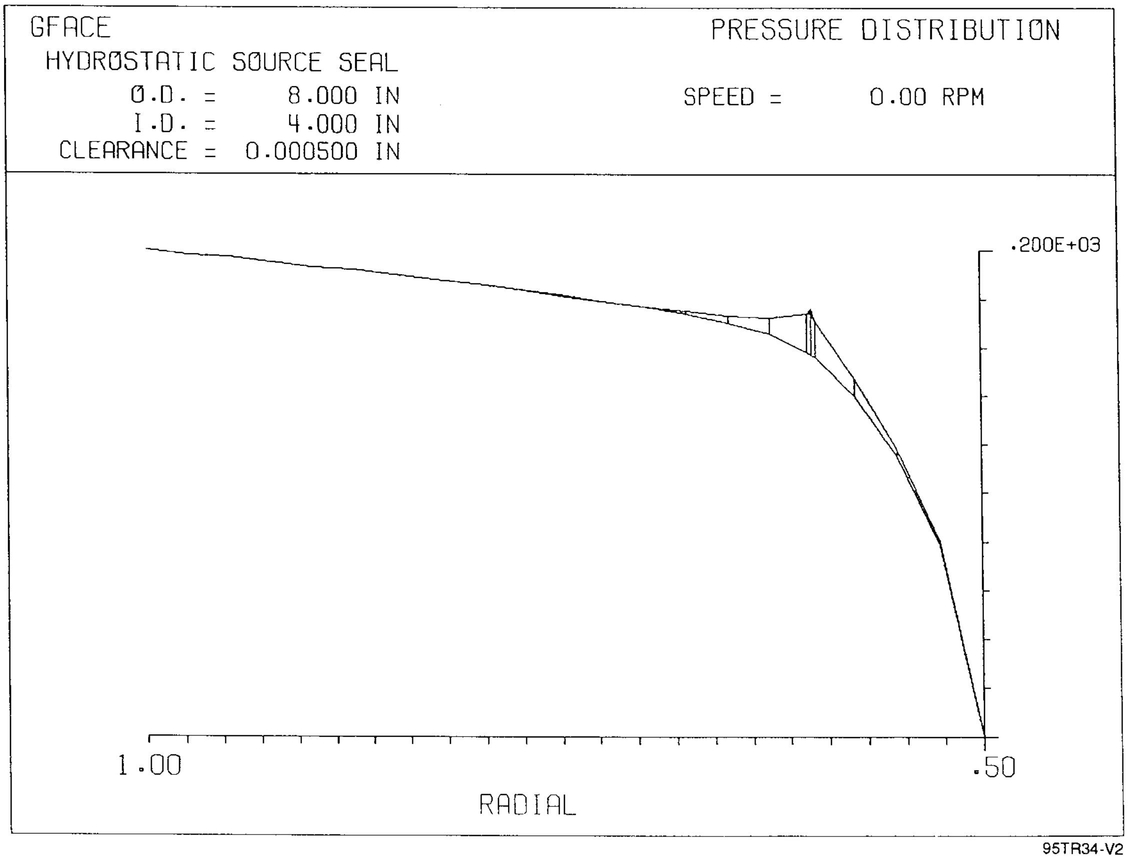

Figure 55. Sample Problem 6, Inherently Compensated Seal, Pressure Distribution Along Radius

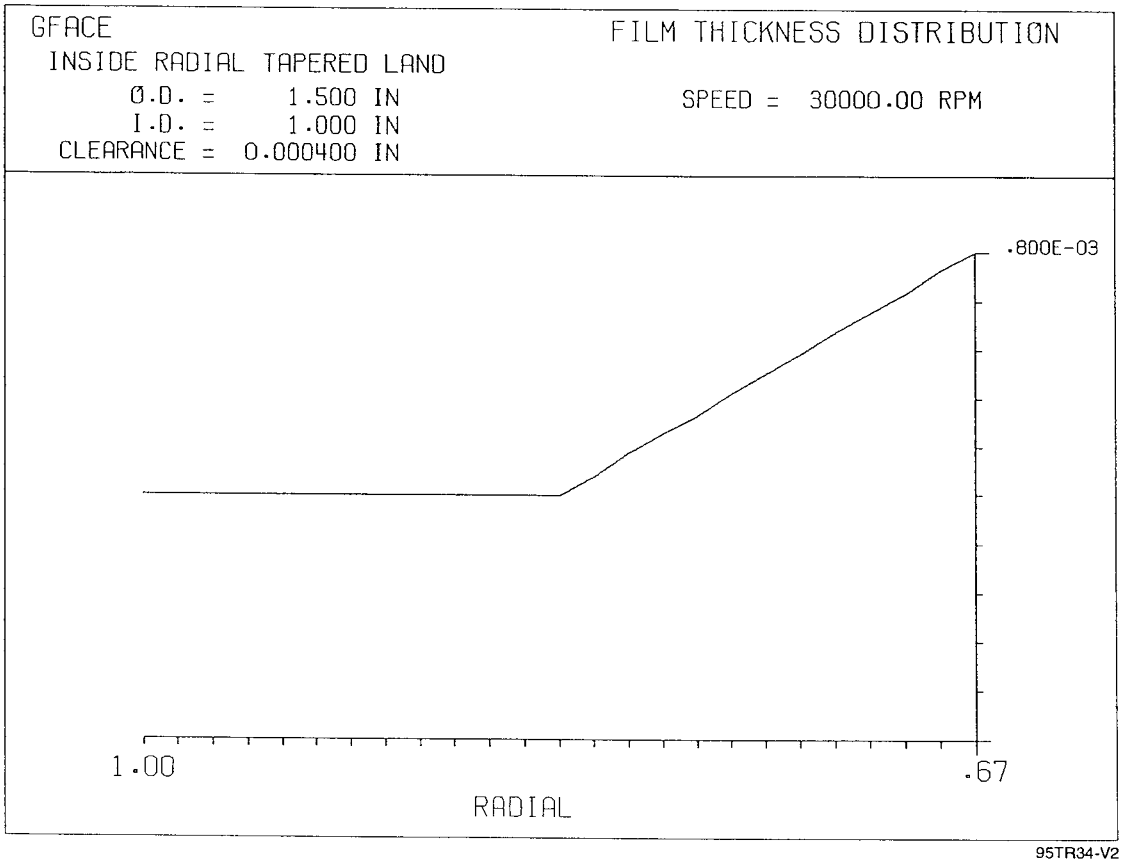

Figure 56. Sample Problem 7, Radial Taper Seal, Clearance Distribution

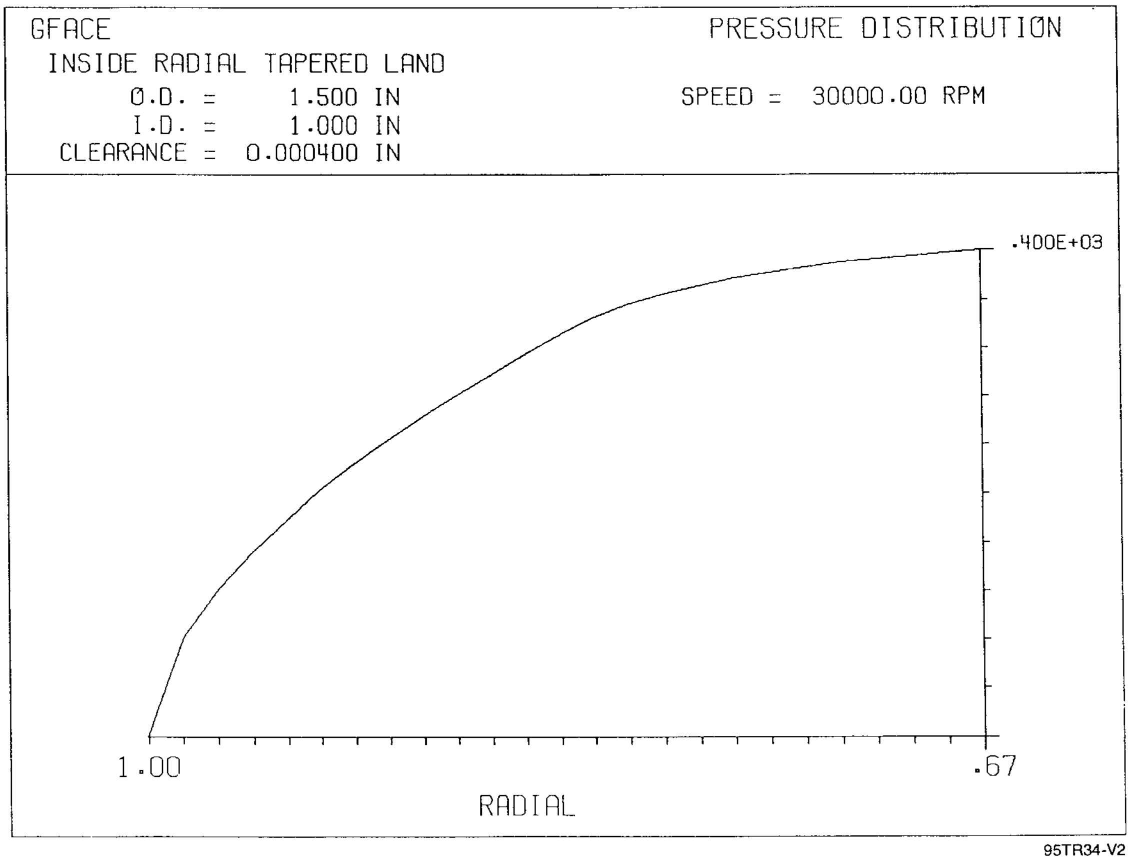

Figure 57. Sample Problem 7, Radial Taper Seal, Pressure Distribution

8.0 VERIFICATION OF CODE GFACE

8.1 Tilted Slider

Etsion and Fleming[9] found that maximum load capacity of a slider occurs when it is tilted about the trailing edge and they produced analytical data for varying compressibility numbers, sector angles and radius ratios. Table 24 below shows comparisons for a 45 degree sector.

Table 24. Comparisons of GFACE with Etsion and Fleming Load Capacity

Λ	ε	ζ degrees	N rpm	W' GFACE	W' Etsion & Fleming	Δ%
1	2.5	.0143	133.69	0.00476	0.0047	1.27
10	2.5	.0143	1,336.9	0.0466	0.0460	1.30
25	3.0	.0172	3,342.25	0.1086	0.1080	0.56
50	3.5	.0201	6,684.5	0.1897	0.1850	2.5
100	4.5	.0258	13,369	0.3014	0.2950	2.17

where:

$$\Lambda = \frac{6\mu\omega r_2^2}{h_2^2 P_a}; \quad \varepsilon = \frac{\zeta' r_2}{h_2}; \quad W' = \frac{2W}{P_a \beta (r_2^2 - r_1^2)}$$

μ = absolute viscosity , $= 1.75 \times 10^{-9} \dfrac{\text{lb} - \text{s}}{\text{in.}^2}$

ω = shaft speed, $\dfrac{\text{rad}}{\text{s}}$

N = shaftspeed, rpm

W = load, lb

P_a = ambient pressure, = 14.7psia

r_2 = outside radius, = 2.0 in.

r_1 = inside radius, = 0.6 in.

ζ' = tilt angle, radians

ζ = tilt angle, degrees

h_2 = trailing edge film thickness = 0.0002 in.

The comparative values of non-dimensional load, W' are within 3%. Comparisons were also made for the Power Loss Coefficient (PLC). Results are indicated on Table 25.

Table 25. Comparison of GFACE with Etsion and Fleming Power Loss

Λ	ε	PLC GFACE	PLC Etsion
1	2.5	49.4	12
10	2.5	12.86	12
25	3.0	12.987	13
50	3.5	14.193	15
100	4.5	16.15	17

$$PLC = \frac{F}{W\omega h_2} \text{ where:}$$

F = Power Loss, in.-lb / s

The correlation is excellent except for Λ =1. The friction levels are on a precipitous upward curve at this value of Λ and it is very easy to be off by a substantial amount. The curve fitting of the Etsion data could easily produce significant error. It is the author's inclination that the GFACE values are accurate.

8.2 Ausman Rayleigh-Step Analysis

In 1961 Ausman produced theoretical results for a Rayleigh step sector[10] for varying radius ratios, number of pads and compressibility parameter Λ. Comparative results with GFACE are indicated on Table 26.

Table 26. GFACE Comparison with Ausman Rayleigh-Step Pad

Λ	n	W	W' GFACE	W' Ausman	Δ %
10	8	0.7539	0.0456	0.046	-.87
20	7	1.821	0.0957	0.103	-7
40	7	3.701	0.1946	0.219	-11
80	6	7.766	0.3479	0.397	-12
160	6	11.71	0.5246	0.572	-8

$$\Lambda = \frac{6\mu\omega r_2^2}{P_a h_2^2}; \quad n = \text{number of pads}; \quad \frac{r_1}{r_2} = 0.5$$

Variables remain as defined above. The correlation as indicated is fair, but not as good as expected. The Ausman analysis was done in 1961, when contemporary numerical analysis was unavailable. Therefore, it is believed that the GFACE data is more accurate.

Further cases were compared with information in Gross[11] for a step pad configuration with the following geometry and operating conditions:

Shaft speed, N	36,000 rpm
Ambient pressure, P_a	42.6 psia
Viscosity, μ	5×10^{-9} lb-s/in.^{2}
Radius ratio, R	0.6
Outside radius, r_2	1.75 in.
Inside radius, r_1	1.05 in.
Pad Angle, β	38^o
Step Angle, β_1	15^o
Land film thickness, h_2	0.0005 in.

Comparative results are shown on Figures 58 and 59. The comparisons are reasonable and discrepancies are probably due to the inaccuracies of the numerical methods utilized by Gross that appears to overestimate load capacity and underestimate power loss. Thus, the application of GFACE would provide conservative designs as compared to Gross.

8.3 Internal Verification

There are a number of internal checks that can be made to assure numerical correctness and accuracy. The first case is a recess hydrostatic bearing without rotation. Then the mass flow entering the recess from an external source should equal the mass flow exiting the pad. A 35 degree pad was examined with variable grid geometry and a recess specified. Four flow paths were specified at the perimeters of the pad. The computer output indicated the following:

Flow exiting from pad:

- Flow path 1 = -0.1968×10^{-4} lb/s
- Flow path 1 = 0.3519×10^{-4} lb/s
- Flow path 1 = -0.6005×10^{-4} lb/s
- Flow path 1 = 0.8530×10^{-4} lb/s
- Total = 2.0022×10^{-4} lb/s

The negative number implies that the flow is in a direction opposite to that of the positive sign convention. In this case all flows are exiting the pad and the total outflow is the absolute sum.

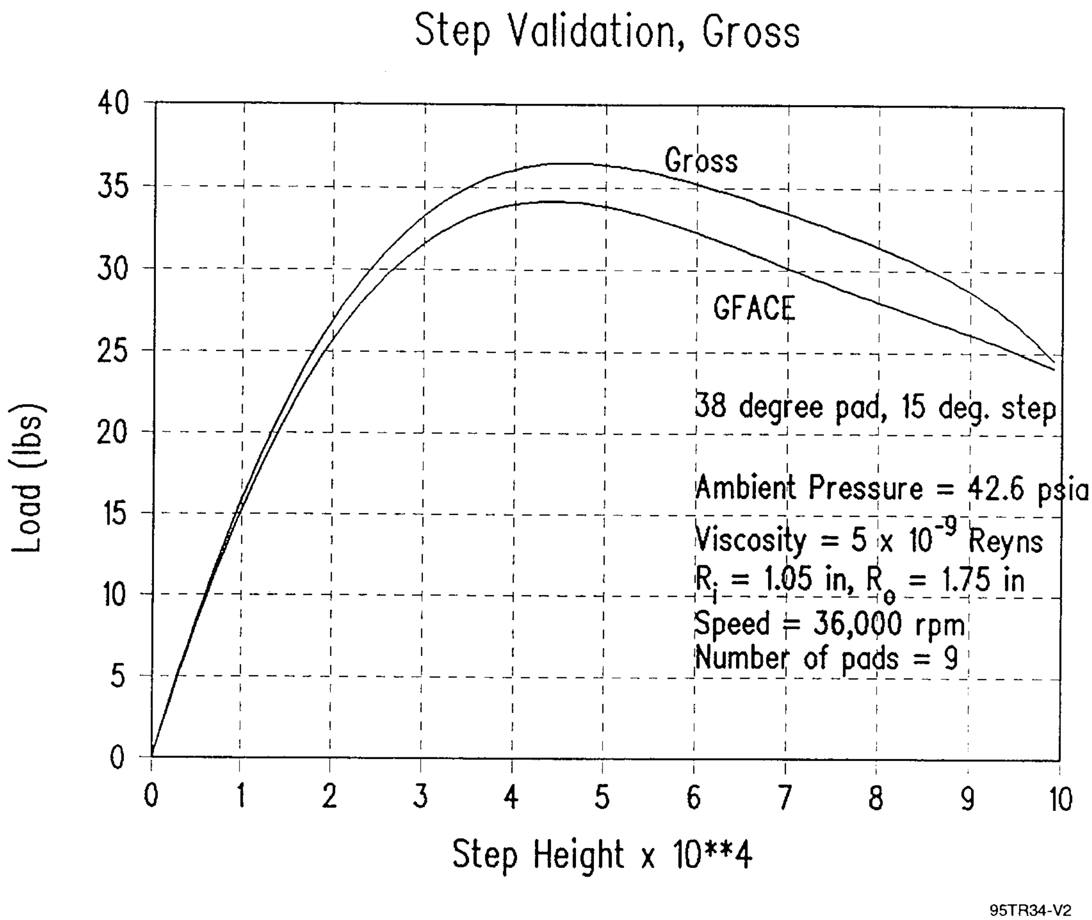

Figure 58. Validation, Step Pad, Load vs. Step Height

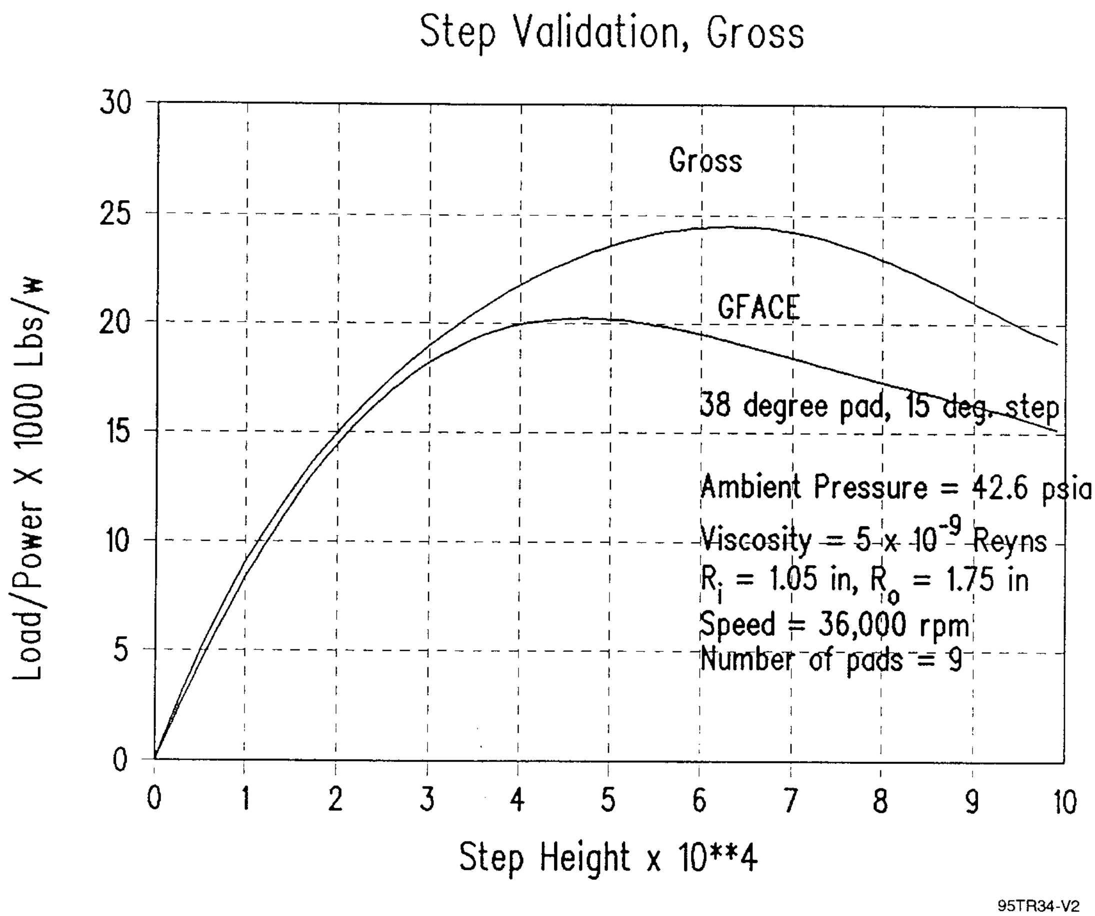

Figure 59. Validation, Step-Pad, Load/Power vs. Step Height

The inflow is the total flow going through the orifice feeding the recess. The following equation applies:

$$f_o = 386.4\ A_o\ C_D\ G_1\ P_S\left\{\left(\frac{P_r}{P_s}\right)^{\frac{2}{\gamma}}\left[1-\left(\frac{P_r}{P_s}\right)^{\frac{\gamma-1}{\gamma}}\right]\right\}^{\frac{1}{2}}$$

A_o = orifice area = $\dfrac{\pi d_o^{\ 2}}{4} = \dfrac{\pi 0.010^2}{4} = 7.854 \text{ x } 10^{-5}$

C_D = Coefficient of Discharge = 0.9

$\dfrac{P_r}{P_s} = \dfrac{\text{recess pressure}}{\text{supply pressure}} = \dfrac{131+14.7}{200+14.7} = 0.678621$

$G_1 = \sqrt{\dfrac{2\gamma}{G_c\Theta(\gamma-1)}}$

where γ = ratio of specific heats = 1.4

G_c = gas constant = 246,900 $\dfrac{\text{in.}^2}{\text{s}^2 - {}^\circ\text{R}}$

Θ = absolute temperature = 1460^0R

$$f_o = 386.4\text{x}7.854\text{x}10^{-5}\text{x}0.9\text{x}1.3935\text{x}10^{-4}\text{x}214.7$$

$$\text{x}\left\{(0.678621)^{\frac{2}{1.4}}\left[1-(0.678621)^{\frac{0.4}{1.4}}\right]\right\}^{\frac{1}{2}} = 2.006\text{x}10^{-4}\ \frac{\text{lb}}{\text{s}}$$

The correlation between the exit and inlet flows is excellent.

A check on the stiffness can be made, at zero excitation frequency, by checking the stiffness values against incremental displacements in the three degrees of freedom. A Rayleigh step pad was examined. Pertinent parameters are as follows:

Outside diameter = 4 in.

Inside diameter = 2.5 in.

Clearance = 0.0002 in.

Step height = 0.004 in.

Specific heat = 1.4

Gas constant = 246,900 in^2/s^2/°R

Absolute temperature = 1460 °R (1000 °F)

Operating Speed = 5000 rpm

Perimeter pressure = 0 psig

Pad angle = 35°

Step angle = 25°

Step width = 0.43 in. (centrally located).

Table 27 shows the results of the displacements on Forces and Moments.

Table 27. Forces and Moments as a Function of Displacements
(δz = 0.0001 in., $\delta\alpha$ = 0.0001 degrees., $\delta\beta$ = 0.0001 degrees)

Displacement	0	Z	α	β
Axial Force, F_Z lb	4.861	4.531	4.854	4.869
Moment about x-axis, M_{XX} in.-lb	3.838	3.571	3.832	3.844
Moment about Y-axis, M_{YY} in.-lb	-6.946	-6.479	-6.936	6.957

The stiffness is computed by subtracting the equilibrium values from the displaced values and dividing by the displacement. Since a positive displacement results in a negative force differential, the quantities are multiplied by -1 to maintain the accepted stiffness sign convention. Table 28 below compares the computed values of stiffness as calculated by the code against those manually computed by the above procedure. The top value is computed by exercising the stiffness option of the code and the bottom value is the manually computed number. The corroboration is excellent. Additional runs were made with full 360° pads with similar results.

Table 28. Stiffness Comparisons Between Automatic and Manual Computed Values; Rayleigh-step Pad
(δz = 0.0001 in., $\delta\alpha$ = 0.0001 degrees., $\delta\beta$ = 0.0001 degrees)

K_{ZZ}	$K_{\alpha Z}$	$K_{\beta Z}$
34,570	27,930	-48,980
33,000	26,700	-46,700
$K_{Z\alpha}$	$K_{\alpha\alpha}$	$K_{\beta\alpha}$
39,900	31,750	-57,150
40,107	34,377	-57296
$K_{Z\beta}$	$K_{\alpha\beta}$	$K_{\beta\beta}$
-44,200	-35,840	62,710
-45,836	-34,337	63,025

9.0 REFERENCES

1. Munson, J., Steinetz, B. "Specific Fuel Consumption and Increased Thrust Performance Benefits Possible with Advanced Seal Technology," Preprint AIAA-94-2700, presented at 1994 Joint Propulsion Conference, Indianapolis, IN, June 27, 1994.
2. Shapiro, W. "Users Manual for Computer Code GCYLT: Gas Lubricated Cylindrical Seals, Laminar and Turbulent" - Mechanical Technology Incorporated Technical Manual 94TM10.
3. Shapiro, W. "Users Manual for Computer Code GFACE - Gas Lubricated Face Seals," Mechanical Technology Incorporated Technical Manual 93TM5.
4. Castelli, V. and Pirvics, J., "Review of Methods in Gas Bearing Film Analysis," *Trans. ASME, Journal of Lubrication Technology*, October 1968, pp 777-792.
5. Artiles, A., Walowit, J., and Shapiro, W., "Analysis of Hybrid, Fluid-Film Bearings with Turbulence and Inertia Effects," *ASME Publication, Advances in Computer-Aided Bearing Design*, Copyright 1982.
6. Castelli, V. and Shapiro, W., "Improved Method of Numerical Solution of the General Incompressible Fluid-Film Lubrication Problem," *Trans. AMSE, Journal of Lubrication Technology*, April 1967, pp 211-218.
7. Shapiro, W. and Colsher, R., "Dynamic Characteristics of Fluid-Film Bearings," *Proceedings of 6th Turbomachinery Symposium*, Gas Turbine Laboratories, Texas A&M University, December 1967.
8. "Design of Gas Bearings," published by Mechanical Technology, Incorporated, 1969.
9. Etsion I. and D. P. Fleming, "An Accurate Solution of the Gas Lubricated, Flat Sector Thrust Bearing," Trans. ASME, *J. Lubr. Technology*, 99:82-88.
10. Ausman J.S. "An Approximate Analytical Solution for Self-Acting Gas Lubrication of Stepped Sector Thrust Bearings," *ASLE Transactions* 4:304-314.
11. Gross, W.A. et. al. "Fluid-Film Lubrication," *John Wiley & Sons*, 1980.

REPORT DOCUMENTATION PAGE	*Form Approved* *OMB No. 0704-0188*

1. AGENCY USE ONLY (*Leave blank*)	2. REPORT DATE	3. REPORT TYPE AND DATES COVERED
	October 2004	Final Contractor Report

4. TITLE AND SUBTITLE

Numerical, Analytical, Experimental Study of Fluid Dynamic Forces in Seals
Volume 2—Description of Gas Seal Codes GCYLT and GFACE

5. FUNDING NUMBERS

WBS–22–5000–0013
NAS3–25644

6. AUTHOR(S)

Wilbur Shapiro

7. PERFORMING ORGANIZATION NAME(S) AND ADDRESS(ES)

Mechanical Technology, Inc. (MTI)
968 Albany-Shaker Road
Latham, New York 12110

8. PERFORMING ORGANIZATION REPORT NUMBER

E–14708–2

9. SPONSORING/MONITORING AGENCY NAME(S) AND ADDRESS(ES)

National Aeronautics and Space Administration
Washington, DC 20546–0001

10. SPONSORING/MONITORING AGENCY REPORT NUMBER

NASA CR—2004-213199-VOL2

11. SUPPLEMENTARY NOTES

Project Manager, Anita D. Liang, Aeronautics Directorate, NASA Glenn Research Center, organization code 2200, 216–977–7439. Responsible person, Robert C. Hendricks, Research and Technology Directorate, NASA Glenn Research Center, organization code 5000, 216–977–7507.

12a. DISTRIBUTION/AVAILABILITY STATEMENT

Unclassified - Unlimited
Subject Categories: 07, 20, and 34 Distribution: Nonstandard

Available electronically at http://gltrs.grc.nasa.gov

This publication is available from the NASA Center for AeroSpace Information, 301–621–0390.

12b. DISTRIBUTION CODE

13. ABSTRACT ***(Maximum 200 words)***

The objectives of the program were to develop computational fluid dynamics (CFD) codes and simpler industrial codes for analyzing and designing advanced seals for air-breathing and space propulsion engines. The CFD code SCISEAL is capable of producing full three-dimensional flow field information for a variety of cylindrical configurations. An implicit multidomain capability allow the division of complex flow domains to allow optimum use of computational cells. SCISEAL also has the unique capability to produce cross-coupled stiffness and damping coefficients for rotordynamic computations. The industrial codes consist of a series of separate stand-alone modules designed for expeditious parametric analyses and optimization of a wide variety of cylindrical and face seals. Coupled through a Knowledge-Based System (KBS) that provides a user-friendly Graphical User Interface (GUI), the industrial codes are PC based using an OS/2 operating system. These codes were designed to treat film seals where a clearance exists between the rotating and stationary components. Leakage is inhibited by surface roughness, small but stiff clearance films, and viscous pumping devices. The codes have demonstrated to be a valuable resource for seal development of future air-breathing and space propulsion engines.

14. SUBJECT TERMS

CFD seal code; Industrial seal codes; User-friendly seal codes; Fluid-film seal codes; Clearance seal codes; Seals; Dynamics; Design; Computational analysis; Fluid forces

15. NUMBER OF PAGES

134

16. PRICE CODE

17. SECURITY CLASSIFICATION OF REPORT	18. SECURITY CLASSIFICATION OF THIS PAGE	19. SECURITY CLASSIFICATION OF ABSTRACT	20. LIMITATION OF ABSTRACT
Unclassified	Unclassified	Unclassified	